Synthesis and Characterization of the Axially Ferrocenyl Substituted Subphthalocyanines

A THESIS
SUBMITTED TO THE FACULTY OF THE
GRADUATE SCHOOL OF THE
UNIVERSITY OF MINNESOTA
BY

Katelynn Louise Spurgin

IN PARTIAL FULFILLMENT OF THE
REQUIREMENTS FOR THE DEGREE OF
MASTER OF SCIENCE

Advised by Dr. Victor Nemykin

October 2013

Acknowledgements

I would like to express my gratitude to my research advisor Dr. Victor Nemykin for all of his guidance and support throughout the last three years. I would also like to show my appreciation to Dr. Pavlo Solentsv for his unending patience and guidance with this project. A big thank you to Dr. Ahmed Heikal for his work with the time resolved fluorescence. Also I would like to thank Jared Sabin for all his help with the instrumentation instruction and for running all the computational chemistry. Finally, I would like to thank UMD for giving me the opportunity to be here and to the National Science Foundation and Minnesota Supercomputing Institution for funding this project.

To My Mom,

Without her unconditional love and support,

None of this would be possible.

Abstract

Two new ferrocenyl-subphthalocyanine dyads with ferrocenenylmethoxide (**2**) and ferrocenyl carboxylate (**3**) substituents directly attached to the subphthalocyanine ligand via the axial position have been prepared and characterized using NMR, UV-vis, and MCD spectroscopies as well as X-ray crystallography. Redox properties of the ferrocenyl-containing dyads **2** and **3** were investigated using the cyclic voltammetry (CV) approach and compared to those in parent subphthalocyanine **1**. CV data reveal that the first reversible oxidation is ferrocene-centered, while the second oxidation and the first reduction are localized on the subphthalocyanine ligand. The electronic structures and the nature of the optical bands observed in UV-vis and MCD spectra of all target compounds were investigated by DFT-PCM and TDDFT-PCM approaches. It has been found that in both dyads **2** and **3** HOMO to HOMO-2 are ferrocene-centered MOs, while HOMO-3 as well as LUMO and LUMO+1 are localized on the subphthalocyanine ligand. Fluorescence properties of the dyads **2** and **3** were investigated using steady-state and time-resolved fluorescence methods. It has been found that the fluorescence quenching is more efficient in dyad **3** as compared to dyad **2**, which was rationalized on the basis of DFT-PCM calculations. Similar tert-butyl SubPc compounds **4** and **5** were synthesized and characterized by UV-Vis, MCD, NMR, Fluorescence and electrochemical methods to determine the effects the tert-butyl groups has on the solubility of SubPc. UV-Vis and MCD show a slight shift in the Q-band to about 570 nm from about 564 nm of that of compounds **1**-**3**. Fluorescent intensities of compounds **4** and **5** were measured under similar conditions and it was found that the addition of ferrocene carboxylate again quenches the emission. CV data for compound **5** suggests that there is a first reversible

oxidation process centered on ferrocene. There are also two irreversible processes belonging to SubPc. Finally, the more electron dense, thiol substituted SubPc compound **10** was synthesized and characterized using UV-Vis, MCD, NMR, Fluorescence and electrochemical methods. Because of the additional electron density there was a shift of 80 nm to lower energy from 564 nm in compound **1** for the Q-band in the UV-Vis spectrum. Similarly, the fluorescent spectrum has a shift of 80 nm and is a mirror image of the Q-band. Finally, CV methods show agreement with compounds **1-5**, that there is an irreversible oxidation and reduction peak belonging to that of the subphthalocyanine core at 0.6987V and -1.893V respectively. The first oxidation process at 0.3943 V however is a reversible process that has not been seen in compounds **1** & **4**. It is possible that it belongs to another process of the compound that is only introduced with the thiol substituents. This can be responsible for the first irreversible reduction process at -1.5063 V as well.

Table of Contents

Acknowledgements i

Abstract ii

Table of Contents iii

Table of Acronyms v

Table of Figures viii

Table of Tables x

Table of Schemes xi

Introduction 1

1. Unsubstituted Subphthalocyanines 3
    a. Introduction 3
    b. Synthesis 4
    c. X-ray Analysis 6
    d. NMR Spectroscopy 13
    e. UV-Vis & MCD 16
    f. Comparative and Time-resolved Fluorescence 18
    g. Electrochemistry 20
    h. Electronic Structure 22
    i. Conclusions 31
2. Tertyl-Butyl Subphthalocyanines 33
    a. Introduction 33
    b. Synthesis 33
    c. NMR Spectroscopy 34

d. UV-Vis & MCD 35

e. Comparative Fluorescence 36

f. Electrochemistry 37

g. Spectroelectrochemistry 38

h. Conclusions 38

3. Thiol Substituted Subphthalocyanines 40

a. Introduction 40

b. Synthesis 40

c. NMR Spectroscopy 43

d. UV-Vis & MCD 45

e. Fluorescence 46

f. Electrochemistry 47

g. Conclusions 48

Experimental Section 49

References 57

Supplemental Information 68

1. Scheme for FcCOOH and $FcCH_2OH$ 68

2. TDDFT 69

3. CIF Information for Compound 1 70

4. CIF Information for Compound 2 76

5. CIF Information for Compound 3 95

Table of Acronyms

DSSC- Dye Sensitizer Solar Cell	2
SubPc- Subphthalocyanine	3
COSY-NMR- Correlation spectroscopy nuclear magnetic resonance	13
TPSPC- Time correlated single-photon counting	19
TDDFT- Time Dependent Density Functional Theory	22

Table of Figures

Figure 1: Dye Sensitizer Solar Cell (DSSC) 2

Figure 2: SubPc-Fc hybrid in a DSSC. 4

Figure 3: Crystal structure of SubPcCl (1) 7

Figure 4: Crystal structure of $SubPcOCH_2Fc$ (2) 7

Figure 5: Crystal structure of $SubPcO_2CFc$ (3) 8

Figure 6: Packing motif for compounds **2** and **3** 9

Figure 7: Packing motif for compound **1** 10

Figure 8: ^{1}H-NMR spectrum of $FcCH_2OH$ and $SubPcOCH_2Fc$ (**2**) in $CDCl_3$. 14

Figure 9: ^{1}H-NMR spectrum of $FcCO_2H$ and $SubPcO_2CFc$ (**3**) in $CDCl_3$. 14

Figure 10: ^{13}C NMR spectrum for compound **2** in $CDCl_3$. 15

Figure 11: ^{13}C NMR spectrum for compound **3** in $CDCl_3$. 16

Figure 12: UV-vis (left) and MCD (right) spectra of **1**-**3**. 16

Figure 13: Comparative fluorescence intensities of compounds **1** – **3**. 19

Figure 14: Room-temperature CV data for compounds **1** – **3** in DMF/TBAP system. 21

Figure 15:MO energy diagram for compounds **1** – **3**. 22

Figure 16: Molecular orbital compositions of compounds **1** – **3** predicted at DFT level. 25

Figure 17: Frontier orbitals of compounds **1** – **3**. 26

Figure 18: Experimental (top) and TDDFT predicted (bottom) UV-vis spectra of compound **1**. *Q*- and *B*-band regions are labeled as *Q* and *B*. 28

Table of Figures

Figure 19: Experimental (top) and TDDFT predicted (bottom) UV-vis spectra of complex **2**. *Q*-, *B*-, and *MLCT* band regions are labeled as *Q*, *B*, and *MLCT*. 28

Figure 20: Experimental (top) and TDDFT predicted (bottom) UV-vis spectra of complex **3**. *Q*-, *B*-, and *MLCT* band regions are labeled as *Q*, *B*, and *MLCT*. 29

Figure 21: Proposed non-radiative deactivation mechanism of the S_1 state in dyads **2** and **3**. 30

Figure 22: ^{1}H-NMR spectrum of tBuSubPcFcCO$_2$ (**5**) in $CDCl_3$ 34

Figure 23: UV-Vis and MCD spectra for compounds **4** and **5**. 35

Figure 24: Comparative Fluorescence of intensities for compounds **4** and **5**. 36

Figure 25: Room-temperature CV data for compound **5** in DCM/TBAP system. 37

Figure 26: Spectroelectrochemistry data for compound **5.** 38

Figure 27: ^{1}H NMR spectrum for compound **8** in $CDCl_3$. 43

Figure 28: ^{1}H NMR spectrum for compound **9** in $CDCl_3$. 44

Figure 29: ^{1}H NMR spectrum for compound **10** in $CDCl_3$. 44

Figure 30: UV-Vis and MCD spectrum for compounds **10**. 45

Figure 31: Fluorescence spectrum for compound **10**. 46

Figure 32: Room-temperature CV data for compound **10** in DCM/TBAP system. 47

Table of Tables

Table 1: Summary of crystallographic data for compounds **1 - 3**. 11

Table 2: Selected bond lengths (Å) and angles (°) for compounds **1- 3.** 12

Table 3: UV-vis absorption and steady-state emission data for compounds **1**-**3**. 18

Table 4: Redox properties of compounds **1 - 3**. 20

Table 5: Comparison of the experimental and DFT predicted bond distances in compounds **1 - 3**. 24

Table 6: Table of oxidation potentials for compound **5**. 37

Table 7: Table of oxidation potentials for compound **10**. 47

Table of Schemes

Scheme 1: Reaction Scheme for compounds **1**-**3**. 6

Scheme 2: Reaction Scheme for synthesis of compound **5.** 34

Scheme 3: Reaction Scheme for synthesis of compound **8.** 41

Scheme 4: Reaction Scheme for synthesis of compound **9.** 42

Scheme 5: Reaction Scheme for synthesis of compound **10.** 42

Supporting Information Scheme 1. 68

Introduction:

Synthesis of functional materials with high solar energy conversion efficiency represents a fundamental goal for a modern science.[1] Effective light-to-energy conversion requires an efficient formation of a long-lived charge-separated (CS) state, which have high energy content.[2] In the natural photosynthetic systems, the sequential electron-transfer processes lead to a spatial separation of ion pairs, which follow a redox gradient created by properly aligned and electronically tuned p-conjugated porphyrinoids.[3] Although a similar strategy has been successfully applied for the formation of the long living CS states in the artificial photosynthetic supramolecular multichromophoric assemblies, one serious drawback is the unacceptable loss of input energy during each electron transfer step.[4] Simple donor-acceptor hybrids represent a very attractive alternative for the preparation of artificial photosynthetic systems, which provide an acceptable compromise between the electronic coupling between the different redox-active substituents and the overall redox gradient.[5] The electron transfer kinetics and the excited state relaxation mechanism in such donor-acceptor hybrids in general depends on the magnitude of electronic coupling between the different substituents, which is dictated by the effective donor-acceptor distance, their orbital and spatial orientation, and the nature of the linking group between them.[6] In addition, charge-recombination and intermolecular interactions could also play a significant role in the kinetics of the CS states formation. The most critical parameter for efficient CS state formation was shown to be the donor-acceptor distance in such a molecular assembly.[7] In particular, it has been demonstrated that a short donor-acceptor distance (~2.6 Å) favors formation of CS states with an

exceptionally long (230 μs) life-time.[8] One way to potentially achieve this is using a dye sensitized solar cell (DSSC). In the cell, an electron donor is axially coordinated to an electron acceptor which is fixed on an electron injection layer within the cell. A photon of light is then absorbed, exciting an electron to its excited state. From there, the donor donates its electron to the acceptor, creating a negative on the acceptor and a positive on the donor. The extra electron on the acceptor is injected to the electron injection layer and the electron is moved through the cell creating electricity. Once the electron has reached the conducting electrode at the top of the cell, the electron is then injected to the positively charged donor, starting the process all over again (Figure 1).

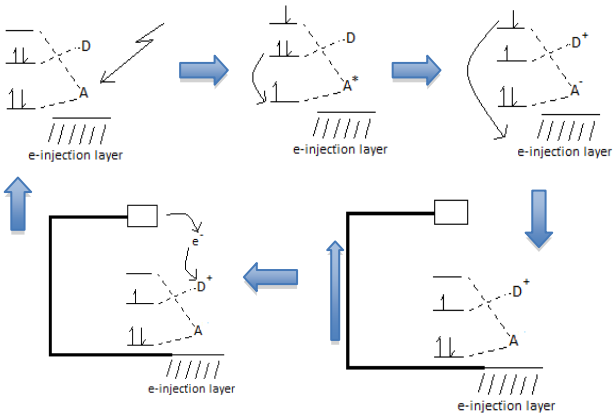

Figure 1: Dye Sensitized Solar Cell (DSSC)

Part 1- Un-substituted subphthalocyanines

Introduction:

Among numerous porphyrinoids used as an antenna in donor-acceptor dyads, the subphthalocyanine (SubPc) macrocycle attracted special attention because of its specific optical properties (a very strong absorption in the visible region) and bowl-shaped geometry, which is potentially useful for covalent as well as non-covalent coordination to acceptors such as C_{60}.[9] In addition, SubPcs exhibit quantum yields higher than the porphyrins for the first excited state and have small reorganization energies.[10] During the last decade, Torres and co-workers as well as the other groups have shown that the C_{60}-SubPc-donor triads could be used as light-harvesting subunits because they can follow a light-triggered multistep charge transfer mechanism, which ultimately leads to formation of a $C_{60}^{-\cdot}$-SubPc-donor$^{+\cdot}$ spatially separated radical ion pair.[9] In particular, ferrocene donors, connected via a *p*-phenyloxy linker to the axial position of the SubPc chromophore provided long-living (up to 231 μs) CS states in the above mentioned triads.[9] It could be anticipated, however, that decreasing the ferrocene-to-SubPc distance should positively affect the CS states formation. However, Fc-SubPc dyads with a direct ferrocene-boron or substituted ferrocene-boron bond have never been prepared and their properties have never been explored. Using a DSSC, a SubPc with a ferrocene substituent axially bound would be coordinated to C_{60} within the cell. SubPc would act as the antenna absorbing a photon of light. A SubPc electron is excited to its excited state and then ferrocene donates an electron to SubPc. From there, SubPc tranfers the electron to C_{60}, creating a positive charge on ferrocene (donor) and a negative charge on C_{60}

(acceptor) which also creates a charge-separated state (CS). The electron from there is then injected to the conducting electrode and moved through the cell creating electricity. When the electron reaches the top of the cell, the electron is injected back to the positively charged ferrocene, and then the process can start all over again (Figure 2).

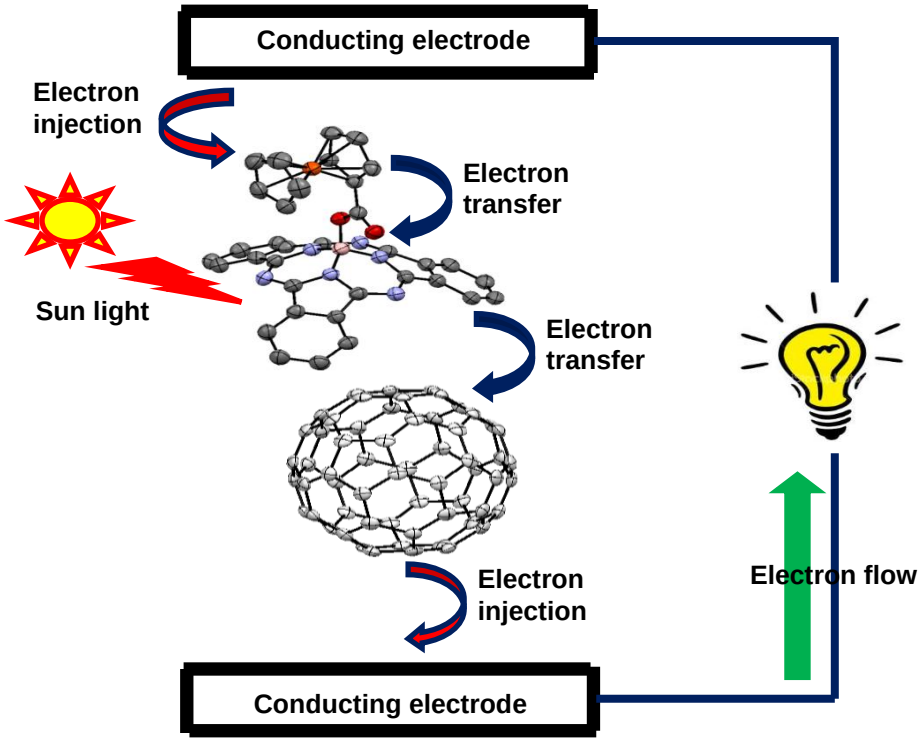

Figure 2: SubPc-Fc hybrid in a DSSC.

Synthesis:

Ferrocenyl methanol (**6**) and ferrocene carboxylic acid (**7**) were prepared in multi-gram quantities using protocols slightly modified from the previously reported methods (Supporting Information Scheme 1).[11,12] Ferrocenyl-containing SubPc dyads **2** and **3** were obtained using the synthetic strategy outlined in Scheme 1. In general, nucleophilic substitution of the chloride atom by alkoxide (OR^-) in SubPcBCl or SubPcBBr can be achieved by refluxing these macrocycles with a corresponding alcohol in toluene.[26] While

this approach is very simple, it is effective only for the thermally stable alcohols. In the case of the reaction between SubPcCl and $FcCH_2OH$ in boiling toluene, no desired $SubPcBOCH_2Fc$ was detected. Instead, bis(ferrocenylmethylene) ether, $(FcCH_2)O$, and unreacted SubPcCl were isolated under these reaction conditions. Thus, in order to obtain target complex **2**, we adopted a new versatile two step strategy described by Toress and co-workers for axial modification of the SubPcCl systems.[27] First, an anion exchange reaction between SubPcCl and silver triflate was conducted followed by quenching of the resulting SubPcOTf by ferrocenylmethanol. Using this strategy, the target subphthalocyanine **2** was obtained in 17 % yield (Scheme 1). Such relatively low yield originates from the low stability of complex **2** on silica gel that was required for its successful purification.

The introduction of a carboxylic acid group into subphthalocyanine systems is not very straightforward. Indeed, only subphthalocyanines axially bonded to acetate, phenylacetate, trifluoroacetate, trichloroacetate, chloroacetate, and benzoate were described so far.[28] Moreover, synthetic procedures for preparation of these complexes requires boiling or melting of the SubPcCl with the corresponding acid. This method, however, is unacceptable in the case of ferrocenecarboxylic acid, because of its well-known thermal decomposition.[29] We found, however, that the substitution of the axial chlorine atom in SubPcBCl by ferrocene carboxylate could be achieved by refluxing of the reagents in *o*-DCB for 3 hours (Scheme 1).

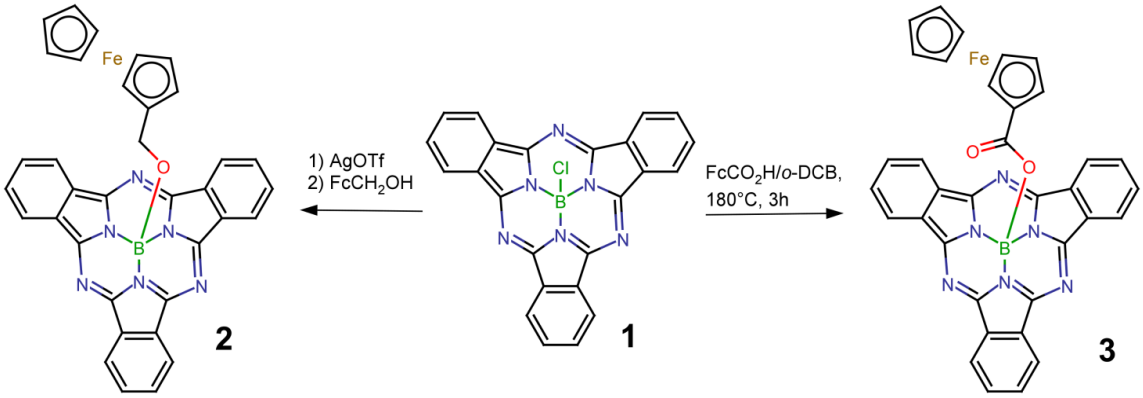

Scheme 1. Reaction Scheme for compounds **1-3**.

X-ray Analysis:

An ultimate knowledge of the structure of the ferrocenyl-subphthalocyanine dyads **2** and **3** was further gained from their X-ray crystal structures. In addition, in order to accurately compare structural changes in complexes **2** and **3** to the parent SubPc **1**, an X-ray structure of compound **1** was also determined at -150^{0}C. Refinement parameters for compounds **1** - **3** are presented in Table 1 while their selected bonds lengths and angles are summarized in the Table 3. ORTEP diagrams of compounds **1** - **3** are shown in Figures 1-3. Similar to all previously known structures of SubPc complexes,[9,26-28,32] the macrocyclic ligand adopts a bowl-shaped conformation with the boron atom pointing away from the macrocyclic base. In all structures boron atoms are located in trigonal pyramidal (3N+Cl for **1** and 3N+O for **2** and **3**) environment.

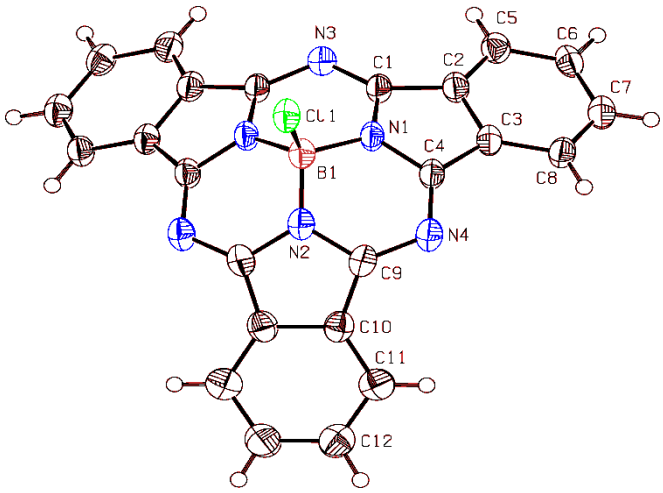

Figure 3: Crystal structure of SubPcCl (**1**).

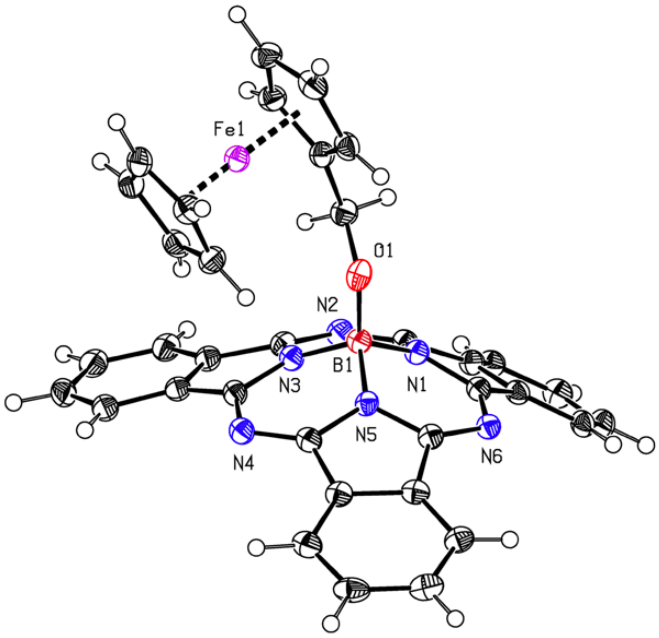

Figure 4: Crystal structure of SubPcOCH$_2$Fc (**2**).

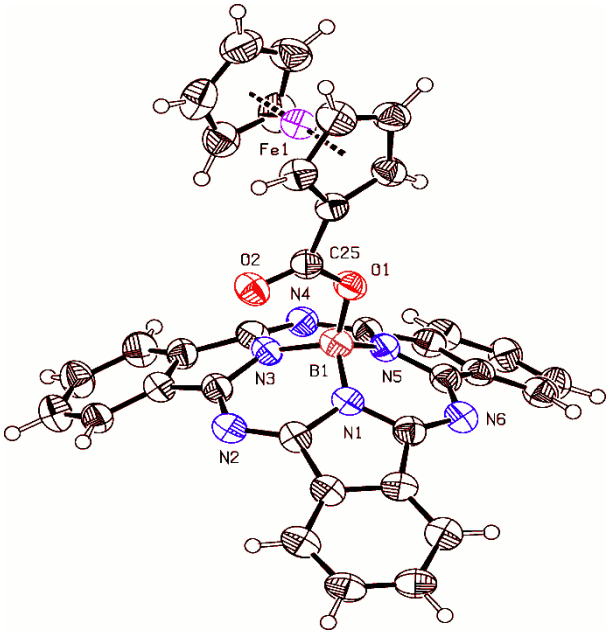

Figure 5: Crystal structure of SubPcO_2CFc (**3**).

The axial B-Cl bond in **1** is expectedly longer, while B-O bonds in **2** and **3** are expectedly shorter compared to the B-N bonds in respective SubPcs. B-O bonds in dyads **2** and **3** are quite different (1.430(4) and 1.467(4) Å for **2** and **3**, respectively) but similar to the other subphthalocyanines with alkoxy- or carboxy- substituents in axial positions.[9,26-28,32] The B-O bond distance difference is reflective of the axial ligand nature and in particular the higher polarity of the B-O bond in complex **3**. The η^1 character in coordination of the axial ferrocenecarboxylate group in dyad **3** could be clearly determined from its X-ray structure (Figure 5, Table 2). Indeed, the X-ray diffraction experiment determined B-O1 and B-O2 bond distances are 1.467(4) and 2.772(5) Å, respectively, while O1-C25 and O2-C25 bond distances are 1.334(4) and 1.218(4) Å, respectively, which is indicative of the η^1 character in coordination of the axial ferrocenecarboxylate group and the presence of C-O and C=O bonds in **3**. The axial ferrocene ligands are tilted toward one of the

nitrogen atoms, which is reflected in the respective O-B-N angles (118.1(2)°, 116.0(2)° and 111.1(2)° in **2** and 108.6(3)°, 117.7(3)°, and 115.1(3)° in **3**). B-N bond distances in dyads **2** and **3** are close to each other, but longer than those in the parent compound **1** (1.489(4)-1.504(4) Å in **2** and 1.480(5)-1.498(5) Å in **3**). O-C bond distance in **2** (1.398(4) Å) is significantly shorter than the same bond distance in the initial $FcCH_2OH$ **6** (for three symmetry unique molecules of **6**: 1.434(6), 1.451(6), and 1.450(5) Å),[11] which is reflective of the electron-acceptor properties of the subphthalocyanine macrocycle. Torsion angles B1-O1-C25-C26 and O1-C25-C26-C27 are -160.9(2)° and 148.1(3)°, in dyads **2** and **3**, respectively. The carboxylic acid group in **3** is almost coplanar with the monosubstituted cyclopentadienyl (Cp) ring (torsion angle O1-C25-C26-C27 is 10.7(5)°). The Fe-C bond distances were observed in the range of 2.031(3) – 2.070(3) Å and 2.016(4) - 2.071(4) Å in dyads **2** and **3**, respectively and adopt close to an eclipsed conformation of Cp rings.

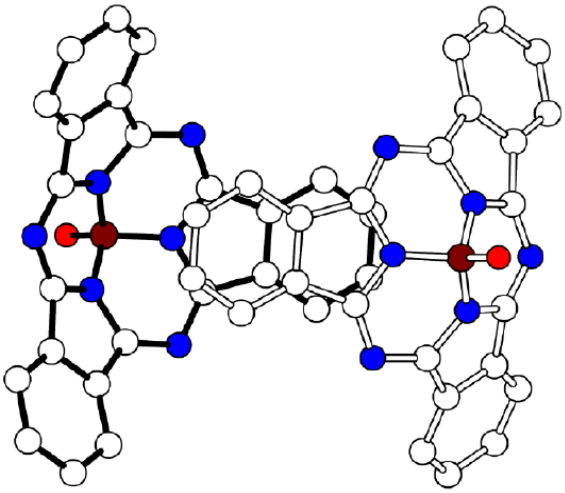

Figure 6: Packing Diagram for compounds **2** and **3.**

The packing motifs in dyads **2** and **3** are very similar and consist of the formation of a π···π stacking between overlapping isoindole fragments of the macrocyclic ligand (Figure

6). On the contrary, π···π stacking in the parent SubPc **1** occurs between isoindole fragment of one molecule and the *meso*-nitrogen containing six-membered fragment of the neighboring macrocycle (Figure 7). Both of these motifs are typical for substituted subphthalocyanines.[9,26-28]

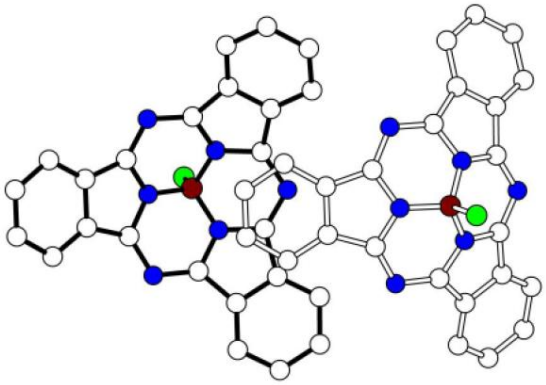

Figure 7: Packing motif for compound **1**.

Table 1. Summary of crystallographic data for compounds **1** - **3**.

	1	**2**	**3**
Empirical formula	$C_{24}H_{12}N_6BCl$	$C_{35}H_{23}N_6OBFe$	$C_{35}H_{21}N_6O_2BFe$
Formula weight	430.66	610.25	624.24
Crystal system	Orthorhombic	Monoclinic	Monoclinic
Space group, Z	Pnma, 4	C2/c, 8	$P2_1/c$, 4
a (Å)	12.1224(2)	28.610(5)	17.2645(8)
b (Å)	14.8449(10)	11.197(5)	7.7863(2)
c (Å)	10.3283(1)	18.146(5)	20.6276(14)
β (°)	90	114.658(5)	95.019(7)
Volume ($Å^3$)	1858.6(1)	5283(3)	2762.3(2)
$\rho_{calc}(g/cm^3)$	1.539	1.535	1.501
$\mu(mm^{-1})$	2.041[a]	0.615[b]	4.757[a]
$\theta_{max}(°)$	68.24[a]	27.49[b]	68.41[a]
Meas./unique reflns	12595/1756	17320/6032	29594/5040
R_{int}	0.0351	0.0492	0.0647
GoF(F^2)	1.156	1.047	1.092
R_1[c], wR_2[d] (I>2σ(I))	0.0668/0.1872	0.0612/0.1553	0.0657/0.1817
R_1[c], wR_2[d] (all data)	0.0852/0.2127	0.0704/0.1625	0.0815/0.2060
$\Delta\rho_{max}/\Delta\rho_{min}$ ($e/Å^3$)	0.838/-0.485	1.067/-0.902	0.618/-0.971

[a]Cu-K_α, [b]Mo- K_α, [c]$R_1(F)=\sum||F_o| - |F_c||/\sum|F_o|$, [d]$wR_2(F^2)=\{\sum[w(F_o^2 - F_c^2)^2]/\sum w(F_o^2)^2]\}^{1/2}$.

Table 2. Selected bond lengths (Å) and angles (°) for compounds **1- 3.**

Compound 1			
Cl(1)-B(1)	1.890(6)	N(2)-B(1)	1.470(8)
N(1)-B(1)	1.473(4)		
N(2)-B(1)-N(1)	105.7(3)	N(2)-B(1)-Cl(1)	112.4(4)
N(1)-B(1)-N(1)#1	106.5(4)	N(1)-B(1)-Cl(1)	113.0(3)
#1 x, 3/2-y, z			
Compound 2			
Fe···π[a](centroid)	1.650(2), 1.659(2)	N(1)-B(1)	1.504(4)
Fe···C(average)	2.049(2)	N(3)-B(1)	1.499(4)
C(25)-O(1)	1.398(4)	N(5)-B(1)	1.489(4)
C(25)-C(26)	1.497(4)	O(1)-B(1)	1.430(4)
O(1)-B(1)-N(5)	111.1(2)	O(1)-B(1)-N(1)	118.1(2)
O(1)-B(1)-N(3)	116.0(2)	N(5)-B(1)-N(1)	104.3(2)
N(5)-B(1)-N(3)	103.1(2)	N(3)-B(1)-N(1)	102.7(2)
C(26)-C(25)-O(1)-B(1)	-160.9(2)	O(1)-C(25)-C(26)-C(27)	148.1(3)
Compound 3			
Fe···π[a](centroid)	1.644(2), 1.648(2)	N(1)-B(1)	1.498(5)
Fe···C(average)	2.039(2)	N(3)-B(1)	1.490(5)
B(1)-O(1)	1.467(4)	N(5)-B(1)	1.480(5)
B(1)-O(2)	2.772(5)	O(2)-C(25)	1.218(4)
C(25)-C(26)	1.472(5)	O(1)-C(25)	1.334(4)
O(2)-C(25)-O(1)	123.1(3)	O(1)-B(1)-N(3)	117.7(3)
O(2)-C(25)-C(26)	124.8(4)	N(5)-B(1)-N(3)	104.5(3)
C(25)-O(1)-B(1)	121.3(3)	N(5)-B(1)-N(1)	104.9(3)
O(1)-B(1)-N(1)	115.1(3)	N(3)-B(1)-N(1)	104.8(3)
O(1)-C(25)-C(26)-C(27)	10.7(5)	B(1)-O(1)-C(25)-C(26)	178.0(3)

[a] Ring centroids were built on C26-C27-C28-C29-C30 and C31-C32-C33-C34-C35.

NMR Spectra:

Introduction of the ferrocenyl substituents into target complexes **2** and **3** significantly increases their solubility in common organic solvents compared to the parent macrocycle **1**. Indeed, both complexes **2** and **3** are reasonably soluble in toluene, DCM, chloroform, and THF. Substitution of the axial chloride in SubPcBCl **1** by the ferrocenyl methanol and the ferrocenecarboxylate could be easily followed by ^{1}H-NMR spectroscopy. Similar to other axially coordinated phthalocyanines and their analogues,[30] the ^{1}H-NMR spectra of complexes **2** and **3** have proton signals of the cyclopentadienyl ligands shifted to higher fields compared to the corresponding signals observed in parent $FcCH_2OH$ and $FcCO_2H$ (Figures 8 and 9). Ring current effects are especially significant with protons located close to the macrocycle. Indeed, protons of the -CH_2- group in complex **2** have a resulting shift in their resonance from 4.27 to 2.34 ppm. Expectedly, NMR signals of the ferrocenyl protons are less shifted compared to the NMR signals of the parent molecules. It is interesting to note, that the chemical shifts of the α-Cp and β-Cp protons in complex **3** are very close to each other and cannot be separated in the COSY experiment, although their integral intensity is in a good agreement with the proposed structure. Macrocyclic aromatic protons in all complexes are close to each other suggesting negligible influence of the axial ligand on the chemical shifts. A similar picture was observed in the case of other axially substituted SubPcs.[9,26-28]

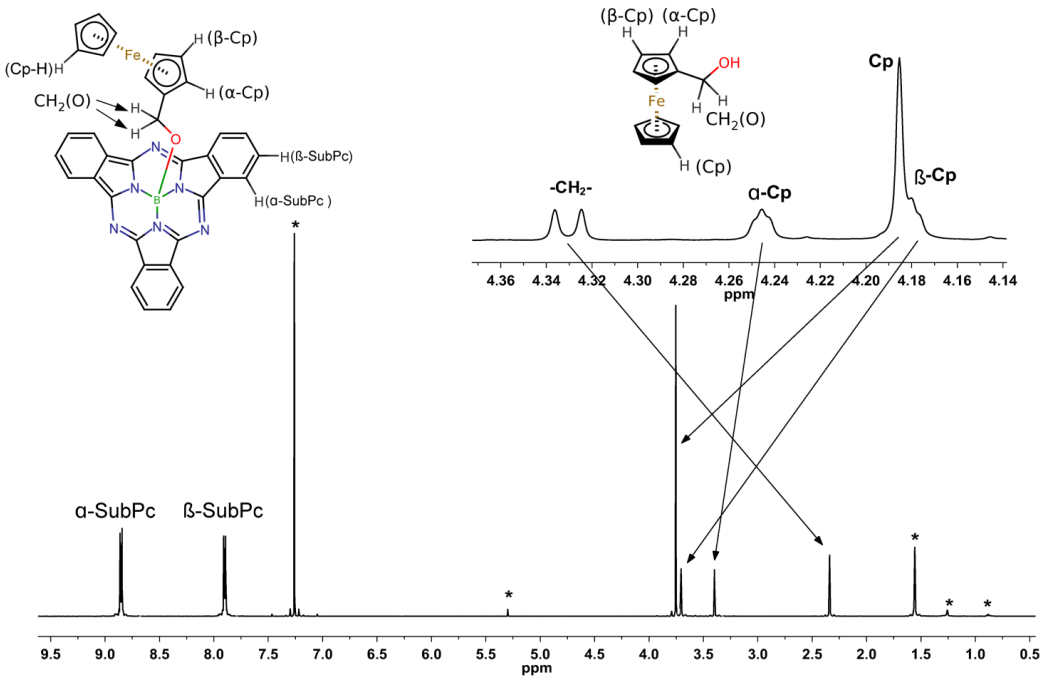

Figure 8. ^{1}H-NMR spectrum of $FcCH_2OH$ and $SubPcOCH_2Fc$ (**2**) in $CDCl_3$.

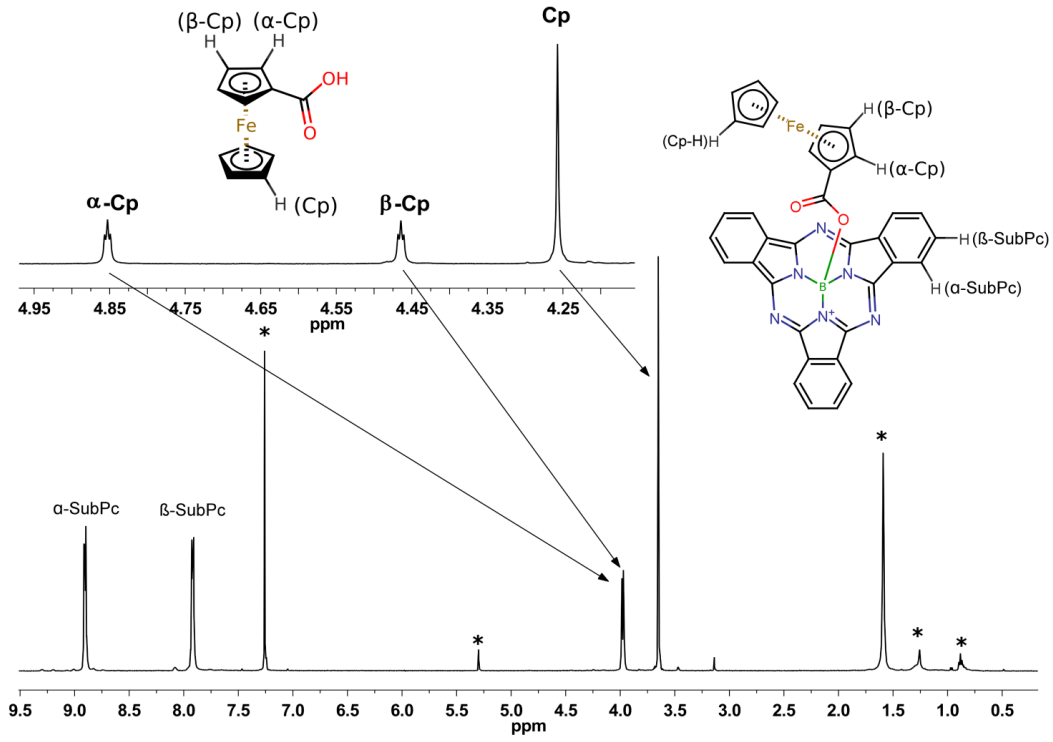

Figure 9. ^{1}H-NMR spectrum of $FcCO_2H$ and $SubPcO_2CFc$ (**3**) in $CDCl_3$.

In the figures below (Figures 10 and 11), ^{13}C NMR was done for further characterization for compounds **2** and **3**. The two compounds have similar peaks such as α and β pyrrole, α, β, and Cp carbons, and a C_{ipso} carbon. The two compounds have different carbon signals that correspond to the linking group that link ferrocene and SubPc. Compound **2** has a CH_2 peak and compound **3** has a CO_2^- peak. These spectra help verify the correct number of carbons within the compounds.

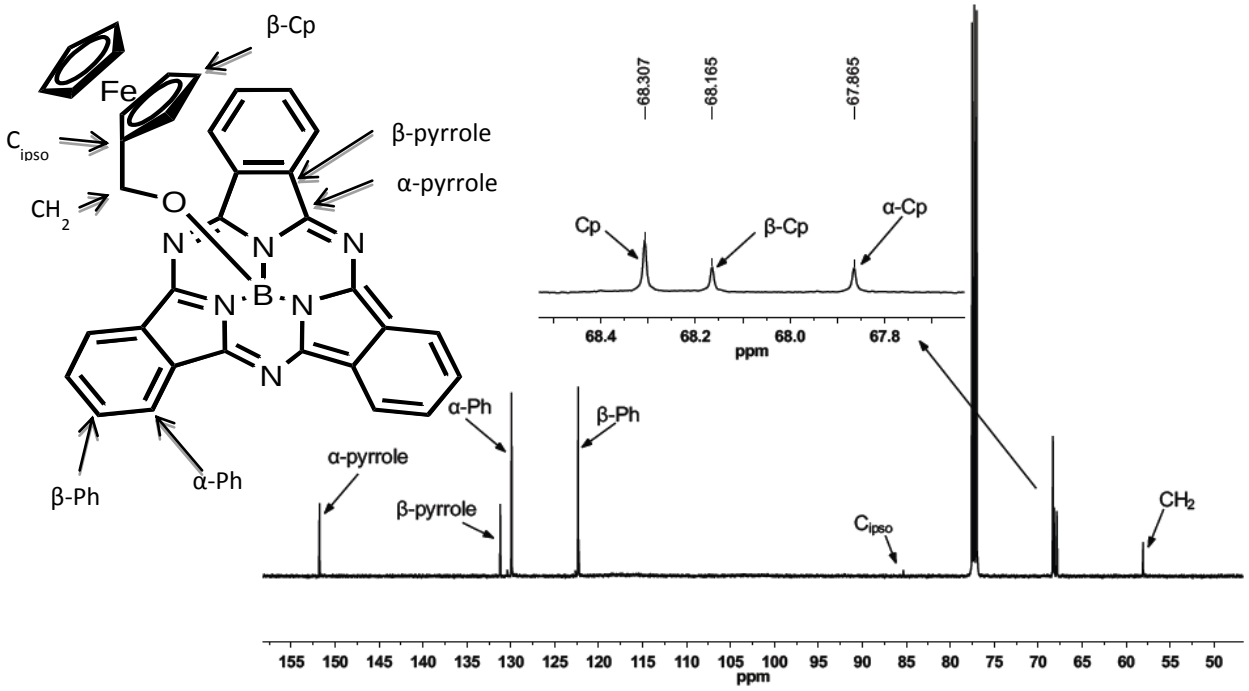

Figure 10. ^{13}C NMR spectrum for compound **2** in $CDCl_3$.

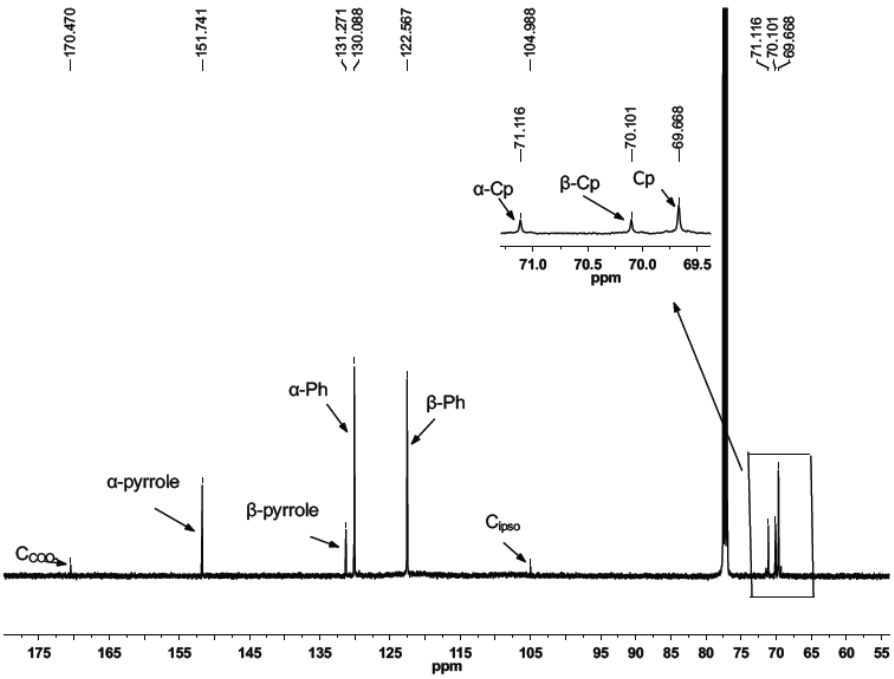

Figure 11. ^{13}C NMR spectrum for compound **3**.

UV-Vis NIR and MCD spectra:

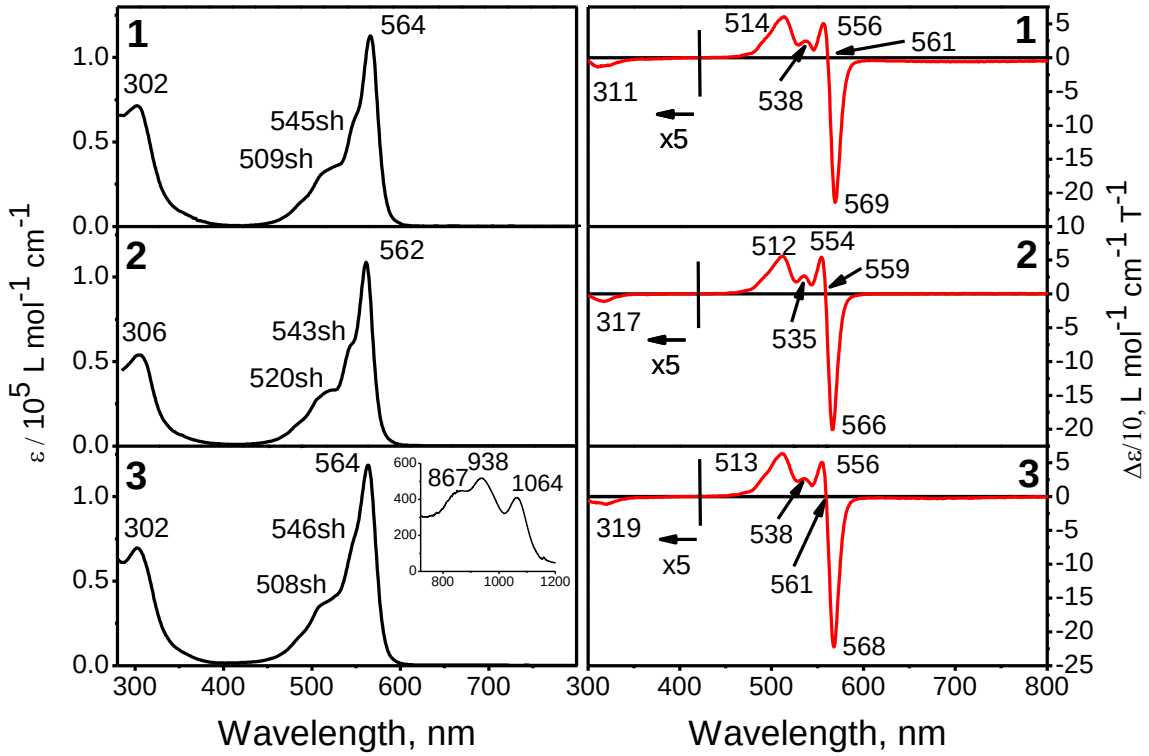

Figure 12. UV-vis (left) and MCD (right) spectra of **1**-**3**.

UV-vis and MCD spectra of SubPcs **1** – **3** are presented in Figure 12 and summarized in Table 3. In agreement with previous publications,[9,26-28,31] axial substitution of the chlorine atom by alkoxy or carboxylate ligands in subphthalocyanines **2** and **3** has a very minor influence on their UV-vis and MCD spectra, which are dominated by the very intense intra-ligand π–π* transitions. Indeed, the low-energy *Q*-band is observed at 564 nm in parent subphthalocyanine **1** and ferrocene-subphthalocyanine dyad **3**, while an only 2 nm shift in the *Q*-band position is observed for complex **2**. Similarly, the MCD spectra of complexes **2** and **3** are almost undistinguished from the MCD spectrum of parent subphthalocyanine **1.** They are dominated by the Faraday *A*-term centered at 558 nm in complex **2** and 561 nm in complex **3** which correspond to the most intense *Q*-band band in the UV-vis spectra of these compounds and confirm their three-fold effective symmetry. Since electrochemical experiments as well as DFT-PCM and TDDFT-PCM calculations predict that ferrocene-centered MOs in dyads **2** and **3** should dominate the HOMO region, we explored the possible presence of metal-to-ligand charge-transfer (MLCT) transitions in the NIR region. Although MLCT bands were not observed in dyad **2** between 600 and 1500 nm, three relatively low intensity bands centered at 850, 938, and 1064 nm were observed for several independently prepared samples of dyad **3** (Figure 6). These weak MLCT transitions could be attributed to charge-transfer from ferrocene-centered HOMO to HOMO-2 to the nearly degenerate subphthalocyanine-centered LUMO and LUMO+1 on the basis of TDDFT-PCM calculations as discussed below. The absence of similar MLCT bands in dyad **2** can be explained by taking into consideration that the higher flexibility of the axial ferrocene-containing substituents should lead to a significantly lower band intensities and thus MLCT bands could be

masked by the low-energy wing of the very intense (ε ~100,000) *Q*-band.

Table 3. UV-vis absorption and steady-state emission data for compounds **1**-**3**.

Compound	UV-vis	Fluorescence			
	λ_{abs}, nm (log ε)	λ_{fl}, nm	τ_1, ns (%)	τ_2, ps (%)	τ_{av}, ps
1	564 (5.05), 545sh (4.79), 527sh (4.56), 302 (4.86)	582	3.11 (100)	-	3110
2	562 (5.04), 543sh (4.77), 524sh (4.52), 306 (4.73)	576	2.92 (30)	5 (70)	882
3	564 (5.07), 546sh (4.86), 518sh (4.58), 303 (4.84)	580[a]	1.65 (3)	21 (97)	65

[a] Crude estimation because of the low emission intensity.

Comparative and Time-resolved Fluorescence:

Axially substituted SubPcs are known as strongly emitting fluorophores and also have been utilized as electron- and energy- donors and acceptors.[10] A high fluorescence quantum yield (Φ_F) of the parent SubPc **1** (Φ_F = 0.25) allows the use of this platform for qualitative and quantitative understanding of the intramolecular fluorescence deactivation process. Indeed, upon excitation of the *Q*-band of parent compound **1**, there is an intense fluorescence peak centered at 582 nm, which is assigned to the $S_1 \rightarrow S_0$ transition (Figure 13). The luminescence observed in SubPcs has shown to be the mirror image of the *Q*-band and almost independent from the solvent and the nature of the axial substituents. When fluorescence spectra for compounds **1** – **3** were recorded under the same experimental conditions, both emission intensities in dyads **2** and **3** were found to be a several orders of magnitude lower than the fluorescence observed in **1**. In spite of the strong quenching, however, the overall fluorescence profile for compounds **1** – **3** remains very similar (Figure 13, Table 3). Such behavior has been observed for several SubPcs with different quenching groups and was attributed to the intrinsically faster singlet

excited state deactivation.[9,10] In order to examine this tentative assignment, we have measured the first excited state lifetimes in compounds **1** - **3** using the TCSPC (time-correlated single-photon counting) approach.[25] The S_1-fluorescence of the parent SubPcCl **1** excited at 475 nm and detected at 585±40 nm decays as a single exponential function with an estimated fluorescence lifetime of τ_{S1} = 3.11 ns. In contrast, the S_1 state fluorescence of ferrocenyl-containing dyads **2** and **3** decays as a biexponential as summarized in Table 3. More importantly, the dominant component in fluorescence emission of ferrocenyl-containing dyads **2** and **3** was found to be 7 ps (70%) and 21 ps (97 %), respectively. It is worth noting that these ultrafast decay components are faster than the full-width-half-maximum (FWHM) of our system response function (~45 ps), which was used in the deconvolution-based fitting algorithm. Thus fluorescence decay measurements confirmed a significant shortening of the first excited-state lifetime of complexes **2** and **3**, which is clearly indicative of an efficient deactivation mechanism in these compounds.

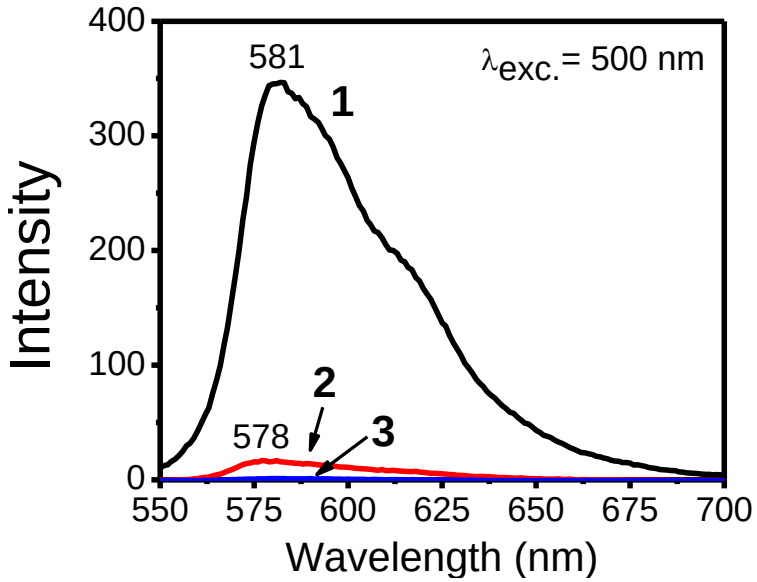

Figure 13. Comparative fluorescence intensities of compounds **1** – **3**.

Electrochemistry:

Redox properties of the ferrocene-subphthalocyanine dyads were examined using the cyclic voltammetry (CV) approach (Table 4). Because of the relatively low solubility of dyads **2** and **3** and especially parent subphthalocyanine **1** in DCM and THF, all electrochemical experiments were conducted in a DMF/TBAP system because most compounds are soluble in DMF. The ferrocene substituents in dyads **2** and **3** exhibit reversible first oxidations at +0.02 and +0.34 V (Figure 14). Oxidation of the axial ferrocenyl substituent in dyad **2** was at a lower potential than dyad **3**.

Table 4. Redox properties of compounds **1 - 3**.

	Oxidation, V		Reduction, V	
	E^{Ox2}	$E_{1/2}{}^{Ox1}$ (Fc)	$E_{1/2}{}^{R1}$	HOMO-LUMO, eV
1	0.655[a]	-	-1.698[a]	2.353
2	0.545[a]	0.020	-1.505	1.526
3	0.724[a]	0.345	-1.323	1.666

[a] Irreversible process; all potentials (±5 mV) are given in volts relative to Fc/Fc^{+}.

This is in good agreement with the electron-donating nature of the ferrocenemethanol group and DFT calculations presented below, which show that the energy of the HOMO in **3** is 0.28 eV lower than that in **2**. All three SubPcs (**1** – **3**) studied exhibit a single reduction peak, at -1.70 , -1.51, and -1.32 V, respectively, which corresponds to the one-electron reduction process centered at the macrocyclic ligand. In agreement with the previous reports,[9,26-28,33] oxidation of the subphthalocyanine ligand was observed as the only partially reversible process at 0.66, 0.54, and 0.66 V, for complexes **1** – **3**, respectively, which is associated with the partial degradation of the

macrocyclic ligand. The degradation of the macrocyclic ligand was further confirmed by CV experiments on dyad **3**. Indeed, when CV experiments were conducted between 0 and -1.75 V potentials, only single a reversible peak of subphthalocyanine reduction was observed at -1.32 V (Figure 14). On the other hand, when CV experiment was conducted by sweeping between +1.25 and -1.75 V, four additional peaks at -0.043, -0.337, -0.698, and -0.958, were observed in the CV. Similar peaks, which are attributed to the degradation of SubPcs were already reported several times in the literature.[33] It is important to note that the oxidation and reduction of subphthalocyanine core potentials in all three systems are ~2 V, which is in typical range for all SubPcs.

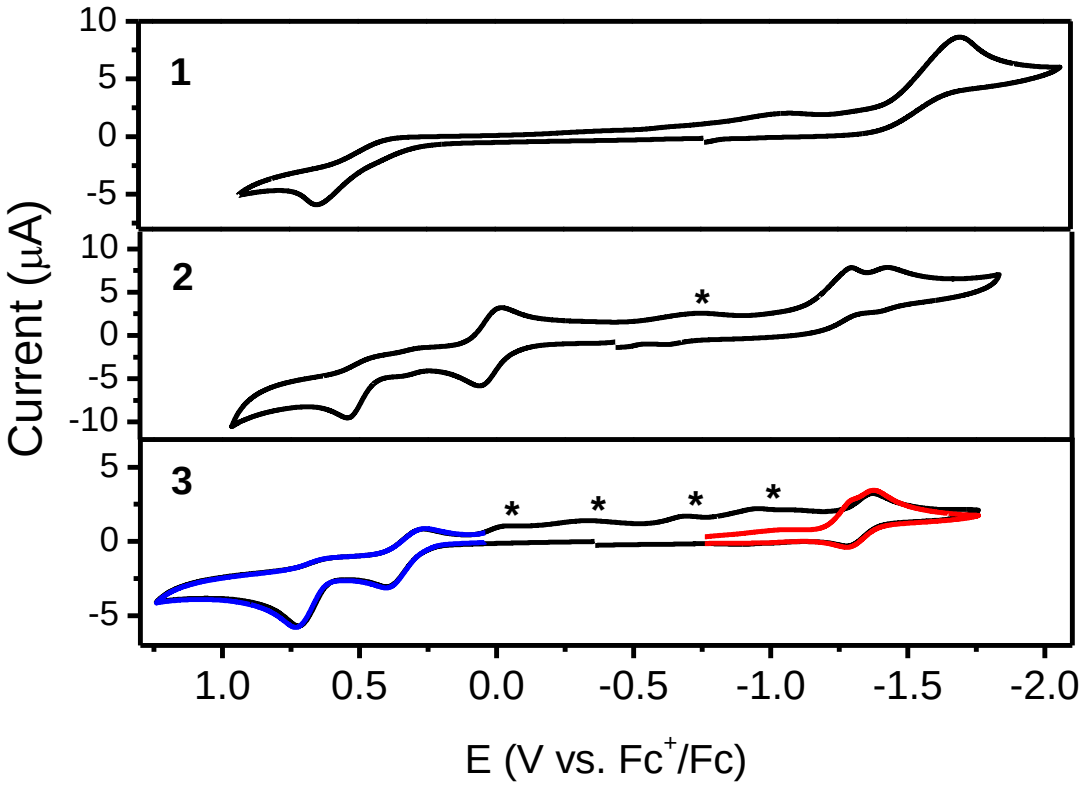

Figure 14. Room-temperature CV data for compounds **1** – **3** in DMF/TBAP system.

Electronic Structure:

Further insight into the electronic structure, spectroscopy, and redox properties of the ferrocene-containing dyads **2** and **3** was gained on the basis of DFT-PCM and TDDFT-PCM calculations, which provide accurate energetic and spectroscopic parameters for a large variety of ferrocene-containing complexes[34] and macrocyclic compounds including SubPcs.[17,35] The comparison between theory and X-ray experiments (Table 5) indicates that the DFT-PCM predicted geometries are in a good agreement with the experimental parameters. The DFT-PCM predicted MO energy diagrams for the target SubPcs **1** – **3** are presented in Figure 15, while an analysis of the orbital compositions is provided in Figure 16.

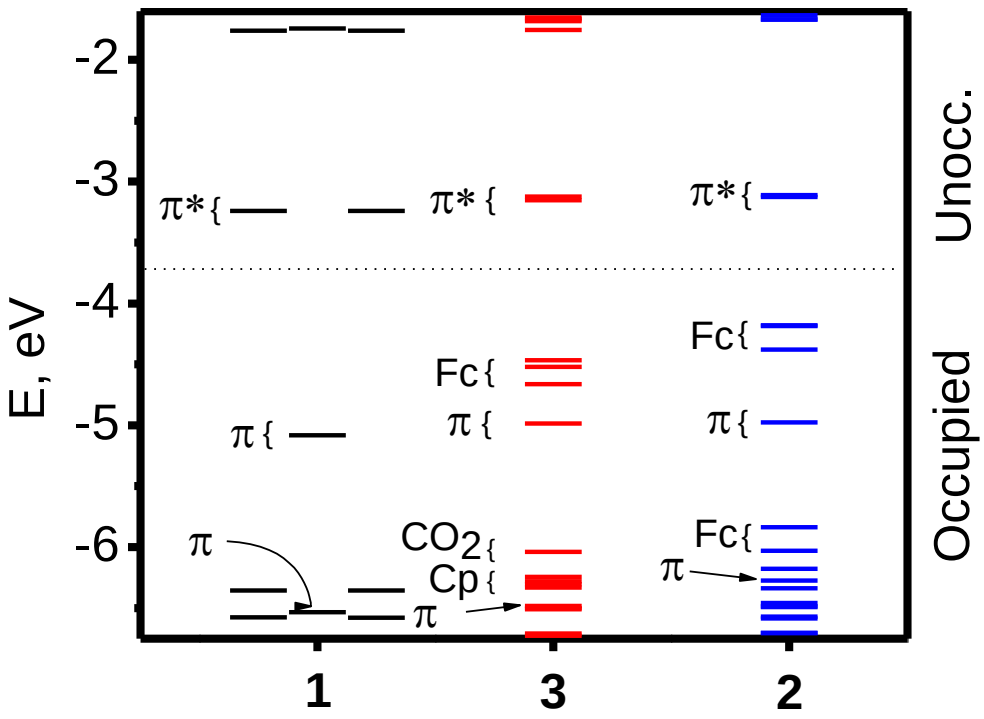

Figure 15. MO energy diagram for compounds **1** – **3**.

In addition, the frontier orbitals of the target SubPc complexes **1** - **3** are pictured in Figure 17. In agreement with the Gouterman's classic four-orbital model for porphyrins and

phthalocyanines,[36] the HOMO in parent SubPcCl **1** has a_2 symmetry (C_{3v} point group) and is a subphthalocyanine-centered π-orbital with an electron density distribution that resembles an a_{1u} MO in the phthalocyanine's D_{4h} point group. Gouterman's model theory states that the absorption bands in porphyrin systems arise from transitions between two HOMOs and two LUMOs. In this theory the HOMOs were calculated to be an a_{1u} and an a_{2u} and the LUMOs were calculated to be a set of degenerate e_g orbitals.[41] In agreement with previous calculations on SubPcs[35] but contrary to closed-shell phthalocyanines and porphyrins,[37] HOMO-1 and HOMO-2 are doubly degenerate MOs, which, as predicted by the TDDFT-PCM calculations, contribute significantly to the *B*-band region intensity of the UV-vis spectrum of SubPcCl **1**. The HOMO-3 again resembles a classic Gouterman's MO with a large contribution from the *meso*-nitrogen atoms (Figure 16). An introduction of axial ferrocenyl-containing ligands in dyads **2** and **3** leads to the situation where HOMO to HOMO-2 become predominantly iron (d_{xy}, d_{x2-y2}, and d_{z2}, respectively) – centered MOs entirely localized on the axial organometallic ligands (Figure 16) with all occupied SubPc-centered π-orbitals having lower energies. Such a molecular orbital description is in excellent agreement with the electrochemical data, which suggests that the first oxidation process in dyads **2** and **3** is ferrocene-centered. As expected from the electron-withdrawing nature of the carboxylic group, the ferrocenyl-centered HOMO to HOMO-2 in dyad **3** are more stable (-4.466, -4.522, and -4.664 eV) compared to the analogue MOs in dyad **2** (-4.180, -4.187, -4.378 eV). In all investigated SubPcs, LUMO and LUMO+1 are, or nearly, doubly degenerate π* MOs entirely localized on the SubPc ligand. These MOs are well separated from the higher energy unoccupied orbitals.

Table 5. Comparison of the experimental and DFT predicted bond distances in compounds **1** - **3**.

Bond	X-ray	DFT
	Compound 1[a]	
B-Cl	1.890(6)	1.855
B-N	1.473(4); 1.470(8)	1.485
	Compound 2[b]	
B-O	1.430(4)	1.416
B-N	1.498(5); 1.490(5); 1.480(5)	1.508; 1.508; 1.496
C-O	1.398(4)	1.408
	Compound 3[b]	
B-O	1.467(4)	1.458
B-N	1.498(5); 1.490(5); 1.480(5)	1.494; 1.494; 1.491
C-O	1.334(4)	1.337
C O	1.218(4)	1.216

[a] C_{3V} point group was used during geometry optimization by DFT and local C_S symmetry was observed in solid state; [b] C_1 point group was used during geometry optimization.

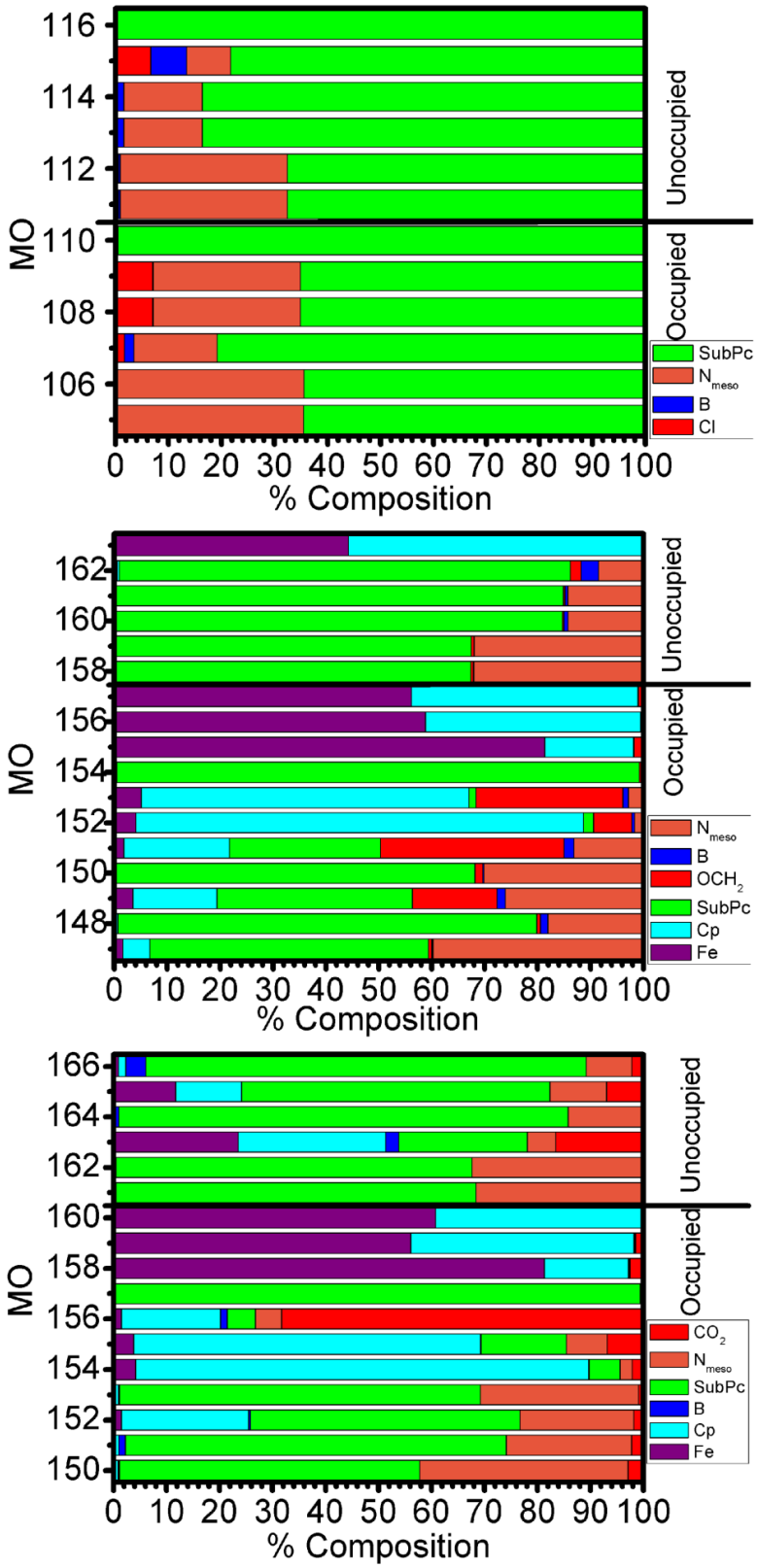

Figure 16. Molecular orbital compositions of compounds **1** – **3** predicted at DFT level.

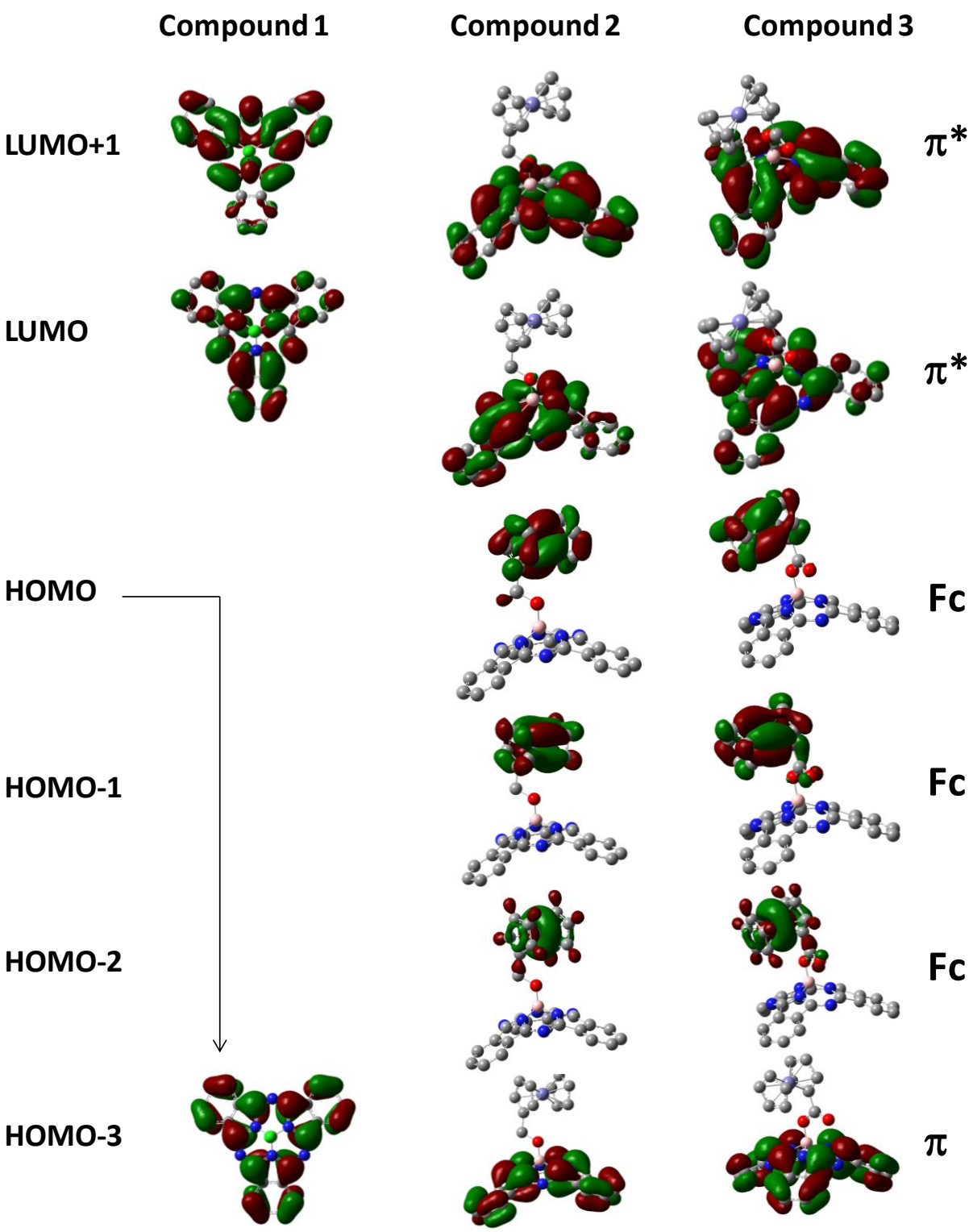

Figure 17. Frontier orbitals of compounds **1** – **3**.

In general, DFT-PCM calculations suggest that the UV-vis spectrum of the parent compound **1** would be dominated by the symmetry allowed π–π* transitions, while in the case of the dyads **2** and **3**, additional low-energy, low-intensity HOMO to HOMO-2 → LUMO, LUMO+1 MLCT transitions are expected in their UV-vis spectra. Further insight into the nature of the experimentally observed transitions was gained using the TDDFT-PCM approach. It was found that in general, TDDFT-PCM calculations reproduce well all experimentally observed features in the SubPc complexes **1** – **3** (Figures 18 – 20) show the experimental and the TDDFT predicted data in cm^{-1} scale, while similar data in nm scale are presented in Supporting Information Figures 1 – 3. In agreement with earlier publications,[17,35,38] the typical TDDFT-PCM errors for complexes **1** – **3** are in a very reasonable range of ~0.1 – 0.2 eV. In agreement with previous calculations, the *Q*-band region in complexes **1** – **3** could be entirely described by the two subphthalocyanine-centered π-π* transitions originating from the HOMO → LUMO, LUMO+1 (complex **1**) or HOMO-3 → LUMO, LUMO+1 (complexes **2** and **3**). Similarly, the *B*-band region in SubPcs **1** – **3** is described by several subphthalocyanine-centered π-π* transitions dominated by Gouterman type transitions from the HOMO-3 → LUMO, LUMO+1 (complex **1**) or HOMO-9 → LUMO, LUMO+1 (complexes **2** and **3**). In addition to *Q*- and *B*-band regions, the MLCT region was predicted by the TDDFT-PCM calculations in the NIR area for ferrocene-containing dyads **2** and **3** (Figures 19 and 20).

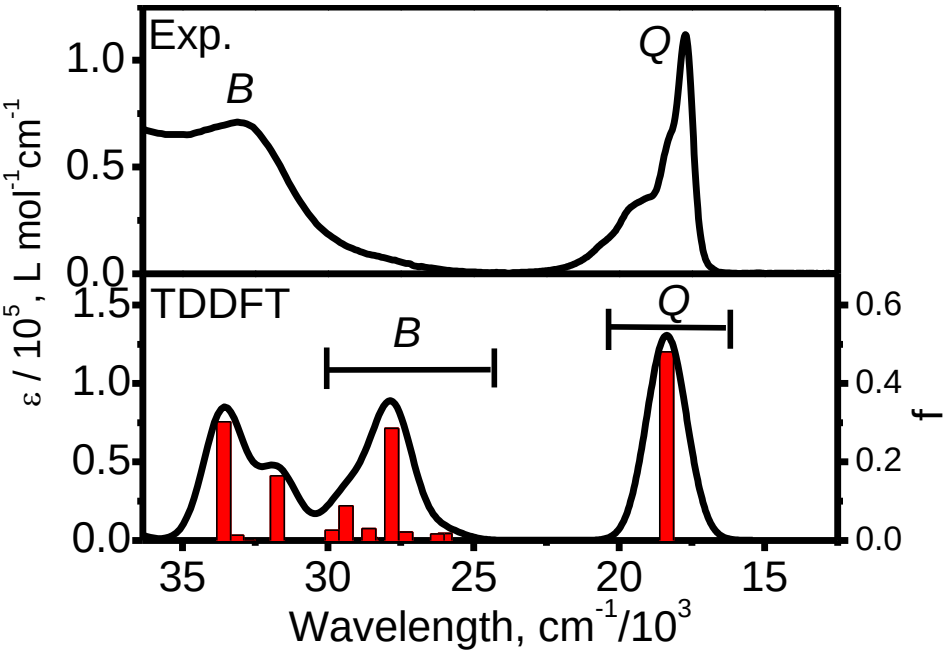

Figure 18. Experimental (top) and TDDFT predicted (bottom) UV-vis spectra of compound **1**. *Q*- and *B*-band regions are labeled as *Q* and *B*.

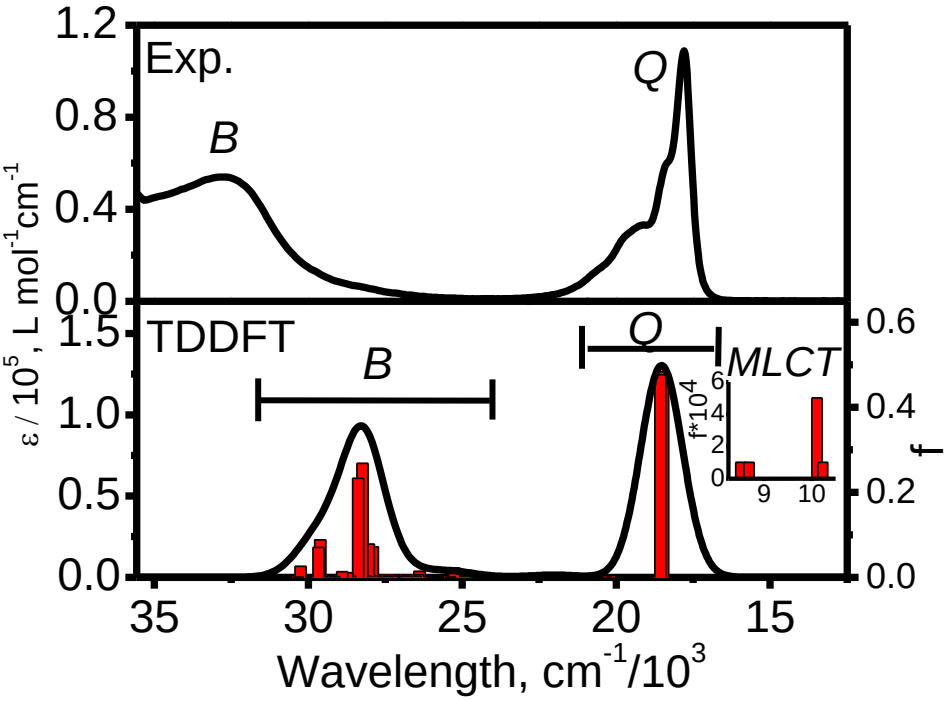

Figure 19. Experimental (top) and TDDFT predicted (bottom) UV-vis spectra of complex **2**. *Q*-, *B*-, and *MLCT* band regions are labeled as *Q*, *B*, and *MLCT*.

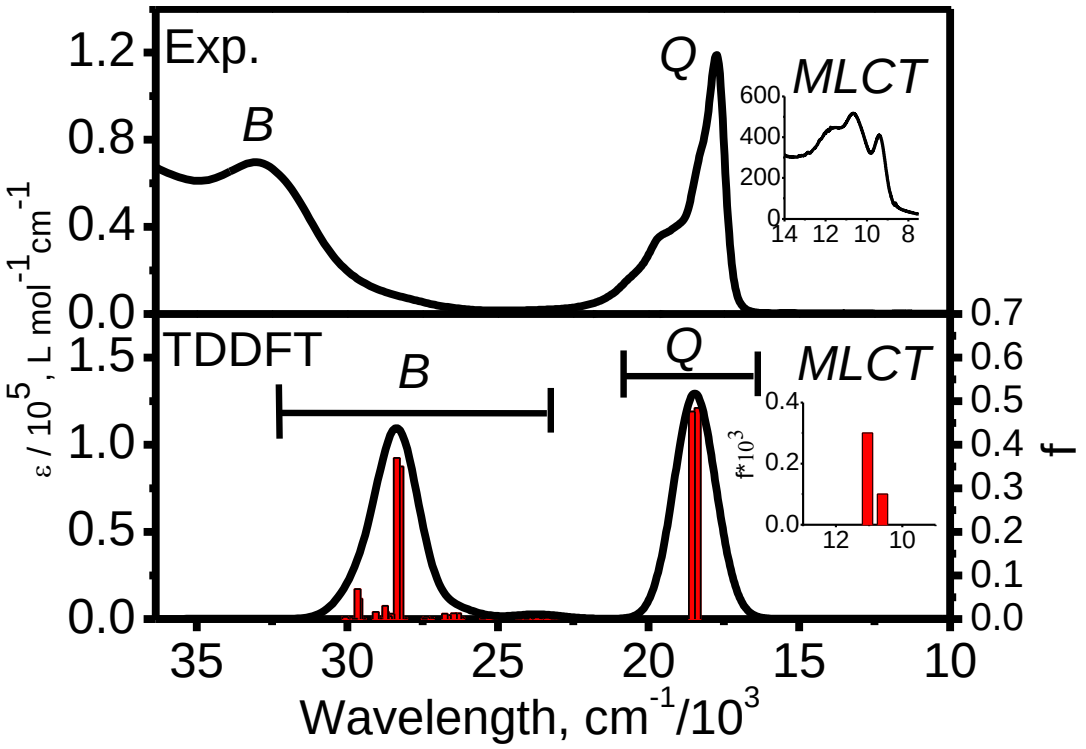

Figure 20. Experimental (top) and TDDFT predicted (bottom) UV-vis spectra of complex **3**. *Q*-, *B*-, and *MLCT* band regions are labeled as *Q*, *B*, and *MLCT*.

The MLCT region originates from the six ferrocene-centered HOMO to HOMO-2 → LUMO, LUMO+1 transitions, which is predicted to have several orders of magnitude lower intensities than the subphthalocyanine-centered π-π* transitions. Both TDDFT-PCM predicted intensities for MLCT transitions and their relative energies (i.e. lower energies for complex **2** as compared to complex **3**) are in a good agreement with the experimental data. In general, TDDFT-PCM data correlate very well with the experimental data although in all cases, the calculated excitation energies for the *Q*-band and MLCT band regions are slightly overestimated, while those for the *B*-band region are slightly underestimated.

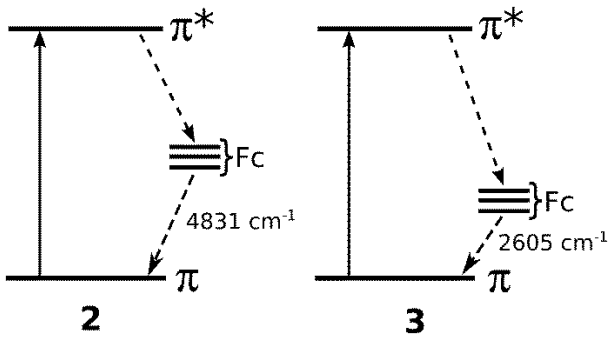

Figure 21. Proposed non-radiative deactivation mechanism of the S_1 state in dyads **2** and **3**.

The DFT-PCM and TDDFT-PCM calculations presented above allow for the explanation of differences observed in the fluorescence lifetime measurements for dyads **2** and **3** as well as the relatively higher steady state fluorescence of dyad **2** compared to dyad **3**. Indeed, although both dyads have much shorter fluorescence lifetime than the parent SubPc **1**, the average lifetime for the S_1 excited state of more rigid dyad **3** is more than 100 times shorter than that in the more structurally flexible dyad **2** (Table 3). A rational explanation of this phenomenon could be achieved by detailed analysis of the electronic structures of dyads **2** and **3**. Thus, population of the S_1 ($S_0 \rightarrow S_1$) state for **2** and **3** rises from HOMO-3 → LUMO, LUMO+1 ($\pi \rightarrow \pi^*$) transitions and SubPc centered HOMO-3 molecular orbital is located below the three ferrocenyl centered MO's (Figure 15). Once the S_1 state has been formed, nonradiative electron transfer from the ferrocene substituent to the half-filled HOMO-3 forms the CS state ($SubPc^{\cdot-}$-$Fc^{\cdot+}$), observed and characterized earlier for several ferrocene-containing SubPcs (Figure 19). Formation of CS states will be especially efficient in the case where there are small difference between the energies of ferrocene and SubPc (π) orbitals. In the case of dyad **3** ferrocene-centered HOMO-2 and SubPc π HOMO-3 are separated only by 2605 cm^{-1}, while the HOMO-2 and HOMO-3 energy difference in dyad **2** is 4831 cm^{-1}. Taking into account the energies of the

vibronic levels (the highest vibronic mode in **3** is 3296.7 cm^{-1}), we can speculate that the S_1 state couples with the CS states through a vibronic coupling mechanism,[39] which is more efficient for dyad **3** than dyad **2**. Accordingly, the average lifetime of the S_1 state in dyad **3** should be shorter compared to that in dyad **2**, which is in agreement with experimental data. Longer average lifetime of the S_1 state in dyad **2** in turn, should lead to a relatively higher fluorescence compared to that in dyad **3**, which is again in agreement with the experimental data.

Conclusions:

Two new ferrocenyl-subphthalocyanine dyads with ferrocenyl methoxide (**2**) and ferrocenyl carboxylate (**3**) substituents directly attached to the subphthalocyanine ligand via the axial position have been prepared and characterized using NMR, UV-vis, and MCD spectroscopies as well as X-ray crystallography. X-ray crystallography of **2** and **3** confirmed the trigonal pyramidal geometry of the boron centers and an axial coordination of the ferrocene substituents to the parent macrocycle. Redox properties of ferrocenyl-containing dyads **2** and **3** were investigated using the CV approach and compared to those in parent subphthalocyanine **1**. It was found that the first reversible oxidation is ferrocene-centered, while the second oxidation and the first reduction are localized on the subphthalocyanine ligand. The electronic structures and the nature of the optical bands observed in UV-vis and MCD spectra of all target compounds were investigated by DFT-PCM and TDDFT-PCM approaches. It has been found that in both dyads **2** and **3** HOMO to HOMO-2 are ferrocene-centered MOs, while HOMO-3 as well as LUMO and LUMO+1 have π or π^* nature and are localized on the subphthalocyanine macrocycle.

The vertical excitation energies calculated using the TDDFT-PCM approach in complexes **1** - **3** are consistent with the experimental data and clearly suggest the dominance of π–π* transitions in the UV-vis spectra of **1** - **2**. In addition, several weak MLCT bands were predicted by the TDDFT-PCM calculations in the NIR region of the UV-vis spectra of dyads **2** and **3**. Fluorescence properties of the dyads **2** and **3** were investigated using steady-state and time-resolved fluorescence methods. It has been found that the fluorescence quenching is more efficient in dyad **3** than dyad **2**, which was rationalized on the basis of DFT-PCM calculations. In general, observed fluorescence quenching trends allow rational design of the new simple donor-acceptor dyads potentially useful in light-harvesting elements.

Part 2: Tert-butyl Subphthalocyanines

Introduction:

Unlike the reasons for synthesizing compounds **1-3**, these tert-butyl subphthalocyanines were used to increase the solubility of these compounds. These compounds were characterized using similar methods as those with of compounds **1-3** in order to compare the effects of substitution on subphthalocyanine. There are four different isomers for each of the compounds **4** and **5** in solution at a given time, which makes obtaining crystals for X-ray analysis nearly impossible.

Synthesis:

Similar to the previous compounds listed (compounds **2** and **3**), ferrocenyl substituted tert-butyl subphthalocyanine (**5**) was prepared from its parent compound, chloro substitutedtert-butyl subphthalocyanine (**4**). This was done in order to determine the effects of increased solubility, compared to the relatively low solubility of compound **1**, and to determine whether there is in fact electronic communication with this type of subphthalocyanine core. This was done by taking milligram quantities of compound **4** and reacting it with a three-fold excess of FcCOOH. Previously reported synthesis of axial substitution on subphthalocyanines indicated the use of boiling toluene for many hours to get the desired product, so that was the procedure used as shown in Scheme 2. Because this was only done to determine if electron communication between ferrocene and the subphthalocyanine core was possible for these complexes, only ferrocene carboxylate substituted tert-butyl subphthalocynine (**5**) was synthesized.

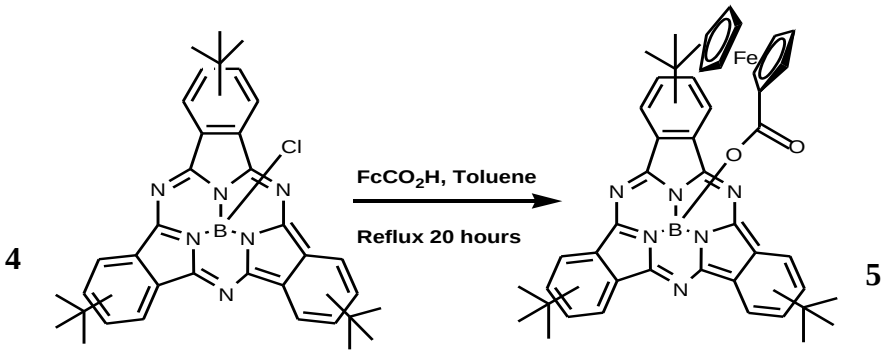

Scheme 2. Reaction Scheme for synthesis of compound **5.**

NMR Spectra:

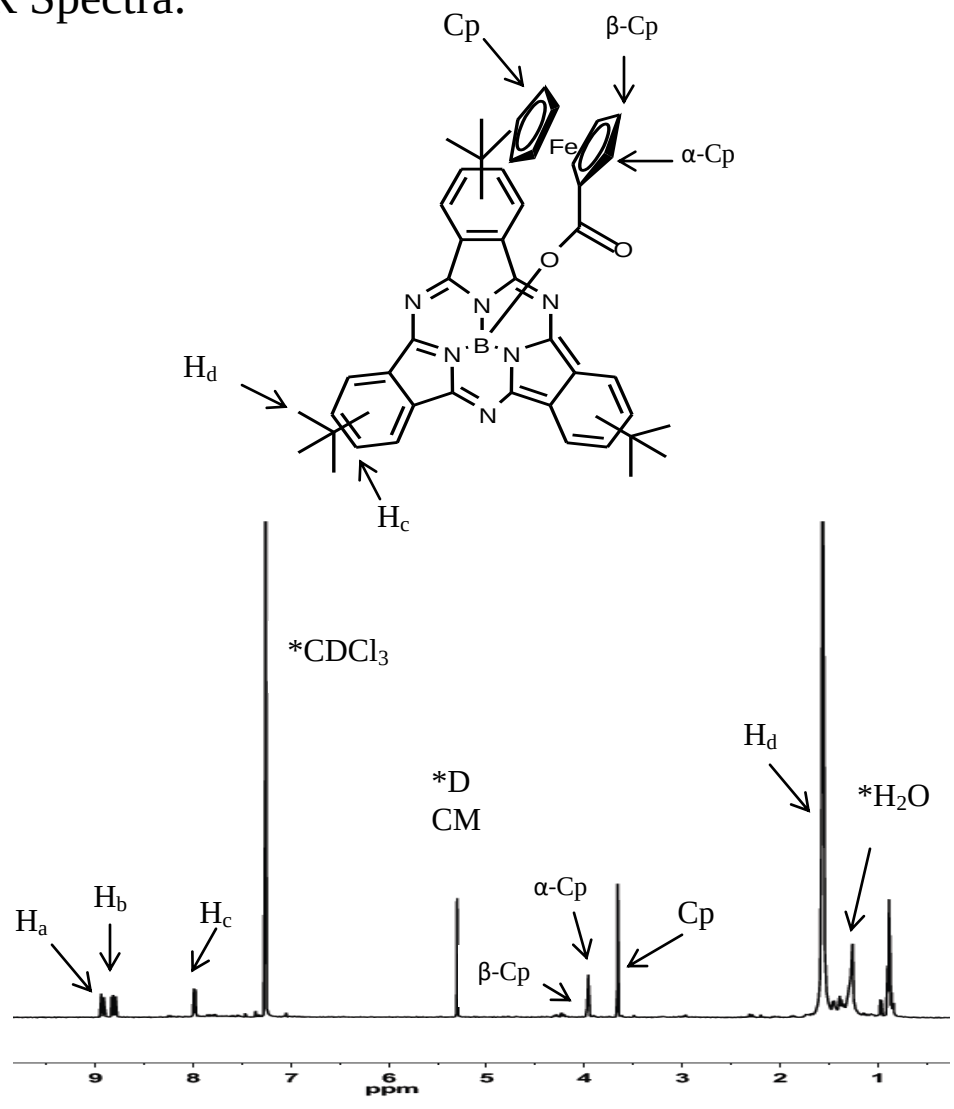

Figure 22. ^{1}H-NMR spectrum of tBuSubPcFcCO$_2$ (**5**) in CDCl$_3$

The ^{1}H-NMR spectrum for compound **5** is shown above in Figure 22. Similar to the other synthesized compounds, there are nine protons belonging to the axial ferrocenyl group. Two of which are α-Cp protons, two β-Cp protons and five Cp protons where the signal for the α and β-Cp protons are almost overlapped making the two signals hard to distinguish. The β-Cp signal lies at the shoulder of the α-Cp signal. For compound **5** however, there are three distinct phenyl protons. Again, there are two α protons in the aromatic region (H_a and H_b), but are different from one another depending on where the functional group lies and a β proton (H_c) opposite of the tert-butyl group. Further upfield there is a very intense peak belonging to all the tert butyl protons for compound **5**. The other peaks belong to common solvents: water, methanol and DCM.

UV-Vis NIR and MCD Spectra:

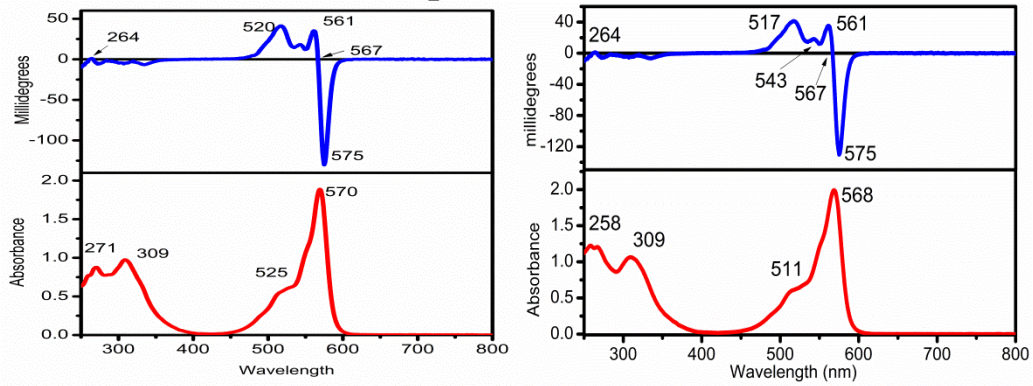

Figure 23. UV-Vis and MCD spectra for compounds **4** and **5**.

UV-Vis and MCD spectra of tBuSubPcs **4** and **5** are presented in Figure 23. In agreement with previous publications[9,26-28,31] and synthesized compound **3,** axial substitution of the chlorine atom by the carboxylate ligand in compound **5** has a very minor influence on the UV-Vis and MCD spectrum, which are dominated by the very intense intra-ligand π-π* transitions. Similarly, the MCD spectrum **5** is almost undistinguished from the MCD

spectrum of parent compound **4.** The Faraday A-term centered at 567 nm in complex **5** that corresponds to the most intense Q-band band in the UV-vis spectrum of this compound and confirms its three-fold effective symmetry dominates it.

Comparative Fluorescence:

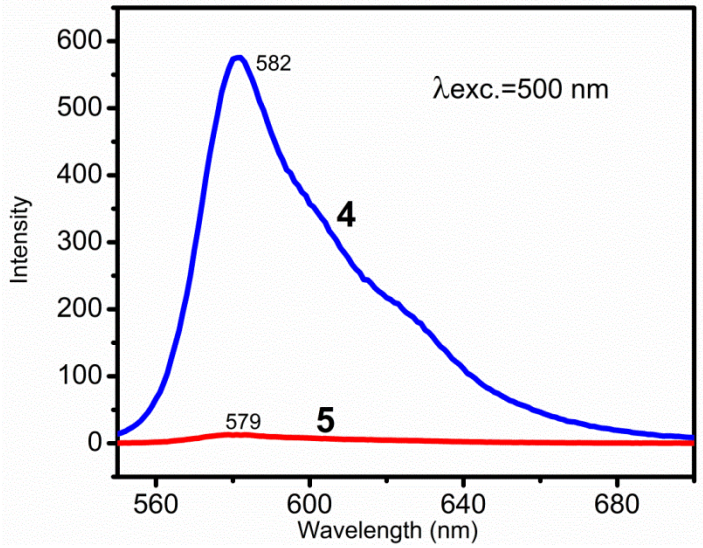

Figure 24. Comparative Fluorescence of intensities for compounds **4** and **5**.

As shown in the figure above (Figure 24) compound **4**, similar to compound **1**, is a known fluorescent chromophore. With the introduction of ferrocene carboxylate into the subphthalocyanine core, the intensity of fluorescence is greatly decreased. Indeed, upon excitation of the *Q*-band of parent compound **4**, an intense fluorescence peak centered at 582 nm, which is assigned to the $S_1 \rightarrow S_0$ transition. Intensities for both compounds were measured under similar conditions and it is clear that the intensity of compound **5** is several orders or magnitude lower than that of compound **4** while still maintaining similar profiles. This is indicative of electron transfer from ferrocene to the subphthalocyanine core.

Electrochemistry:

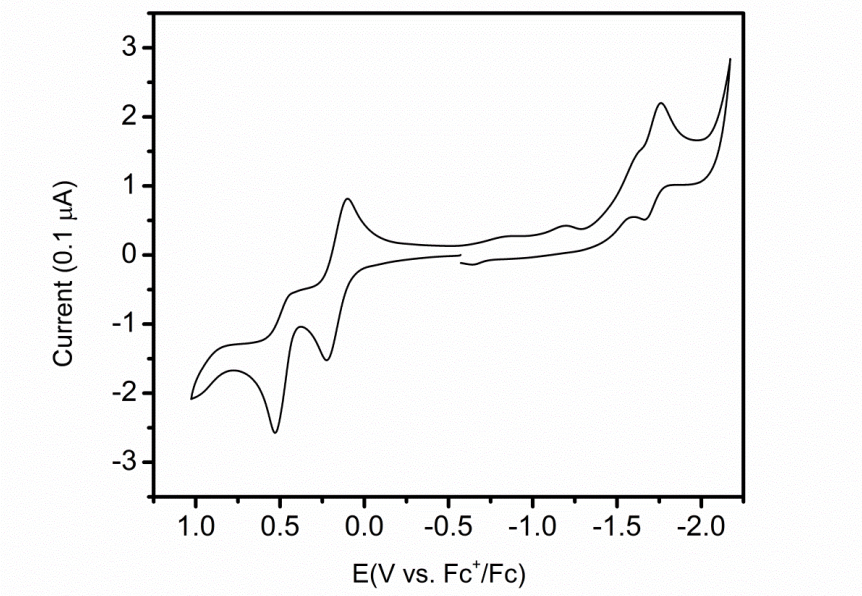

Figure 25. Room-temperature CV data for compound **5** in DCM/TBAP system.

The redox properties of the ferrocene substituted tert-butyl subphthalocyanine were also investigated using the CV (cyclic voltammetry) approach. Similar to the CV data of compounds **2** and **3**, the first reversible process for compound **5** is ferrocene centered at +0.146 V. Also, similar to compounds **2** and **3**, there is an irreversible second oxidation process at +0.45 V belonging to that of the macrocycle ligand itself, which is indicative of the degradation of the compound. There is a reduction process that occurs at -1.71V also belonging to the macrocycle ligand. Due to the fact that this compound is much more soluble in common solvents, this experiment was run in a DCM/TBAP system.

Table 6. Table of oxidation potentials for compound **5**.

Compound	$E_{1/2}(ox)_1$ (V)	$E_{1/2}(ox)_2$ (V)	$E_{1/2}(red)_1$ (V)
5	0.146	0.450[a]	-1.71

[a] Irreversible process; all potentials (±5 mV) are given in volts relative to Fc/Fc^+.

Spectroelectrochemistry:

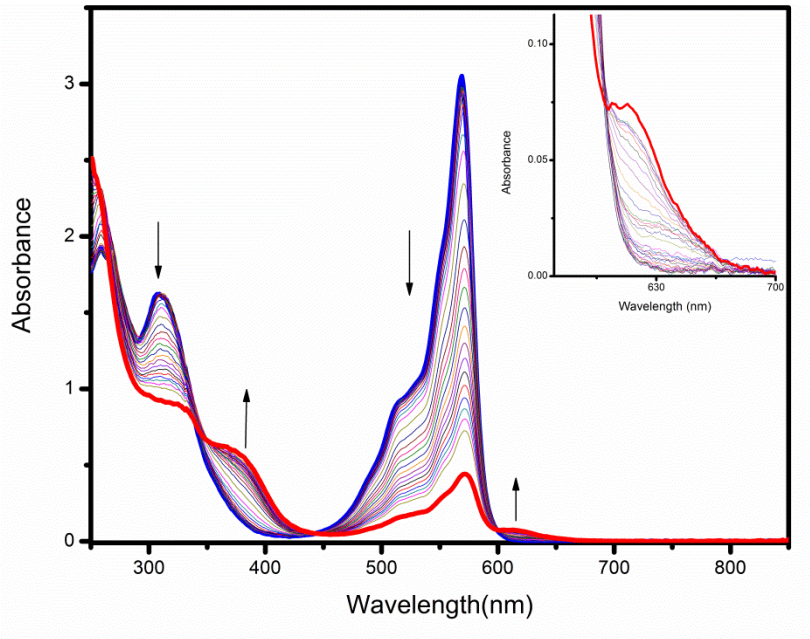

Figure 26. Spectroelectrochemistry data for compound **5**

In compounds **2** and **3**, spectroelectrochemistry created the degradation of the compound in the electrochemical cell. In the case of compound **5**, the oxidation of the π cation radical of the subphthalocyanine core is located on the shoulder of the Q-band around 600 nm. The compound was unable to be reduced back down, leading to the eventual degradation of the compound. Unfortunately, there was no evidence of oxidation of Fe(II) within ferrocene because there is no evidence of increased absorbance within the IVCT section (inter valence charge transfer) of the spectrum.

Conclusion:

Another new ferrocene substituted subphthalocyanine has been prepared and characterized using UV-Vis, MCD, NMR, Fluorescence and electrochemical methods. UV-Vis and MCD were shown to be very similar to that of compounds **1-3** with only a small shift from 564 nm to 570 nm in the Q-band. The MCD signal contained a

characteristic A term which is indicative of its three fold symmetry and double degeneracy in its excited state. NMR shows typical placement of subphthalocyanine and ferrocene protons. Comparative Fluorescence indicated that when compounds **4** and **5** were measured under similar conditions, the intensity of compound **5** is several orders of magnitude lower than that of compound **4** indicating the electron transfer between ferrocene and subphthalocyanine. Electrochemical CV methods indicate a first reversible oxidation process centered on ferrocene making other two irreversible processes belong to the subphthalocyanine core itself. Spectroelectrochemistry indicates the possible oxidation of the π cation radical of compound **5**. Unlike compounds **2-3**, compounds **4** and **5** have much better solubility in common solvents such as DCM, Toluene, and THF.

Part III. Thio-substituted Subphthalocyanines

Introduction:

As previously stated, effective light-to-energy conversion requires an efficient formation of a long-lived charge-separated (CS) states, which have high-energy content. Subphthalocyanines (SubPcs) as a whole make excellent antenna complexes due to their optical properties. In order to induce electron transfer, the axial bound chlorine needs to be replaced by an electron-donating group such as ferrocene. If ferrocene substituted SubPc's can coordinate to an electron acceptor such as C_{60} then electron transfer can occur upon the excitation of an electron from a photon of light, creating a charge separated state. Previously synthesized ferrocene substituted SubPc compounds **2** and **3** were unable to coordinate to C_{60} due to the poor electron densisty of the subphthalocyanine core. In order to increase electron density, electron rich subphthalocyanines need to be synthesized. By increasing the electron density around the subphthalocyanine core, the ability to coordinate to C_{60} also increases, thus creating a potential light-harvesting unit.

Synthesis:

As stated above, more electron rich SubPc's needed to be synthesized. One way of achieving this is with the addition of thiol substituents to the subphthalocyanine core. Using a previously reported procedure, compound **8** was synthesized by taking multigram quantities of 2,3-dicyanohydroquinone along with para-toluenesulfonyl chloride and potassium carbonate and refluxing it in acetone for a couple hours and later stirring in

water for an additional hour (Scheme 3).[40] The yield for this reaction was very high. (89%)

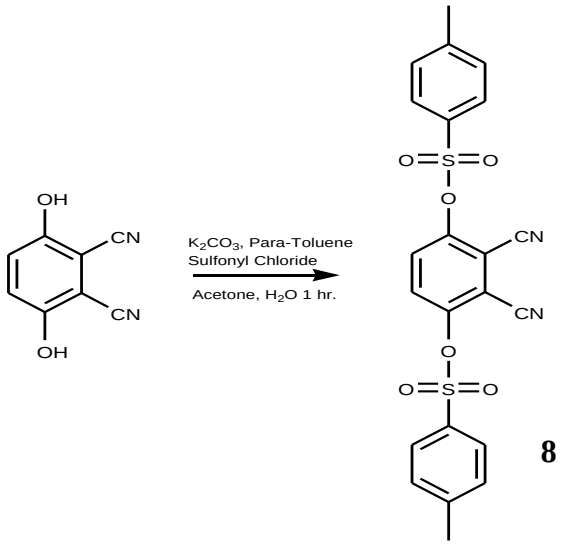

Scheme 3. Reaction Scheme for synthesis of compound **8.**

The next step in the reaction was to prepare a thio-substituted nitrile in preparation for making the subphthalocyanine. Thiophenol was used because if its large phenyl groups, with the intention that it would better coordinate to C_{60}. The nitrile was synthesized by taking compound **8** and thiophenol and stirring it in DMSO for 24 hours. Multigram quantities of potassium carbonate were added portion wise over a six hour period and compound **9** later extracted using DCM and water (Scheme 4). The yield for this reaction was relatively low (32%).

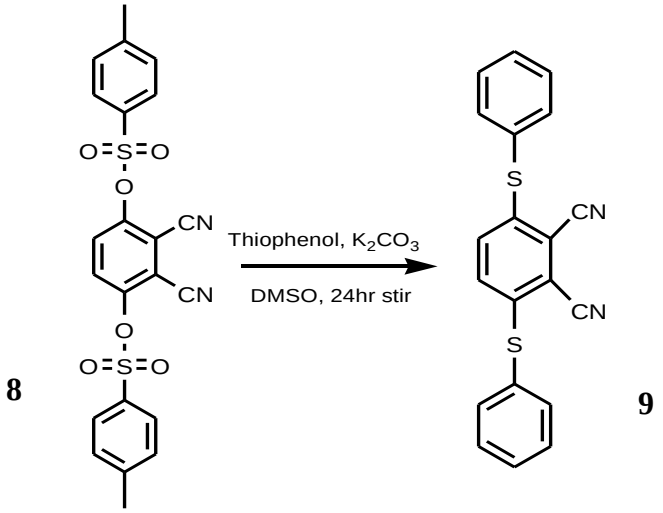

Scheme 4. Reaction Scheme for synthesis of compound **9.**

Finally in preparing compound **10**, compound **9** was dissolved in a 1M solution of BCl_3 in *p*-xylene and refluxed for 40 min. Compound **10** was then washed with toluene, dried and finally washed with methanol (Scheme 5).

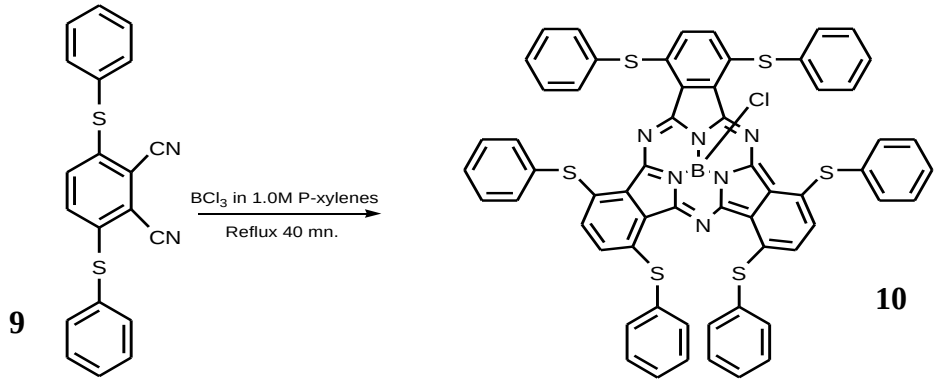

Scheme 5. Reaction Scheme for synthesis of compound **10**.

NMR Spectra:

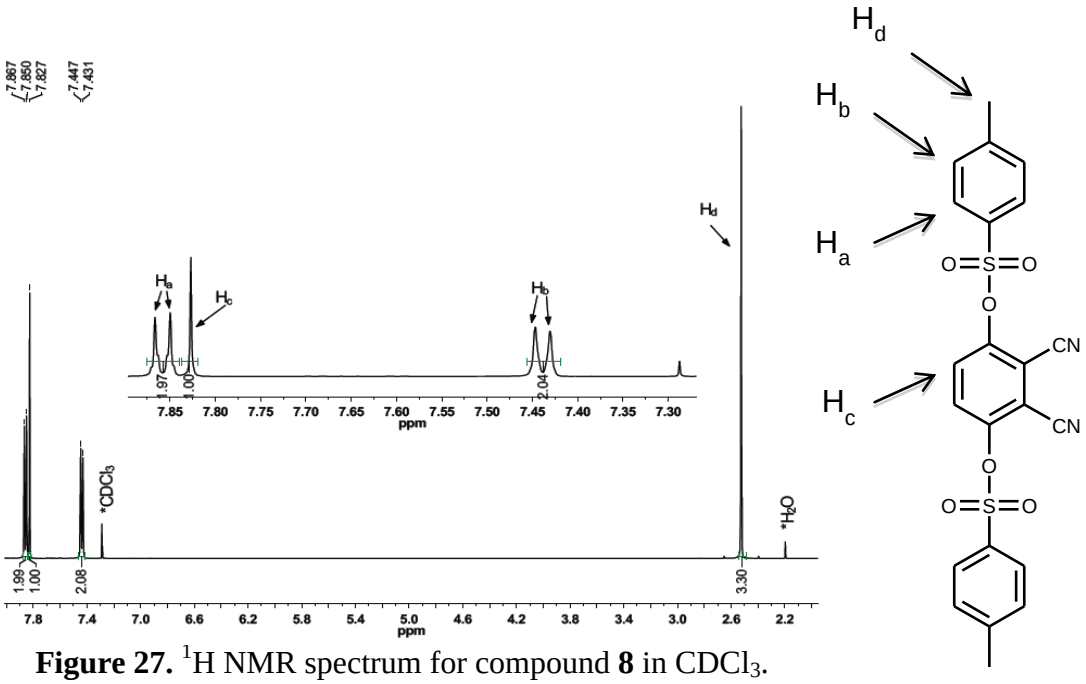

Figure 27. ^{1}H NMR spectrum for compound **8** in $CDCl_3$.

The ^{1}H NMR spectrum shown above is for the first compound, compound **8**, synthesized in the reaction scheme for synthesizing compound **10**. No further characterization of compound **8** was required because it is a well known compound and is only an intermediate to the final compound **10**. There are three distinct peaks in the aromatic region belonging to the compound **8**. The only other peak is that belonging to the methyl group. The NMR is very clean and thus allowed the next step in the reaction to take place.

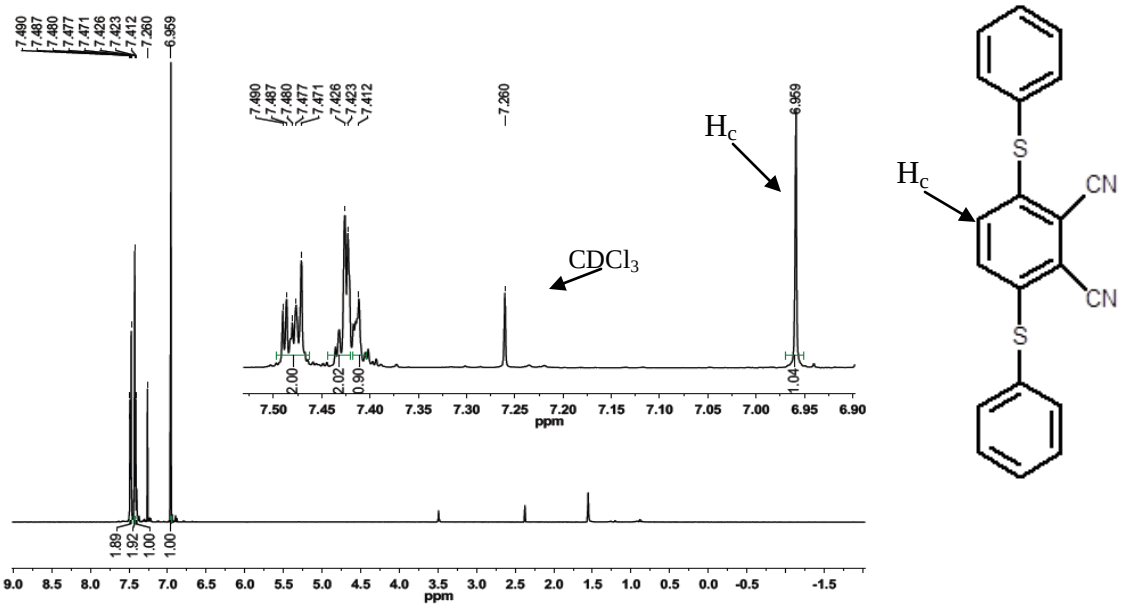

Figure 28. ^{1}H NMR spectrum for compound **9** in $CDCl_3$.

Due to the complex formation of this compound, compound **9**, the aromatic protons are very hard to distinguish. From the integration, there is the correct number of hydrogens in the aromatic region of the NMR for the proposed compound. Again this spectrum is really clean and allowed for the continuation of the reaction.

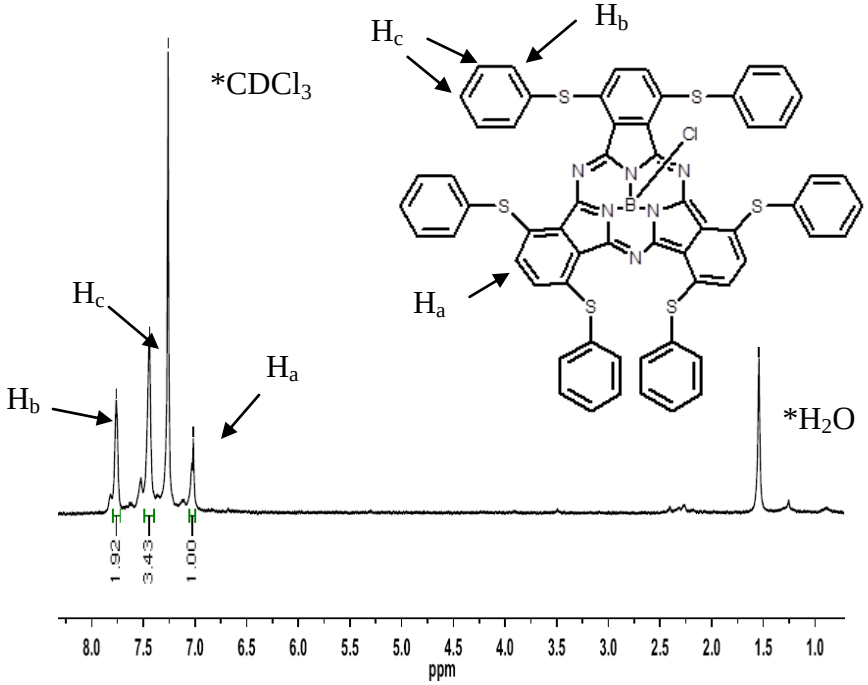

Figure 29. ^{1}H NMR spectrum for compound **10** in $CDCl_3$

The ^{1}H NMR of the final parent compound **10** is shown above (Figure 29). There are three distinct peaks for this compound belonging to aromatic protons. It is assumed that there should be four distinct peaks, but because of the close proximity of the three protons on the thio phenyls, they appear as one signal with an integration of three. The other two peaks have correct integration, one proton belonging to the β-Ph of the subphthalocyanine core. It is noticeable that the β-Ph proton peak from compound **9** is at 6.95 ppm whereas the same proton peak is shifted downfield to 7.10 ppm in compound **10**.

UV-Vis & MCD Spectra:

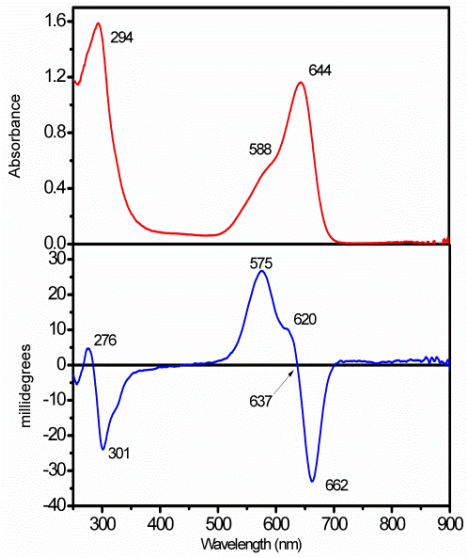

Figure 30. UV-Vis and MCD spectrum for compounds **10**.

The UV-Vis and MCD spectra for compound **10** are shown above (Figure 30). In the UV-Vis spectrum the shape of the Q-band is characteristic of that of other subphthalocyanines, such as compounds **1**-**5** listed previously, and is indicative of the Q-band representing the π to π* transitions of the HOMO to LUMO orbitals. Alternatively,

unlike compounds **1-5** whose Q-bands were somewhere between 560-580 nm, compound **10** has a Q-band peak at 644 nm. This is in agreement with the fact that thiol-substituted SubPc's have more electron density around the subphthalocyanine core, thus shifting the Q-band to lower energy within the visible region. As for the MCD spectrum, SubPc's that have been explored in this discussion have all exhibited a characteristic Farday A term. In the spectrum of compound **10**, there are two B terms.

Fluorescence:

Compound **10** was further characterized by fluorescence. It is expected that this compound, like the other two parent compounds **1** and **4**, is also a fluorescent chromophore. As you can see from the figure below (Figure 31), that is in fact the case. Also similar to the other parent compounds, the fluorescent spectrum is a mirror image of the intense Q-band of the UV-Vis spectrum which is centered at 662 nm.

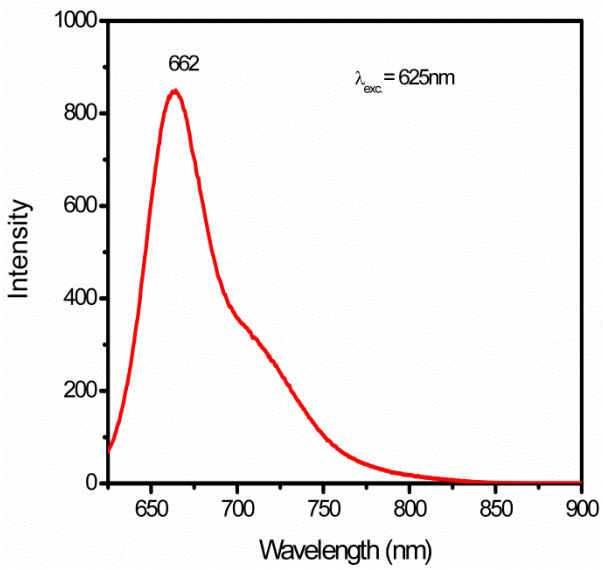

Figure 31. Fluorescence spectrum for compound **10**.

Electrochemistry:

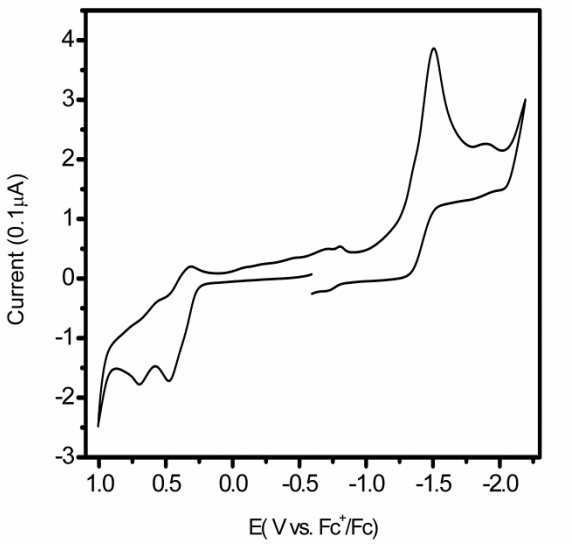

Figure 32. Room-temperature CV data for compound **10** in DCM/TBAP system.

Similar to all compounds reported above (compounds **1-5**) compound **10** was further characterized using CV (cyclic voltammetry) electrochemical methods (Figure 32). In agreement with compounds **1-5**, there is an irreversible oxidation and reduction peak belonging to that of the subphthalocyanine core at 0.6987V and -1.893V respectively (Table 7). The first oxidation process at 0.3943 V however is a reversible process that has not been seen in compounds **1** & **4**. It is possible that it belongs to another process of the compound that is only introduced with the thiol substituents. This can be responsible for the first irreversible reduction process at -1.5063 V as well. Because there are several sulfur groups in this compound, the process is very intense.

Table 7. Table of oxidation potentials for compound **10**.

Compound	$E_{1/2}(ox)_1$ (V)	$E_{1/2}(ox)_2$ (V)	$E_{1/2}(red)_1$ (V)	$E_{1/2}(red)_2$ (V)
10	0.3943	0.6987[a]	-1.5063[a]	-1.893[a]

[a] Irreversible process; all potentials (±5 mV) are given in volts relative to Fc/Fc^+.

Conclusion:

In this chapter, a thiol substituted subphthalocyanine was prepared and characterized with the idea to potentially utilize it as a light-harvesting unit. Characterization techniques used were UV-Vis, MCD, NMR, Fluorescence and electrochemical methods. It was found that there was an 80 nm blue shift to lower energy of the Q-band in the UV-Vis spectrum. In the MCD there were two uncharacteristic B terms, unlike the A terms seen previously. NMR showed a shift downfield for the β-SubPc proton in compound **10** from that of compound **9**. Also, due to the dominance of the thiophenol protons in the aromatic region the β-SubPc proton is shifted upfield from 8-8.5 ppm to 7.0 ppm. Fluorescence maintains the common image among other SubPcs investigated in this paper, that the spectrum is a mirror image of the Q-band. Also similar to the UV spectrum, there is about an 80 nm blue shift to lower energy. Like compounds **1** and **4**, compound **10** is also a fluorescent chromophore. Electrochemical CV methods show the irreversible oxidation and reduction processes centered on the subphthalocyanine compound. Two new processes appear in this parent compound that has not been seen in the other two parent compounds, compounds **1** and **4**. These are likely due to the introduction of the thiol substituents in the compound.

Experimental Section:

Reagents and materials. All reactions were performed under an argon atmosphere using standard Schlenk techniques. All solvents were purified by standard methods: THF was distilled over sodium-potassium alloy, toluene was distilled over sodium metal, DCM and hexane were distilled over calcium hydride, *o*-DCB was distilled over P_2O_5 under reduced pressure, and methanol was distilled over magnesium under an argon atmosphere. $NaBH_4$, NH_4Cl, *tert*-butyl lithium solution in hexanes, SubPcCl (**1**), ferrocene and ferrocenecarboxaldehyde were purchased from Aldrich and used without further purification. Silica gel (60 Å, 60-100 μm) was purchased from Dynamic Adsorbents Inc.

Preparation of $FcCH_2OH$ **(6)**. This compound was prepared using a slightly modified earlier reported procedure.[11] $NaBH_4$ (30.0 mg; 0.79 mmol) was added to a solution of ferrocenecarboxaldehyde (500.0 mg; 2.34 mmol) in 20 ml of THF and 0.4 ml of methanol and the reaction mixture was stirred at room temperature for 24 h. At this time, solid $NaBH_4$ was completely dissolved and the reaction mixture changed color from orange to yellow-brown. After the reaction was completed, a solution of NH_4Cl (333 mg; 6.22 mmol) in 20 ml of water was added drop-wise to the reaction mixture (*Caution: gas evolution*). Next, 75 ml of ethyl acetate and 50 ml of water were added to the reaction mixture. The organic layer was separated from water and the water layer was extracted with 15 ml of ethyl acetate. The combined organic layers were washed with water (3x20 ml) and dried over sodium sulfate. Ethyl acetate was removed under reduced pressure and the resulting oil was recrystallized from hexane. The needle-crystalline solid was filtered off, washed with cold hexane, and dried on air. Yield: 391 mg (77 %). NMR data are in

agreement with those previously reported: ^{1}H NMR (δ, ppm, $CDCl_3$) 4.33 (2H, s, CH_2), 4.27 (2H, t, α-Cp), 4.19 (5H, s, Cp), 4.18 (2H, t, β-Cp), 1.51 (H, s, OH),

Preparation of $FcCO_2H$ **(7)**. This compound was prepared using a slightly modified earlier reported procedure.[12] Solution of *tert*-butyllithium (13.4 ml; 22.7 mmol) in hexane was added during 15 min to a stirred solution of ferrocene (5.0 g; 26.9 mmol) in 23 ml of THF at 0°C. After additional stirring for 15 min at 0°C, the solution was warmed up to room temperature and poured out on to 1L beaker with crashed dry ice. Next, 300 ml of water was slowly added to the resulting mixture and solution was filtered in order to remove unreacted ferrocene. A solution of hydrochloric acid (0.1 M) was added to a stirred filtrate to achieve pH = 7. The resulting precipitate was filtered, washed with cold water and dried first in air and then under reduced pressure. The yield of yellow-brown powder was 3.41 g (56.3 %). The compound purity was confirmed by ^{1}H-NMR and compared to a purchased sample. ^{1}H NMR (δ, ppm, $CDCl_3$): 7.36 (1H, s, OH), 4.85 (2H, m, α-Cp), 4.46 (2H, m, β-Cp), 4.26 (5H, s, Cp).

Preparation of $SubPcOCH_2Fc$ **(2).** Mixture of SubPcCl (**1**) (50 mg; 0.116 mmol) and silver triflate (37 mg; 0.148 mmol) was dissolved in 3 ml of dry toluene and stirred for 2.5 h at room temperature. After this period of time, a solution of $FcCH_2OH$ **6** (50 mg; 0.233 mmol) and $(i\text{-Pr})_2NEt$ (20.5 µL; 0.145 mmol) in 3 ml of toluene was added as a single portion and the reaction mixture was stirred for an additional 8 h. Solvent was removed under vacuum and the solid was redissolved in 5 ml of DCM and loaded on a short chromatographic column (SiO_2, toluene : THF (5:2 v/v)). The first pink fraction was collected, its solvent was evaporated under reduced pressure and the resulting solid was recrystallized from a water/THF mixture. Yield: 12 mg (17 %). Elemental analysis

calculated for $C_{35}H_{23}BN_6OFe$: C(68.89), H(3.80), N(13.77); found C(68.01), H(3.83), N(13.47). ^{1}H NMR (δ, ppm, $CDCl_3$): 8.85 (6H, dd, α-SubPc), 7.90 (6H, dd, β- SubPc), 3.75 (5H, s, Cp), 3.71 (2H, m, β-Cp), 3.40 (2H, m, α-Cp), 2.34 (2H, s, CH_2); ^{13}C NMR (δ, ppm, TMS, $CDCl_3$): 151.7 (α-pyrrole), 131.1 (β-pyrrole), 129.8 (α- SubPc), 122.2 (β-SubPc), 85.3 (C_{ipso}) 68.2 (Cp), 68.1 (α-Cp), 67.8 (β-Cp), 58.0 (CH_2).

Preparation of SubPcO$_2$CFc **(3).** A mixture of ferrocenecarboxylic acid (321 mg; 1.395 mmol) and subphthalocyanine chloride (**1**) (200 mg; 0.465 mmol) in 3 ml of *o*-dichlorobenzene was refluxed for 3 h, cooled down, filtered, and the remaining residue was washed with DCM. Combined organic layers were evaporated under reduced pressure, and the resulting solid was redissolved in toluene and filtered. The toluene was evaporated under reduced pressure and the remaining solid was redissolved in dichloromethane and separated on a short chromatography column (SiO_2, DCM/THF (1:15 v/v)). The first red fraction was collected and solvent was evaporated under reduced pressure. 280 mg of the crude product was recrystallized first from THF/water and then from DCM/hexane systems. Yield: 185 mg (64 %). Elemental analysis calculated for $C_{35}H_{21}BN_6O_2Fe$: C(67.34), H(3.39), N(13.46); found C(66.77), H(3.53), N(12.67). ^{1}H NMR (δ, ppm, $CDCl_3$): 8.90 (6H, m, α- SubPc), 7.92 (6H, m, β- SubPc), 3.98 (2H, m, β-Cp), 3.97 (2H, m, α-Cp), 3.65 (5H, m, Cp); ^{13}C NMR (δ, ppm, TMS, $CDCl_3$): 170.47 (CO_2), 151.7 (α-pyrrole), 131.3 (β-pyrrole), 130.1 (α- SubPc), 122.6 (β- SubPc), 105.0 (C_{ipso}) , 71.1 (α-Cp), 70.1 (β-Cp), 69.7 (Cp).

Preparation of tert-butylSubPcO$_2$CFc **(5).** The compound was prepared by taking tert-butylSubPcCl **(4)** (150mg) and a threefold excess of $FcCO_2H$ (450 mg) and refluxing it in

toluene (3ml) for 20 hours. The compound was then dried under reduced pressure. The compound was further purified by column chromatography on silica gel in a DCM/THF system (1:20 (v/v)). Solvent was evaporated and compound was dried under reduced pressure. Yield 28 mg. ^{1}H NMR (δ, ppm, $CDCl_3$): 8.93 (3H, d, H_a), 8.81 (3H, m, H_b), 7.98 (3H, d, H_c) 3.96 (2H, m, β-Cp), 3.95 (2H, m, α-Cp), 3.65 (5H,m, Cp), 1.56 (18H, m, CH_3), 1.38 (9H,m, CH_3).

Preparation of 3,6-bis(4-methylphenyl sulfonyloxy) phthalonitrile **(8).** This compound was prepared using a previously reported procedure[40] by taking 2,3-dicyanohydroquinone (2.0 grams, 12.5 mmol) and refluxing with potassium carbonate (7.0 grams, 50 mmol) and para-toluene sulfonyl chloride (5.2 grams, 27mmol) in acetone (15 ml) for 2 hours. The mixture was then added to 40 ml of water and stirred for an additional hour. The product was then filtered off and dried overnight. The next morning the light brown product was dried under reduced pressure in a 50°C water bath. Yield 5.2g (89%). ^{1}H NMR (δ, ppm, $CDCl_3$): 7.860 (4H, d, H_a), 7.827 (2H, d, H_c), 7.435 (4H, d, H_b) 2.522 (6H,m, H_d).

Preparation of 3,6-di(thiophenol)-4,5-dicyanobenzene **(9).** This compound was prepared by a mixture of thiophenol (2.8 g, 25.4 mmol) and 3,6 bis(4-methylphenyl sulfonyloxy) phthalonitrile **(8)** (5 g, 9.2 mmol) in dimethylsulfoxide (30ml) that stirred for 24 hours. Potassium carbonate was added in 2 gram portions every two hours for the first six hours. After 24 hours, 40ml of water was added to the flask. The aqueous phase was extracted using dichloromethane (3 x 50 ml). The extracts were further treated with 5% sodium

bicarbonate solution (2 x 250 ml) and then again with water (2 x 250 ml). The solvent was then distilled off and the compound was re-crystallized from methanol. The compound was then washed with cold hexane and left to dry. Yield 1.2 g (33%). ^{1}H NMR (δ, ppm, $CDCl_3$): 7.48 (4H, m, Thiophenol), 7.42 (6H, m, Thiophenol), 6.96 (2H, s, H_c).

Preparation of SubPc(SPh)$_8$ **(10).** Using a similar procedure as previously reported, this compound was prepared from 3,6-di(thiophenol)-4,5-dicyanobenzene **(9)** (750 mg, 0.69 mmol) and was dissolved in a 0.1M solution of boron trichloride in p-xylene (3 ml). The reaction mixture refluxed for 45 min, was cooled, and flushed with argon gas to get rid of excess boron trichloride. The remaining solvent was evaporated under reduced pressure and the subsequent crude product was washed several times with toluene. The compound was then filtered and the blue solution was evaporated using rotovapor. The compound was then washed with methanol, filtered, and left to dry overnight. Yield 68 mg (2.9 %). Elemental analysis calculated for $C_{60}H_{36}BN_6S_6Cl$: C(65.31), H(3.53), N(7.62); found C(65.75), H(3.39), N(7.37). ^{1}H NMR (δ, ppm, $CDCl_3$): 7.75 (6H, m, H_b), 7.49 (18H, m, H_c), 7.10 (6H, m, H_a).

DFT-PCM and TDDFT-PCM Calculations. The initial geometries of complexes **1** - **3** were taken from the X-ray data and optimized at the DFT level, using a hybrid PBE1PBE exchange-correlation functional.[13] This exchange-correlation functional was shown to provide a good agreement between theoretical and experimental bond distances and angles in ferrocene-containing compounds.[14] Equilibrium geometries were confirmed by frequency calculations and specifically by the absence of the imaginary frequencies.

Solvation effects were modeled using the polarized continuum model (PCM) approach.[15] DCM was used as the solvent in all calculations. All single-point DFT-PCM and TDDFT-PCM calculations were conducted using a pure BP86 functional,[16] which accurately describes vertical excitation energies in a variety of porphyrinoids.[17] The first 35 states were considered in all PCM-TDDFT calculations. In all cases, Wachter's full-electron basis set[18] was used for iron centers and 6-31G(d)[19] for all other atoms. All calculations were performed using Gaussian 09 software.[20] Molecular orbital analysis was conducted using the QMForge program.[21]

X-ray crystallography. Single crystals of complexes **1**, **2**, and **3** suitable for X-ray crystallographic analysis were obtained by the slow evaporation of *o*-DCB, dichloromethane/hexane, and toluene solutions, respectively. X-ray diffraction data were collected on a Rigaku RAPID-II diffractometer using a graphite monochromator using Cu Kα (λ=1.5418 Å) or Mo Kα (λ=0.71073 Å) radiation at -150 ^{0}C. Multi-scan absorption correction[22] was applied to the data in all cases. The crystal structures were solved by the direct method (SIR-92)[23] and refined by full-matrix least-squares method on F^2 using the SHELXL-97 program.[24] PLATON program was used for visualization of the results. Crystal data for complexes **1** – **3** are summarized in Table 1, while selected bond distances and angles are presented in Table 3. CCDC 861030, 861031, and 861032 contain the supplementary crystallographic data for all compounds. These data can be obtained free of charge via www.ccdc.cam.ac.uk/conts/retrieving.html (or from Cambridge Crystallographic Data Centre, 12 Union Road, Cambridge CB2 1EZ, UK; fax: (+44) 1223-336-033 or deposit@ccdc.cam.ac.uk).

Table 1. Summary of crystallographic data for compounds **1** - **3**.

	1	**2**	**3**
Empirical formula	$C_{24}H_{12}N_6BCl$	$C_{35}H_{23}N_6OBFe$	$C_{35}H_{21}N_6O_2BFe$
Formula weight	430.66	610.25	624.24
Crystal system	Orthorhombic	Monoclinic	Monoclinic
Space group, Z	Pnma, 4	C2/c, 8	$P2_1/c$, 4
a (Å)	12.1224(2)	28.610(5)	17.2645(8)
b (Å)	14.8449(10)	11.197(5)	7.7863(2)
c (Å)	10.3283(1)	18.146(5)	20.6276(14)
β (°)	90	114.658(5)	95.019(7)
Volume ($Å^3$)	1858.6(1)	5283(3)	2762.3(2)
$\rho_{calc}(g/cm^3)$	1.539	1.535	1.501
$\mu(mm^{-1})$	2.041[a]	0.615[b]	4.757[a]
$\theta_{max}(°)$	68.24[a]	27.49[b]	68.41[a]
Meas./unique reflns	12595/1756	17320/6032	29594/5040
R_{int}	0.0351	0.0492	0.0647
GoF(F^2)	1.156	1.047	1.092
R_1[c], wR_2[d] (I>2σ(I))	0.0668/0.1872	0.0612/0.1553	0.0657/0.1817
R_1[c], wR_2[d] (all data)	0.0852/0.2127	0.0704/0.1625	0.0815/0.2060
$\Delta\rho_{max}/\Delta\rho_{min}$ ($e/Å^3$)	0.838/-0.485	1.067/-0.902	0.618/-0.971

[a]Cu-K_α, [b]Mo- K_α, [c]$R_1(F)=\sum||F_o| - |F_c||/\sum|F_o|$, [d]$wR_2(F^2)=\{\sum[w(F_o^2 - F_c^2)^2]/\sum w(F_o^2)^2]\}^{1/2}$.

Spectroscopy Measurements. UV-Vis data were obtained on Jasco-720 or Cary 17 spectrophotometers. MCD data were recorded using OLIS DCM 17 CD

spectropolarimeter with a 1.4 T DeSa magnet. The MCD spectra were measured in mdeg = [θ] and converted to Δε (M^{-1} cm^{-1} T^{-1}) using the regular conversion formula: Δε=θ/(32980 • Bdc), where B is the magnetic field, d is the path length, and c is the concentration. Complete spectra were recorded at room temperature in parallel and anti-parallel directions with respect to the magnetic field. Electrochemical measurements were conducted using a CH Instruments electrochemical analyzer utilizing a three-electrode scheme with platinum working, auxiliary and Ag/AgCl reference electrodes in 0.1 M solution of TBAP in DMF with redox potentials corrected using an internal standard (decamethylferrocene, Fc*) in all cases. The redox potentials were then corrected to ferrocene using appropriate oxidation potentials for Fc^*/Fc^{*+} vs. Fc/Fc^+ in the DMF/TBAP system. NMR spectra were recorded on a Varian INOVA instrument with a 500 MHz frequency for protons and 125 MHz for carbon. Chemical shifts are reported in parts per million (ppm) and referenced to TMS as an internal standard. In all cases, final assignments of ^1H and ^{13}C signals were made using COSY and HMQC spectra. Elemental analyses were conducted by Atlantic Microlab. Steady-state fluorescence data were collected using Cary Eclipse fluorimeter at room temperature.

Time-resolved fluorescence data measurements were carried out using time-correlated single-photon counting (TCSPC) technique, which was described in details elsewhere.[25] Briefly, femtosecond laser pulses (475 nm, 4.2 MHz, 120 fs) were generated using a Titanium-Sapphire laser system (950 nm, 760 MHz, Mira 900-F, Coherent), a pulse picker (Mira 9200, Coherent) and a second harmonic generator for one-photon excitation of compounds **1** - **3**. The samples were prepared in a deep-well slide and a coverslip, sealed with nail polish, and positioned in the focal plane of 1.2NA microscope

objective (Olympus) in an inverted IX81 microscope (Olympus). The epifluorescence signal was directed toward a microchannel plate photomultiplier tube, MCP-PMT, (R3809U, Hamamatsu) through a filter (585±40 nm) and a Glan-Thompson polarizer, which was set at the magic angle (54.7^0). A histogram of fluorescence photon arrival times (i.e., a fluorescence decay) was recorded using a SPC 830 module (Becker and Hickl, Berlin, Germany) and analyzed using SPCImage software.

References

(1) (a) Sun, Y.; Welch, G. C.; Leong, W. L.; Takacs, C. J.; Bazan, G. C.; Heeger, A.J. *Nature Materials* **2012**, 11, 44–48. (b) Whittell, G. R.; Hager, M. D.; Schubert, U. S.; Manners, I. *Nature Materials* **2011**, 10, 176–188. (c) *Electron Transfer in Chemistry*; Balzani, V., Ed.; Wiley-VCH: Weinheim, Germany, 2001; Vol. I-V. (d) Melkozernov, A. N.; Barber, J.; Blankenship, R. E. *Biochemistry* **2006**, 331–345. (e) Guenes, S.; Neugebauer, H.; Sariciftci, N. S. *Chem. Rev.* **2007**, *107*, 1324–1338.

(2) (a) Imahori, H.; Mori, Y.; Matano, Y. *J. Photochem. Photobiol. C* **2003**, *4*, 51–83. (b) Imahori, H.; Tamaki, K.; Araki, Y.; Sekiguchi, Y.; Ito, O.; Sakata, Y.; Fukuzumi, S. *J. Am. Chem. Soc.* **2002**, *124*, 5165–5174. (c) D'Souza, F.; Chitta, R.; Gadde, S.; Islam, D.-M. S.; Schumacher, A. L.; Zandler, M. E.; Araki, Y.; Ito, O. *J. Phys. Chem. B* **2006**, *110*, 25240–25250. (d) Springer, J.; Kodis, G.; De La Garza, L.; Moore, A. L.; Moore, T. A.; Gust, D. *J. Phys. Chem. A* **2003**, *107*, 3567–3575. (e) Gonza´lez-Rodrı´guez, D.; Bottari, G. *J. Porphyrins Phthalocyanines* **2009**, *13*, 624–636.

(3) *Molecular Mechanisms of Photosynthesis*; Blankenship, R. E., Ed.; Blackwell Science: Malden, MA, 2002.

(4) (a) Aratani, N.; Osuka, A. in: *Handbook of Porphyrin Science*. Kadish, K. M.; Smith,

K. M.; Guilard, R. (Eds.); World Scientific Publishing Co. Pte. Ltd. 2010, Vol. 1, pp 1 – 132. (b) Balaban, T. S. in: *Handbook of Porphyrin Science*. Kadish, K. M.; Smith, K. M.; Guilard, R. (Eds.); World Scientific Publishing Co. Pte. Ltd. 2010, Vol. 1, pp 221 – 306. (c) Verreet, B.; Rand, B. P.; Cheyns, D.; Hadipour, A.; Aernouts, T.; Heremans, P.; Medina, A.; Claessens, C. G.; Torres, T. *Adv. Energy Mater.* **2011**, *1*, 565-568. (d) Zhao, Z.; Cammidge, A. N.; Cook, M. J. *Chem. Commun.* **2009**, 7530-7532.

(5) (a) Yoon, Z. S.; Yang, J.; Yoo, H.; Cho, S.; Kim, D. in: *Handbook of Porphyrin Science*. Kadish, K. M.; Smith, K. M.; Guilard, R. (Eds.); World Scientific Publishing Co. Pte. Ltd. 2010, Vol. 1, pp 439 – 506. (b) Gonzalez-Rodriguez, D.; Carbonell, E.; Rojas, G. M.; Castellanos, C. A.; Guldi, D. M.; Torres, T. *J. Am. Chem. Soc.* **2010**, *132*, 16488-16500. (c) El-Khouly, M. E.; Shim, S. Hee; Araki, Y.; Ito, O.; Kay, K.-Y. *Journal of Physical Chemistry B* **2008**, *112*, 3910-3917. (d) Solntsev, P. V.; Sabin, J. R.; Dammer, S. J.; Gerasimchuk, N. N.; Nemykin, V. N. *Chem. Commun.* **2010**, 6581-6583. (e) Ziessel, R.; Ulrich, G.; Elliott, K. J.; Harriman, A. *Chem. Eur. J.* **2009**, 4980-4984. (f) Mauldin, C. E.; Piliego, C.; Poulsen, D.; Unruh, D. A.; Woo, C.; Ma, B.; Mynar, J. L.; Frechet, J. M. J. *Appl. Mater. Interf.* **2010**, *2*, 2833-2838.

(6) (a) Grimm, B.; Hausmann, A.; Kahnt, A.; Seitz, W.; Spanig, F.; Guldi, D. M. in: *Handbook of Porphyrin Science*. Kadish, K. M.; Smith, K. M.; Guilard, R. (Eds.); World Scientific Publishing Co. Pte. Ltd. 2010, Vol. 1, pp 133 – 220. (b) Araki, Y.; Ito, O. *J. Photochem. Photobiol. C* **2008**, *9*, 93 –110. (c) Guldi, D. M.; Hirsch, A.; Scheloske, M.; Dietel, E.; Troisi, A.; Zerbetto, F.; Prato, M. *Chem. Eur. J.* **2003**, *9*, 4968 – 4979. (d) Albinsson, B.; Eng, M. P.; Pettersson, K.; Winters, M. U. *Phys.*

Chem. Chem. Phys. **2007**, 5847 – 5864. (e) Nieto, C. R.; Guilleme, J.; Villegas, C.; Delgado, J. L.; Gonzalez-Rodriguez, D.; Martin, N.; Torres, T.; Guldi, D. M. *J. Mater. Chem.* **2011**, *21*, 15914-15918. (f) Rohde, G. T.; Sabin, J. R.; Barrett, C. D.; Nemykin, V. N. *New J. Chem.*, **2011**, *35*, 1440-1448. (g) Nemykin, V. N.; Rohde, G. T.; Barrett, C. D.; Hadt, R. G.; Sabin, J. R.; Reina, G.; Galloni, P.; Floris, B. *Inorg. Chem.* **2010**, *49*, 7497-7509. (h) Nemykin, V. N.; Rohde, G. T.; Barrett, C. D.; Hadt, R. G.; Bizzarri, C.; Galloni, P.; Floris, B.; Nowik, I.; Herber, R. H.; Marrani, A. G.; Zanoni, R.; Loim, N. M. *J. Am. Chem. Soc.* **2009**, *131*, 14969-14978. (i) Nemykin, V. N.; Galloni, P.; Floris, B.; Barrett, C. D.; Hadt, R. G.; Subbotin, R. I.; Marrani, A. G.; Zanoni, R.; Loim, N. M. *Dalton Trans.* **2008**, 4233-4246. (j) Nemykin, V. N.; Barrett, C. D.; Hadt, R. G.; Subbotin, R. I.; Maximov, A. Y.; Polshin, E. V.; Koposov, A. Y. *Dalton Trans.* **2007**, 3378-3389.

(7) (a) D'Souza, F.; Ito, O. in: *Handbook of Porphyrin Science*. Kadish, K. M.; Smith, K. M.; Guilard, R. (Eds.); World Scientific Publishing Co. Pte. Ltd. 2010, Vol. 1, pp 307 – 438. (b) (a) El-Khouly, M. E.; Ito, O.; Smith, P. M.; D'Souza, F. *J. Photochem. Photobiol., C* **2004**, *5*, 79–104. (b) Fukuzumi, S. *Phys. Chem. Chem. Phys.* **2008**, *10*, 2283–2297. (c) D'Souza, F.; Ito, O. *Organic Electronics and Photonics*; Nalwa, H. R., Ed.; American Scientific Publishers: Stevenson Ranch, CA, 2008; Vol. 1, Chap. 13. (d) Ohkubo, K.; Fukuzumi, S. *Bull. Chem. Soc. Japan* **2009**, *82*, 303–315.

(8) Ohkubo, K.; Kotani, H.; Shao, J.; Ou, Z.; Kadish, K. M.; Li, G.; Pandey, R. K.; Fujitsuka, M.; Ito, O.; Imahori, H.; Fukuzumi, S. *Angew. Chem., Int. Ed.* **2004**, 853-856.

(9) (a) Verreet, B.; Rand, B. P.; Cheyns, D.; Hadipour, A.; Aernouts, T.; Heremans, P.;

Medina, A.; Claessens, C. G.; Torres, T. *Adv. Energy Mater.* **2011**, *1*, 565-568. (b) Luhman, W. A.; Holmes, R. J. *Adv. Funct. Mater.* **2011**, *21*, 764-771. (c) Shimizu, S.; Nakano, S.; Hosoya, T.; Kobayashi, N. *Chem. Commun.* **2011**, *47*, 316-318. (d) Gonzalez-Rodriguez, D.; Carbonell, E.; Guldi, D. M.; Torres, T. *Angew. Chem., Int. Ed.* **2009**, *48*, 8032-8036. (e) Verreet, B.; Schols, S.; Cheyns, D.; Rand, B. P.; Gommans, H.; Aernouts, T.; Heremans, P.; Genoe, J. *J. Mater. Chem.* **2009**, *19*, 5295-5297. (f) Gonzalez-Rodriguez, D.; Torres, T.; Herranz, M. A.; Echegoyen, L.; Carbonell, E.; Guldi, D. M. *Chem. Eur. J.* **2008**, *14*, 7670-7679. (g) Kim, J.-H.; El-Khouly, M. E.; Araki, Y.; Ito, O.; Kay, K.-Y. *Chem. Lett.* **2008**, *37*, 544-545. (h) Iglesias, R. S.; Claessens, C. G.; Rahman, G. M. A.; Herranz, M. A.; Guldi, D. M.; Torres, T. *Tetrahedron* **2007**, *63*, 12396-12404. (i) Claessens, C. G.; Gonzalez-Rodriguez, D.; Iglesias, R. S.; Torres, T. *C. R. Chimie* **2006**, *9*, 1094-1099. (j) Claessens, C. G.; Torres, T. *Chem. Commun.* **2004**, 1298-1299. (k) Gonzalez-Rodriguez, D.; Torres, T.; Guldi, D. M.; Rivera, J.; Herranz, M. A.; Echegoyen, L. *J. Am. Chem. Soc.* **2004**, *126*, 6301-6313.

(10) (a) Wrobel, D.; Boguta, A.; Mazurkiewicz, P. *Spectrochim. Acta. A* **2003**, *59*, 2841-54. (b) Kobayashi, N. *J. Chem. Soc., Chem. Commun.* **1991**, 1203-1205. (c) Yanagi, H.; Mukai, H.; Nair, M. *Thin Solid Films* **2006**, *499*, 123-128. (d) Xu, S.; Chen, K.; Tian, H. *J. Mater. Chem.* **2005**, *15*, 2676-2680. (e) Gonzalez-Rodriguez, D.; Claessens, C. G.; Torres, T.; Liu, S.; Echegoyen, L.; Vila, N.; Nonell, S. *Chem. Eur. J.* **2005**, *11*, 3881-3893. (f) Ohno-Okumura, E.; Sakamoto, K.; Kato, T.; Hatano, T.; Fukui, K.; Karatsu, T.; Kitamura, A.; Urano, T. *Dyes Pigments* **2002**, *53*, 57-65. (g) Rahman, G. M. A.; Lueders, D.; Rodriguez-Morgade, M. S.; Caballero, E.; Torres, T.;

Guldi, D. M. *ChemSusChem* **2009**, *2*, 330-335. (h) Xu, H.; Ng, D. K. P. *Chem. Asian J.* **2009**, *4*, 104-110. (i) Diaz, D. D.; Bolink, H. J.; Cappelli, L.; Claessens, C. G.; Coronado, E.; Torres, T. *Tetr. Lett.* **2007**, *48*, 4657-4660. (j) Geyer, M.; Plenzig, F.; Rauschnabel, J.; Hanack, M.; Del Rey, B.; Sastre, A.; Torres, T. *Synthesis* **1996**, 1139-1151. (k) Medina, A.; Claessens, C. G.; Rahman, G. M. A.; Lamsabhi, A. M.; Mo, O.; Yanez, M.; Guldi, D. M.; Torres, T. *Chem. Commun.* **2008**, 1759-1761. (l) Xu, H.; Jiang, X.-J.; Chan, E. Y. M.; Fong, W.-P.; Ng, D. K. P. *Org. Biomol. Chem.* **2007**, *5*, 3987-3992.

(11) Bellouard, F.; Chuburu, F.; Chuburu, F.; Yaouanc, J.-J.; Handel, H.; Le Mest, Y. *New J. Chem.* **1999**, *23*, 1133-1135.

(12) Goldberg, S. I.; Keith, L. H.; Prokopov, T. S. *J. Org. Chem.* **1963**, *28*, 850-851.

(13) (a) Adamo, C.; Barone, V. *J. Chem. Phys.*, **1999**, *110*, 6158-6169. (b) Perdew, J. P.; Burke, K.; Ernzerhof, M. *Phys. Rev. Lett.*, **1996**, *77*, 3865-3868. (c) Perdew, J. P.; Burke, K.; Ernzerhof, M. *Phys. Rev. Lett.*, **1997**, *78*, 1396-1396.

(14) (a) Firme, C. L.; Pontes, D. de L.; Antunes, O. A. C. *Chem. Phys. Lett.* **2010**, *499*, 193-198. (b) Kalamse, V.; Wadnerkar, N.; Chaudhari, A. *J. Phys. Chem. C* **2010**, *114*, 4704-4709. (c) Meylemans, H. A.; Damrauer, N. H. *Inorg. Chem.* **2009**, *48*, 11161-11175. (d) Alparone, A.; Reis, H.; Papadopoulos, M. G. *J. Phys. Chem. A* **2006**, *110*, 5909-5918. (e) Solntsev, P. V.; Dudkin, S. V.; Sabin, J. R.; Nemykin, V. N. *Organometallics*, **2011**, *30*, 3037-3046.

(15) Tomasi, J.; Mennucci, B.; Cammi, R. *Chem. Rev.*, **2005**, *105*, 2999-3093.

(16) (a) Becke, A. D. *Phys. Rev. A* **1988**, *38*, 3098-3100. (b) Perdew, J. P. *Phys. Rev. B*,

1986, *33*, 8822-8824.

(17) (a) Nemykin, V. N.; Hadt, R. G. *J. Phys. Chem. A* **2010**, *114*, 12062-12066. (b) Nemykin, V. N.; Hadt, R. G.; Belosludov, R. V.; Mizuseki, H.; Kawazoe, Y. *J. Phys. Chem. A* **2007**, *111*, 12901-12913. (c) Zhang, L.; Qi, D.; Zhang, Y.; Bian, Y.; Jiang, J. *J. Mol. Graph. Model.* **2011**, *29*, 717-725. (d) Zarate, X.; Schott, E.; Arratia-Perez, R. *Int. J. Quant. Chem.* **2011**, *111*, 4186-4196. (e) Soldatova, A. V.; Kim, J.-H.; Rizzoli, C.; Kenney, M. E.; Rodgers, M. A. J.; Rosa, A.; Ricciardi, G. *Inorg. Chem.* **2011**, *50*, 1135-1149. (f) Ricciardi, G.; Soldatova, A. V.; Rosa, A. *J. Porphyrins Phthalocyanines* **2010**, *14*, 689-700.

(18) Wachters, A. J. H. *J. Chem. Phys.*, **1970**, *52*, 1033-1036.

(19) McLean, A. D.; Chandler, G. S. *J. Chem. Phys.*, **1980**, *72*, 5639-5648.

(20) Gaussian 09, Revision **A.1**, Frisch, M. J.; Trucks, G. W.; Schlegel, H. B.; Scuseria, G. E.; Robb, M. A.; Cheeseman, J. R.; Scalmani, G.; Barone, V.; Mennucci, B.; Petersson, G. A.; Nakatsuji, H.; Caricato, M.; Li, X.; Hratchian, H. P.; Izmaylov, A. F.; Bloino, J.; Zheng, G.; Sonnenberg, J. L.; Hada, M.; Ehara, M.; Toyota, K.; Fukuda, R.; Hasegawa, J.; Ishida, M.; Nakajima, T.; Honda, Y.; Kitao, O.; Nakai, H.; Vreven, T.; Montgomery, Jr., J. A.; Peralta, J. E.; Ogliaro, F.; Bearpark, M.; Heyd, J. J.; Brothers, E.; Kudin, K. N.; Staroverov, V. N.; Kobayashi, R.; Normand, J.; Raghavachari, K.; Rendell, A.; Burant, J. C.; Iyengar, S. S.; Tomasi, J.; Cossi, M.; Rega, N.; Millam, N. J.; Klene, M.; Knox, J. E.; Cross, J. B.; Bakken, V.; Adamo, C.; Jaramillo, J.; Gomperts, R.; Stratmann, R. E.; Yazyev, O.; Austin, A. J.; Cammi, R.; Pomelli, C.; Ochterski, J. W.; Martin, R. L.; Morokuma, K.; Zakrzewski, V. G.; Voth, G. A.; Salvador, P.; Dannenberg, J. J.; Dapprich, S.; Daniels, A. D.; Farkas, Ö.;

Foresman, J. B.; Ortiz, J. V.; Cioslowski, J.; Fox, D. J. Gaussian, Inc., Wallingford CT, 2009.

(21) Tenderholt, A. L. *QMForge, Version 2.1*. Stanford University, Stanford, CA, USA.

(22) Otwinowski, Z.; Minor, W. *Methods in Enzymology*, New York: Academic Press; **1997**. Vol. 276, Carter Jr, C. W.; Sweet, R. M. (Eds.), pp. 307—326.

(23) Altomare, A.; Cascarano, G.; Giacovazzo, C.; Guagliardi, A.; Burla, M. C.; Polidori, G.; Camalli, M. *J. Appl. Cryst.* **1994**, *27*, 435.

(24) Sheldrick, G. M. *Acta Cryst.* **2008**, *A64*, 112-122.

(25) (a) Yu, Q.; Proia, M.; Heikal, A. A. *J. Biomedical Optics*, **2008**, *13*, 041315. (b) Heikal, A.A. In: *Advances in Planar Lipid Bilayers and Liposomes*, Iglic, A. (Ed.); Elsevier, Inc.; 2011, Vol. 13, pp. 169-197.

(26) (a) Del Rey, B.; Keller, U.; Torres, T.; Rojo, G.; Agullo-Lopez, F.; Nonell, S.; Marti, C.; Brasselet, S.; Ledoux, I.; Zyss, J. *J. Am. Chem. Soc.* **1998**, *120*, 12808-12817. (b) Kasuga, K.; Idehara, T.; Handa, M.; Ueda, Y.; Fujiwara, T.; Isa, K. *Bull. Chem. Soc. Japan* **1996**, *69*, 2559-2563. (c) Gonzalez-Rodriguez, D.; Torres, T.; Denardin, E. L. G.; Samios, D.; Stefani, V.; Correa, D. S. *J. Organomet. Chem.* **2009**, *694*, 1617-1622. (d) Morse, G. E.; Paton, A. S.; Lough, A.; Bender, T. P. *Dalton Trans.* **2010**, 3915 – 3922. (e) Lapok, L.; Claessens, C. G.; Woehrle, D.; Torres, T. *Tetr. Lett.* **2009**, *50*, 2041-2044. (f) Claessens, C. G.; Gonzalez-Rodriguez, D.; del Rey, B.; Torres, T.; Mark, G.; Schuchmann, H.-P.; von Sonntag, C.; MacDonald, J. G.; Nohr, R. S. *Eur. J. Org. Chem.* **2003**, 2547-2551.

(27) Guilleme, J.; Gonzalez-Rodriguez, D.; Torres, T. *Angew. Chem., Int. Ed.* **2011**, *50*,

3506-3509.

(28) Potz, R.; Goldner, M.; Huckstadt, H.; Cornelissen, U.; Tutass, A.; Homborg, H. *Z. Anorg. Allg. Chem.* **2000**, *626*, 588-596.

(29) (a) *Ferrocenes: Ligands, Materials and Biomolecules*, Stepnicka, P. (Ed.), John Wiley & Sons, Ltd., Chichester, England, **2008**, 655 pp. (b) Koslova, I. K.; Luk'yanov, O. A.; Tartakovskii, V. A. *Izv. Akad. Nauk SSSR, Ser. Khim.* **1981**, 2563-2571.

(30) (a) Ona-Burgos, P.; Casimiro, M.; Fernandez, I.; Navarro, A. V.; Fernandez Sanchez, J. F.; Carretero, A. S.; Gutierrez, A. F. *Dalton Trans.* **2010**, *39*, 6231-6238. (b) Koyama, T.; Suzuki, T.; Hanabusa, K.; Shirai, H.; Kobayashi, N. *Inorg. Chim. Acta* **1994**, *218*, 41-45. (c) Abraham, R. J.; Medforth, C. J. *Magn. Res. Chem.* **1988**, *26*, 803-812. (d) Nemykin, V. N.; Kobayashi, N.; Chernii, V. Y.; Belsky, V. K. *Eur. J. Inorg. Chem.* **2001**, 733-743. (e) Nemykin, V. N.; Polshina, A. E.; Chernii, V. Y.; Polshin, E. V.; Kobayashi, N. *Dalton* **2000**, 1019-1025

(31) (a) Claessens, C. G.; Gonzalez-Rodriguez, D.; Torres, T. *Chem. Rev.* **2002**, *102*, 835-853. (b) Kobayashi, N. in: The Porphyrin Handbook. Kadish, K. M.; Smith, K. M.; Guilard, R. (Eds.), Academic Press, New York, 2003, Vol 15, pp 161 – 262.

(32) (a) Engel, M. K.; Yao, J.; Maki, H.; Takeuchi, H.; Yonehara, H.; Pac, C.; *Report of Kawamura Institute of Chem. Res.*, **1997**, *9*, 53-128. (b) Tippmann, E. M.; Schultz, P. G. *Tetrahedron* **2007**, 63, 6182-6184. (c) Kato, T.; Tham, F. S.; Boyd, P. D. W.; Reed, C. A. *Heteroatom Chem.* **2006**, *17*, 209 – 216.

(33) (a) Gonzalez-Rodriguez, D.; Martinez-Diaz, M. V.; Abel, J.; Perl, A.; Huskens, J.;

Echegoyen, L.; Torres, T. *Org. Lett.* **2010**, *12*, 2970-2973. (b) Sakamoto, K.; Ohno-Okumura, E. *Materials* **2009**, *2*, 1127-1179. (c) Camerel, F.; Ulrich, G.; Retailleau, P.; Ziessel, R. *Angew. Chem., Int. Ed.* **2008**, *47*, 8876-8880. (d) Iglesias, R. S.; Claessens, C. G.; Herranz, M. A.; Torres, T. *Org. Lett.* **2007**, *9*, 5381-5384. (e) Iglesias, R. S.; Claessens, C. G.; Torres, T.; Herranz, M. A.; Ferro, V. R.; Garcia de la Vega, J. M. *J. Org. Chem.* **2007**, *72*, 2967-2977.

(34) (a) Galangau, O.; Dumas-Verdes, C.; Schmidt, E. Y.; Trofimov, B. A.; Clavier, G. *Organometallics* **2011**, *30*, 6476-6481. (b) Herber, R. H.; Nowik, I. Grosland, J. O.; Hadt, R. G..; Nemykin, V. N. *J. Organomet. Chem.* **2008**, *693*, 1850-1856. (c) Nemykin, V. N.; Makarova, E. A.; Grosland, J. O.; Hadt, R. G.; Koposov, A. Y. *Inorg. Chem.* **2007**, *46*, 9591-9601. (d) Nemykin, V. N.; Maximov, A. Y.; Koposov, A. Y. *Organometallics* **2007**, *26*, 3138-3148. (e) Nemykin, V. N.; Olsen, J. G.; Perera, E.; Basu, P. *Inorg. Chem.* **2006**, *45*, 3557 - 3568. (f) Nemykin, V. N.; Hadt, R. G. *Inorg. Chem.* **2006**, *45*, 8297 - 8307. (g) Li, Y. L.; Han, L.; Mei, Y.; Zhang, J. Z. H. *Chem. Phys. Lett.* **2009**, *482*, 217-222. (h) Fabrizi de Biani, F.; Manca, G.; Marchetti, L.; Leoni, P.; Bruzzone, S.; Guidotti, C.; Atrei, A.; Albinati, A.; Rizzato, S. *Inorg. Chem.* **2009**, *48*, 10126-10137. (i) Li, F.; Sa, R.; Wu, K. *Mol. Phys.* **2008**, *106*, 2537-2544. (j) Santi, S.; Orian, L.; Donoli, A.; Durante, C.; Bisello, A.; Ganis, P.; Ceccon, A.; Crociani, L.; Benetollo, F. *Organometallics* **2007**, *26*, 5867-5879. (k) Zhang, W.-W.; Yu, Y.-G.; Lu, Z.-D.; Mao, W.-L.; Li, Y.-Z.; Meng, Q.-J. *Organometallics* **2007**, *26*, 865-873. (l) Parac, M.; Grimme, S. *J. Phys. Chem. A* **2002**, *106*, 6844-6850.

(35) (a) Lamsabhi, A. M.; Yanez, M.; Mo, O.; Trujillo, C.; Blanco, F.; Alkorta, I.; Elguero, J.; Caballero, E.; Rodriguez-Morgade, M. S.; Claessens, C. G.; Torres, T. *J.*

Porphyrins Phthalocyanines **2011**, *15*, 1220-1230. (b) Xue, Z. L.; Mack, J.; Lu, H.; Zhang, L.; You, X. Z.; Kuzuhara, D.; Stillman, M.; Yamada, H.; Yamauchi, S.; Kobayashi, N. *Chem. Eur. J.* **2011**, *17*, 4396-4407. (c) Jakubikova, E.; Campbell, I. H.; Martin, R. L. *J. Phys. Chem. A* **2011**, *115*, 9265-9272. (d) Zhong, A.; Zhang, Y.; Bian, Y. *J. Mol. Graph. Model.* **2010**, *29*, 470-480. (e) Mack, J.; Kobayashi, N.; Stillman, M. J. *J. Inorg. Biochem.* **2010**, *104*, 310-317. (f) Quartarolo, A. D.; Lanzo, I.; Sicilia, E.; Russo, N. *Phys. Chem. Chem. Phys.* **2009**, *11*, 4586-4592. (g) Eriksson, E. S. E.; Eriksson, L. A. *Phys. Chem. Chem. Phys.* **2011**, *13*, 7207-7217. (h) Galinato, M. G. I.; Spolitak, T.; Ballou, D. P.; Lehnert, N. *Biochemistry* **2011**, *50*, 1053-1069. (i) Uoyama, H.; Kim, K. S.; Kuroki, K.; Shin, J.-Y.; Nagata, T.; Okujima, T.; Yamada, H.; Ono, N.; Kim, D.; Uno, H. *Chem. Eur. J.* **2010**, *16*, 4063-4074.

(36) Gouterman, M. *J. Mol. Spectrosc.* **1961**, *6*, 138–163.

(37) (a) Stuzhin, P. A.; Pimkov, I. V.; Ul'-Khak, A.; Ivanova, S. S.; Popkova, I. A.; Volkovich, D. I.; Kuz'mitskii, V. A.; Donzello, M.-P. *Russ. J. Org. Chem.* **2007**, *43*, 1854-1863. (b) Matsushita, O.; Muranaka, A.; Kobayashi, Y.; Kobayashi, N. *Heterocycles* **2007**, *74*, 321-329. (c) Maslov, V. G. *Optics Spectroscopy* **2006**, *101*, 853-861. (d) Kobayashi, N.; Nakajima, S.-I.; Ogata, H.; Fukuda, T. *Chem. Eur. J.* **2004**, *10*, 6294-6312. (e) Stillman, M.; Mack, J.; Kobayashi, N. *J. Porphyrins Phthalocyanines* **2002**, *6*, 296-300. (f) Zhang, X.-B.; Feng, J.-K.; Ren, A.-M.; Sun, C.-C. *J. Mol. Struct. THEOCHEM* **2006**, *767*, 165-173. (g) Mack, J.; Stillman, M. J. *J. Porphyrins Phthalocyanines* **2001**, *5*, 67-76.

(38) (a) Tokura, S.; Sato, T.; Tsuneda, T.; Nakajima, T.; Hirao, K. *J. Comp. Chem.* **2008**, *29*, 1187-1197. (b) Chiba, M.; Fedorov, D. G.; Kitaura, K. *J. Chem. Phys.* **2007**, *127*,

104108-104118. (c) Seth, M.; Ziegler, T. *J. Chem. Phys.* **2006**, *124*, 144105-1441016. (d) Tawada, Y.; Tsuneda, T.; Yanagisawa, S.; Yanai, T.; Hirao, K. *J. Chem. Phys.* **2004**, *120*, 8425-8433. (e) Hirata, S.; Zhan, C.-G.; Apra, E.; Windus, T. L.; Dixon, D. A. *J. Phys. Chem. A* **2003**, *107*, 10154-10158.

(39) Lahmani, F.; Tramer, A.; Tric, C. *J. Chem. Phys.* **1974**, *60*, 4431-4447.

(40) Mbambisa, G.; Nyokong, T. *Polyhedron* **2008**, *27*, 2799-2804.

(41) Ceulemans, W. Oldendorf, C. Gorller-Walrand, L. Vanquickenborne, G. *J. Am. Chem. Soc.* **1986**, *108*, 1155-1163.

Supplemental Information:

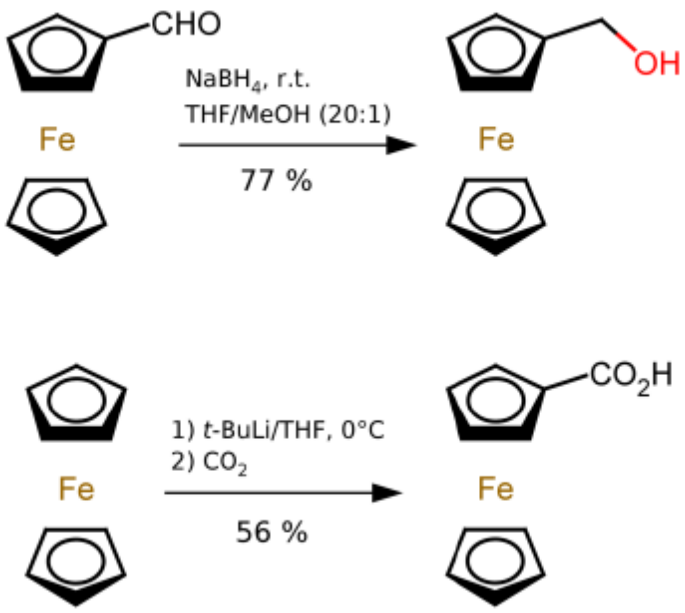

Supporting Information Scheme 1.

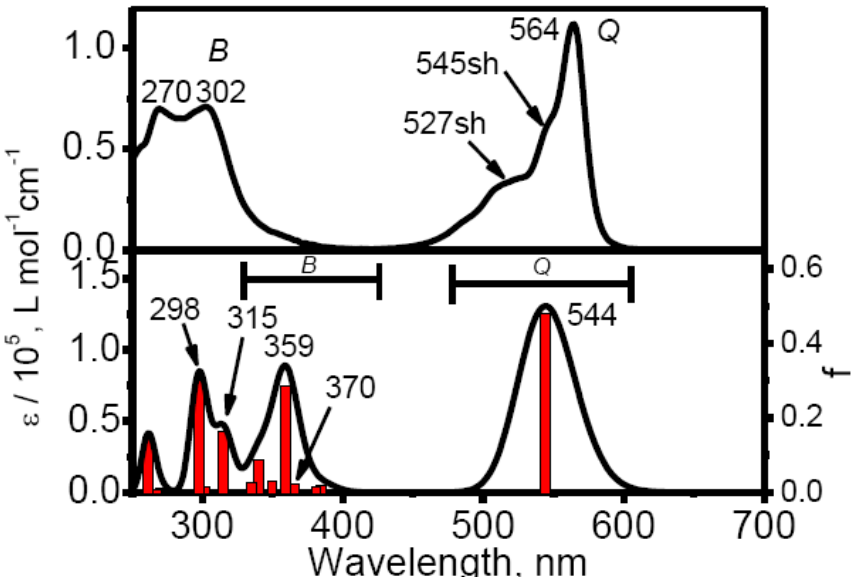

Supporting Information Figure 1. Experimental (top) and TDDFT predicted (bottom) UV-vis spectra of compound 1. *Q*- and *B*-band regions are labeled as *Q* and *B*.

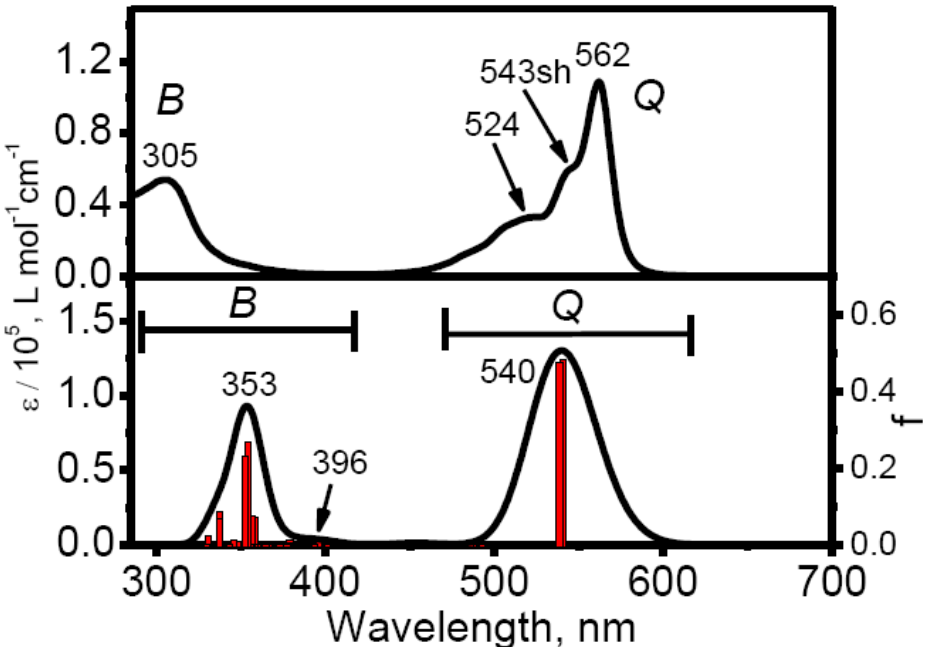

Supporting Information Figure 2. Experimental (top) and TDDFT predicted (bottom) UV-vis spectra of compound 2. *Q*- and *B*-band regions are labeled as *Q* and *B*.

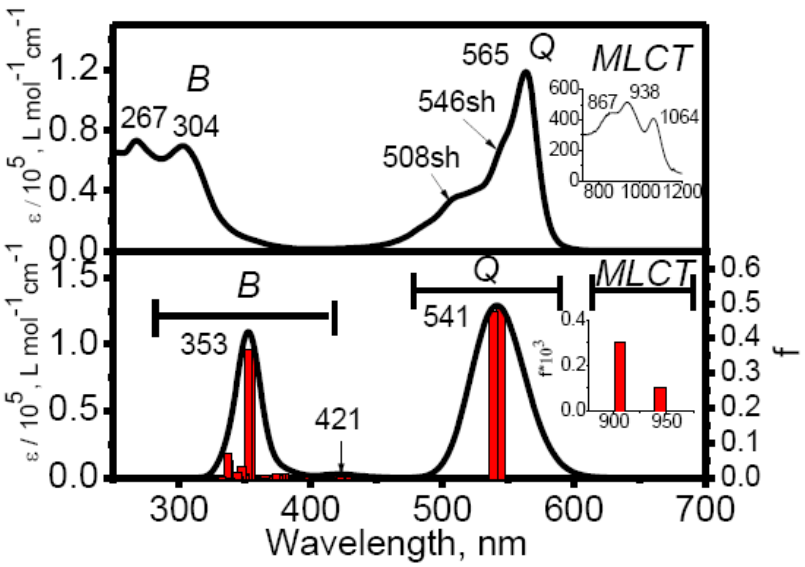

Supporting Information Figure 3. Experimental (top) and TDDFT predicted (bottom) UV-vis spectra of compound 3. *Q*- and *B*-band regions are labeled as *Q* and *B*.

CIF Information for Compound 1:

Table 1. Crystal data and structure refinement for a0011.

Identification code	a0011
Empirical formula	C24 H12 B Cl N6
Formula weight	430.66
Temperature	123(2) K
Wavelength	1.54187 A
Crystal system, space group	Orthorhombic, Pnma
Unit cell dimensions	a = 12.1224(2) A alpha = 90 deg. b = 14.8449(10) A beta = 90 deg. c = 10.32830(10) A gamma = 90 deg.
Volume	1858.64(13) A^3
Z, Calculated density	4, 1.539 Mg/m^3
Absorption coefficient	2.041 mm^-1

F(000)	880
Crystal size	0.21 x 0.2 x 0.16 mm
Theta range for data collection	7.31 to 68.24 deg.
Limiting indices	-13<=h<=14, -17<=k<=17, -12<=l<=11
Reflections collected / unique	12595 / 1756 [R(int) = 0.0351]
Completeness to theta = 68.24	99.1 %
Absorption correction	Semi-empirical from equivalents
Max. and min. transmission	1.000 and 0.705
Refinement method	Full-matrix least-squares on F^2
Data / restraints / parameters	1756 / 0 / 151
Goodness-of-fit on F^2	1.156
Final R indices [I>2sigma(I)]	R1 = 0.0668, wR2 = 0.1872
R indices (all data)	R1 = 0.0852, wR2 = 0.2127
Largest diff. peak and hole	0.838 and -0.485 e.A^-3

Table 2. Atomic coordinates (x 10^4) and equivalent isotropic displacement parameters (A^2 x 10^3) for a0011.
U(eq) is defined as one third of the trace of the orthogonalized Uij tensor.

	x	y	z	U(eq)
Cl(1)	3129(1)	7500	2388(1)	39(1)
N(1)	3377(2)	6705(2)	-69(3)	33(1)
N(2)	1724(4)	7500	234(4)	37(1)
N(3)	4932(3)	7500	-920(4)	36(1)
N(4)	1663(3)	5935(2)	-270(3)	39(1)
C(1)	4384(3)	6730(2)	-682(4)	33(1)
C(2)	4536(3)	5823(2)	-1197(3)	36(1)

C(3)	3539(3)	5337(2)	-990(3)	34(1)
C(4)	2773(3)	5956(2)	-346(3)	35(1)
C(5)	5413(3)	5433(2)	-1890(4)	38(1)
C(6)	5280(3)	4544(2)	-2291(4)	40(1)
C(7)	4310(3)	4067(3)	-2059(4)	40(1)
C(8)	3430(3)	4458(2)	-1424(4)	38(1)
C(9)	1144(3)	6731(2)	-61(3)	37(1)
C(10)	36(3)	7018(2)	-346(3)	37(1)
C(11)	-918(3)	6533(3)	-663(4)	44(1)
C(12)	-1857(3)	7033(3)	-952(4)	51(1)
B(1)	2901(5)	7500	578(6)	36(1)

Table 3. Bond lengths [A] and angles [deg] for a0011.

Cl(1)-B(1)	1.890(6)
N(1)-C(4)	1.361(4)
N(1)-C(1)	1.376(4)
N(1)-B(1)	1.473(4)
N(2)-C(9)	1.375(4)
N(2)-C(9)#1	1.375(4)
N(2)-B(1)	1.470(8)
N(3)-C(1)#1	1.344(4)
N(3)-C(1)	1.344(4)
N(4)-C(4)	1.348(5)
N(4)-C(9)	1.356(5)
C(1)-C(2)	1.460(5)
C(2)-C(5)	1.407(5)
C(2)-C(3)	1.423(5)
C(3)-C(8)	1.387(5)
C(3)-C(4)	1.466(5)
C(5)-C(6)	1.392(5)
C(5)-H(5)	0.9500
C(6)-C(7)	1.394(6)
C(6)-H(6)	0.9500
C(7)-C(8)	1.380(5)
C(7)-H(7)	0.9500
C(8)-H(8)	0.9500
C(9)-C(10)	1.439(5)
C(10)-C(11)	1.400(5)
C(10)-C(10)#1	1.433(7)
C(11)-C(12)	1.391(6)
C(11)-H(11)	0.9500
C(12)-C(12)#1	1.388(8)
C(12)-H(12)	0.9500

B(1)-N(1)#1	1.473(4)
C(4)-N(1)-C(1)	113.7(3)
C(4)-N(1)-B(1)	122.7(3)
C(1)-N(1)-B(1)	122.3(3)
C(9)-N(2)-C(9)#1	112.3(4)
C(9)-N(2)-B(1)	123.4(2)
C(9)#1-N(2)-B(1)	123.4(2)
C(1)#1-N(3)-C(1)	116.4(4)
C(4)-N(4)-C(9)	116.9(3)
N(3)-C(1)-N(1)	123.1(3)
N(3)-C(1)-C(2)	130.9(3)
N(1)-C(1)-C(2)	104.7(3)
C(5)-C(2)-C(3)	120.7(3)
C(5)-C(2)-C(1)	131.3(3)
C(3)-C(2)-C(1)	107.8(3)
C(8)-C(3)-C(2)	120.6(3)
C(8)-C(3)-C(4)	132.6(3)
C(2)-C(3)-C(4)	106.8(3)
N(4)-C(4)-N(1)	122.9(3)
N(4)-C(4)-C(3)	130.1(3)
N(1)-C(4)-C(3)	105.5(3)
C(6)-C(5)-C(2)	117.0(4)
C(6)-C(5)-H(5)	121.5
C(2)-C(5)-H(5)	121.5
C(5)-C(6)-C(7)	121.9(4)
C(5)-C(6)-H(6)	119.1
C(7)-C(6)-H(6)	119.1
C(8)-C(7)-C(6)	121.3(4)
C(8)-C(7)-H(7)	119.3
C(6)-C(7)-H(7)	119.3
C(7)-C(8)-C(3)	118.4(4)
C(7)-C(8)-H(8)	120.8
C(3)-C(8)-H(8)	120.8
N(4)-C(9)-N(2)	121.4(4)
N(4)-C(9)-C(10)	131.2(3)
N(2)-C(9)-C(10)	106.1(3)
C(11)-C(10)-C(10)#1	120.9(2)
C(11)-C(10)-C(9)	131.8(4)
C(10)#1-C(10)-C(9)	107.2(2)
C(12)-C(11)-C(10)	116.9(4)
C(12)-C(11)-H(11)	121.6
C(10)-C(11)-H(11)	121.6
C(12)#1-C(12)-C(11)	122.2(2)
C(12)#1-C(12)-H(12)	118.9
C(11)-C(12)-H(12)	118.9

N(2)-B(1)-N(1)	105.7(3)
N(2)-B(1)-N(1)#1	105.7(3)
N(1)-B(1)-N(1)#1	106.5(4)
N(2)-B(1)-Cl(1)	112.4(4)
N(1)-B(1)-Cl(1)	113.0(3)
N(1)#1-B(1)-Cl(1)	113.0(3)

Symmetry transformations used to generate equivalent atoms:
#1 x,-y+3/2,z

Table 4. Anisotropic displacement parameters (A^2 x 10^3) for a0011.
The anisotropic displacement factor exponent takes the form:
-2 pi^2 [h^2 a*^2 U11 + ... + 2 h k a* b* U12]

	U11	U22	U33	U23	U13	U12
Cl(1)	53(1)	25(1)	40(1)	0	0(1)	0
N(1)	38(2)	19(2)	41(2)	-1(1)	2(1)	-0(1)
N(2)	44(3)	25(2)	41(3)	0	2(2)	0
N(3)	38(2)	29(2)	42(2)	0	-2(2)	0
N(4)	47(2)	26(2)	45(2)	-2(1)	4(1)	-2(1)
C(1)	39(2)	22(2)	39(2)	1(1)	-3(2)	0(1)
C(2)	44(2)	25(2)	38(2)	-1(2)	-5(2)	2(2)
C(3)	44(2)	23(2)	36(2)	-2(1)	-2(2)	2(2)
C(4)	39(2)	23(2)	42(2)	-2(2)	2(2)	-0(1)
C(5)	47(2)	29(2)	37(2)	2(2)	-5(2)	2(2)
C(6)	47(2)	30(2)	42(2)	-4(2)	0(2)	9(2)
C(7)	53(2)	28(2)	39(2)	-2(2)	-4(2)	2(2)
C(8)	44(2)	25(2)	43(2)	-1(2)	-4(2)	-2(2)
C(9)	45(2)	28(2)	39(2)	-2(2)	2(2)	-4(2)
C(10)	42(2)	33(2)	37(2)	-4(2)	5(2)	-2(2)
C(11)	43(2)	49(2)	40(2)	-3(2)	4(2)	-0(2)
C(12)	49(3)	46(2)	58(3)	-2(2)	1(2)	-3(2)
B(1)	41(3)	25(3)	41(3)	0	0(3)	0

Table 5. Hydrogen coordinates (x 10^4) and isotropic displacement parameters (A^2 x 10^3) for a0011.

	x	y	z	U(eq)
H(5)	6067	5761	-2075	45
H(6)	5867	4254	-2736	48
H(7)	4253	3460	-2344	48
H(8)	2766	4132	-1288	45
H(11)	-923	5893	-679	53
H(12)	-2520	6723	-1157	62

Table 6. Torsion angles [deg] for a0011.

C(1)#1-N(3)-C(1)-N(1)	-8.4(7)
C(1)#1-N(3)-C(1)-C(2)	156.8(3)
C(4)-N(1)-C(1)-N(3)	156.1(4)
B(1)-N(1)-C(1)-N(3)	-10.8(6)
C(4)-N(1)-C(1)-C(2)	-12.4(4)
B(1)-N(1)-C(1)-C(2)	-179.3(4)
N(3)-C(1)-C(2)-C(5)	14.3(7)
N(1)-C(1)-C(2)-C(5)	-178.4(4)
N(3)-C(1)-C(2)-C(3)	-160.3(4)
N(1)-C(1)-C(2)-C(3)	6.9(4)
C(5)-C(2)-C(3)-C(8)	2.5(5)
C(1)-C(2)-C(3)-C(8)	177.8(3)
C(5)-C(2)-C(3)-C(4)	-175.2(3)
C(1)-C(2)-C(3)-C(4)	0.1(4)
C(9)-N(4)-C(4)-N(1)	8.3(5)
C(9)-N(4)-C(4)-C(3)	-155.6(4)
C(1)-N(1)-C(4)-N(4)	-154.7(3)
B(1)-N(1)-C(4)-N(4)	12.2(6)
C(1)-N(1)-C(4)-C(3)	12.5(4)
B(1)-N(1)-C(4)-C(3)	179.4(4)
C(8)-C(3)-C(4)-N(4)	-18.6(7)
C(2)-C(3)-C(4)-N(4)	158.7(4)
C(8)-C(3)-C(4)-N(1)	175.4(4)
C(2)-C(3)-C(4)-N(1)	-7.3(4)
C(3)-C(2)-C(5)-C(6)	-3.5(5)
C(1)-C(2)-C(5)-C(6)	-177.5(4)
C(2)-C(5)-C(6)-C(7)	2.1(5)
C(5)-C(6)-C(7)-C(8)	0.4(6)
C(6)-C(7)-C(8)-C(3)	-1.5(6)
C(2)-C(3)-C(8)-C(7)	0.0(5)
C(4)-C(3)-C(8)-C(7)	177.0(4)

C(4)-N(4)-C(9)-N(2)	-8.6(5)
C(4)-N(4)-C(9)-C(10)	156.2(4)
C(9)#1-N(2)-C(9)-N(4)	157.2(3)
B(1)-N(2)-C(9)-N(4)	-11.5(7)
C(9)#1-N(2)-C(9)-C(10)	-10.9(6)
B(1)-N(2)-C(9)-C(10)	-179.7(4)
N(4)-C(9)-C(10)-C(11)	15.8(7)
N(2)-C(9)-C(10)-C(11)	-177.6(4)
N(4)-C(9)-C(10)-C(10)#1	-160.2(3)
N(2)-C(9)-C(10)-C(10)#1	6.4(3)
C(10)#1-C(10)-C(11)-C(12)	-1.0(4)
C(9)-C(10)-C(11)-C(12)	-176.6(4)
C(10)-C(11)-C(12)-C(12)#1	1.1(4)
C(9)-N(2)-B(1)-N(1)	27.4(6)
C(9)#1-N(2)-B(1)-N(1)	-140.0(4)
C(9)-N(2)-B(1)-N(1)#1	140.0(4)
C(9)#1-N(2)-B(1)-N(1)#1	-27.4(6)
C(9)-N(2)-B(1)-Cl(1)	-96.3(4)
C(9)#1-N(2)-B(1)-Cl(1)	96.3(4)
C(4)-N(1)-B(1)-N(2)	-27.7(5)
C(1)-N(1)-B(1)-N(2)	138.1(4)
C(4)-N(1)-B(1)-N(1)#1	-139.7(3)
C(1)-N(1)-B(1)-N(1)#1	26.0(6)
C(4)-N(1)-B(1)-Cl(1)	95.6(4)
C(1)-N(1)-B(1)-Cl(1)	-98.6(4)

Symmetry transformations used to generate equivalent atoms:
#1 x,-y+3/2,z

Table 7. Hydrogen bonds for a0011 [A and deg.].

D-H...A	d(D-H)	d(H...A)	d(D...A)	<(DHA)

CIF Information for Compound 2

Table 1. Crystal data and structure refinement for a0022.

Identification code	a0022
Empirical formula	C35 H23 B Fe N6 O
Formula weight	610.25

Temperature	123(2) K
Wavelength	0.71073 A
Crystal system, space group	Monoclinic, C2/c
Unit cell dimensions	a = 28.610(5) A alpha = 90 deg. b = 11.197(5) A beta = 114.658(5) deg. c = 18.146(5) A gamma = 90 deg.
Volume	5283(3) A^3
Z, Calculated density	8, 1.535 Mg/m^3
Absorption coefficient	0.615 mm^-1
F(000)	2512
Crystal size	0.76 x 0.21 x 0.10 mm
Theta range for data collection	3.08 to 27.49 deg.
Limiting indices	-37<=h<=37, -14<=k<=14, -20<=l<=23
Reflections collected / unique	17320 / 6032 [R(int) = 0.0492]
Completeness to theta = 27.49	99.4 %
Absorption correction	Semi-empirical from equivalents
Max. and min. transmission	1.0000 and 0.5820
Refinement method	Full-matrix least-squares on F^2
Data / restraints / parameters	6032 / 0 / 397
Goodness-of-fit on F^2	1.047
Final R indices [I>2sigma(I)]	R1 = 0.0612, wR2 = 0.1553
R indices (all data)	R1 = 0.0704, wR2 = 0.1625
Largest diff. peak and hole	1.067 and -0.902 e.A^-3

Table 2. Atomic coordinates (x 10^4) and equivalent isotropic displacement parameters (A^2 x 10^3) for a0022.
U(eq) is defined as one third of the trace of the orthogonalized Uij tensor.

	x	y	z	U(eq)
C(1)	5755(1)	475(3)	3582(2)	21(1)
C(2)	5640(1)	722(3)	2738(2)	21(1)
C(3)	5798(1)	1918(3)	2697(2)	22(1)
C(4)	6012(1)	2385(3)	3519(2)	22(1)
C(5)	5467(1)	-2(3)	2052(2)	24(1)
C(6)	5446(1)	482(3)	1336(2)	28(1)
C(7)	5592(1)	1662(3)	1293(2)	28(1)
C(8)	5778(1)	2392(3)	1973(2)	25(1)
C(9)	6648(1)	3235(3)	4634(2)	22(1)
C(10)	7129(1)	3832(3)	5130(2)	24(1)
C(11)	7362(1)	3172(3)	5861(2)	24(1)
C(12)	7021(1)	2171(3)	5810(2)	22(1)
C(13)	7362(1)	4852(3)	4993(2)	27(1)
C(14)	7815(1)	5234(3)	5619(2)	31(1)
C(15)	8043(1)	4594(3)	6342(2)	31(1)
C(16)	7831(1)	3541(3)	6469(2)	28(1)
C(17)	6759(1)	254(3)	5875(2)	22(1)
C(18)	6805(1)	-1034(3)	5986(2)	23(1)
C(19)	6403(1)	-1568(3)	5300(2)	23(1)
C(20)	6119(1)	-591(2)	4770(2)	21(1)
C(21)	7163(1)	-1742(3)	6589(2)	28(1)
C(22)	7101(1)	-2971(3)	6519(2)	33(1)
C(23)	6704(1)	-3494(3)	5853(2)	32(1)
C(24)	6357(1)	-2805(3)	5227(2)	26(1)
C(25)	5581(1)	3212(3)	5034(2)	26(1)
C(26)	5368(1)	3596(3)	5623(2)	23(1)
C(27)	5377(1)	4772(3)	5926(2)	27(1)
C(28)	5135(1)	4732(3)	6471(2)	30(1)
C(29)	4974(1)	3545(3)	6500(2)	30(1)
C(30)	5118(1)	2840(3)	5978(2)	26(1)
C(31)	6515(1)	3463(3)	7084(2)	30(1)
C(32)	6332(1)	2394(3)	7300(2)	29(1)
C(33)	6163(1)	2694(3)	7914(2)	28(1)
C(34)	6227(1)	3931(3)	8059(2)	29(1)
C(35)	6454(1)	4409(3)	7558(2)	30(1)
N(1)	5922(1)	1531(2)	3982(1)	20(1)

N(2)	6343(1)	3295(2)	3835(1)	23(1)
N(3)	6591(1)	2369(2)	5117(1)	21(1)
N(4)	7099(1)	1140(2)	6225(1)	23(1)
N(5)	6313(1)	428(2)	5197(1)	20(1)
N(6)	5815(1)	-575(2)	3967(1)	21(1)
O(1)	5756(1)	2035(2)	5203(1)	25(1)
Fe(1)	5758(1)	3631(1)	6854(1)	23(1)
B(1)	6111(1)	1638(3)	4887(2)	20(1)

Table 3. Bond lengths [A] and angles [deg] for a0022.

C(1)-N(6)	1.343(4)
C(1)-N(1)	1.366(4)
C(1)-C(2)	1.452(4)
C(2)-C(5)	1.391(4)
C(2)-C(3)	1.424(4)
C(3)-C(8)	1.398(4)
C(3)-C(4)	1.452(4)
C(4)-N(2)	1.346(4)
C(4)-N(1)	1.367(3)
C(5)-C(6)	1.387(4)
C(5)-H(5)	0.9500
C(6)-C(7)	1.397(4)
C(6)-H(6)	0.9500
C(7)-C(8)	1.387(4)
C(7)-H(7)	0.9500
C(8)-H(8)	0.9500
C(9)-N(2)	1.345(4)
C(9)-N(3)	1.363(4)
C(9)-C(10)	1.455(4)
C(10)-C(13)	1.395(4)
C(10)-C(11)	1.419(4)
C(11)-C(16)	1.397(4)
C(11)-C(12)	1.462(4)
C(12)-N(4)	1.345(4)
C(12)-N(3)	1.363(3)
C(13)-C(14)	1.387(4)
C(13)-H(13)	0.9500
C(14)-C(15)	1.395(5)
C(14)-H(14)	0.9500
C(15)-C(16)	1.390(5)
C(15)-H(15)	0.9500
C(16)-H(16)	0.9500
C(17)-N(4)	1.348(4)

C(17)-N(5)	1.367(3)
C(17)-C(18)	1.454(4)
C(18)-C(21)	1.392(4)
C(18)-C(19)	1.427(4)
C(19)-C(24)	1.392(4)
C(19)-C(20)	1.460(4)
C(20)-N(6)	1.349(3)
C(20)-N(5)	1.361(4)
C(21)-C(22)	1.387(5)
C(21)-H(21)	0.9500
C(22)-C(23)	1.396(5)
C(22)-H(22)	0.9500
C(23)-C(24)	1.388(4)
C(23)-H(23)	0.9500
C(24)-H(24)	0.9500
C(25)-O(1)	1.398(4)
C(25)-C(26)	1.497(4)
C(25)-H(25A)	0.9900
C(25)-H(25B)	0.9900
C(26)-C(27)	1.422(4)
C(26)-C(30)	1.422(4)
C(26)-Fe(1)	2.039(3)
C(27)-C(28)	1.425(4)
C(27)-Fe(1)	2.031(3)
C(27)-H(27)	0.9500
C(28)-C(29)	1.415(5)
C(28)-Fe(1)	2.037(3)
C(28)-H(28)	0.9500
C(29)-C(30)	1.420(4)
C(29)-Fe(1)	2.062(3)
C(29)-H(29)	0.9500
C(30)-Fe(1)	2.058(3)
C(30)-H(30)	0.9500
C(31)-C(35)	1.421(4)
C(31)-C(32)	1.427(5)
C(31)-Fe(1)	2.036(3)
C(31)-H(31)	0.9500
C(32)-C(33)	1.426(4)
C(32)-Fe(1)	2.039(3)
C(32)-H(32)	0.9500
C(33)-C(34)	1.408(4)
C(33)-Fe(1)	2.070(3)
C(33)-H(33)	0.9500
C(34)-C(35)	1.422(4)
C(34)-Fe(1)	2.060(3)
C(34)-H(34)	0.9500

C(35)-Fe(1)	2.056(3)
C(35)-H(35)	0.9500
N(1)-B(1)	1.504(4)
N(3)-B(1)	1.499(4)
N(5)-B(1)	1.489(4)
O(1)-B(1)	1.430(4)

N(6)-C(1)-N(1)	122.7(2)
N(6)-C(1)-C(2)	129.8(2)
N(1)-C(1)-C(2)	105.8(2)
C(5)-C(2)-C(3)	120.3(3)
C(5)-C(2)-C(1)	132.2(3)
C(3)-C(2)-C(1)	107.2(2)
C(8)-C(3)-C(2)	121.1(3)
C(8)-C(3)-C(4)	131.5(3)
C(2)-C(3)-C(4)	107.0(2)
N(2)-C(4)-N(1)	123.2(2)
N(2)-C(4)-C(3)	129.2(3)
N(1)-C(4)-C(3)	105.8(2)
C(6)-C(5)-C(2)	118.1(3)
C(6)-C(5)-H(5)	121.0
C(2)-C(5)-H(5)	121.0
C(5)-C(6)-C(7)	121.6(3)
C(5)-C(6)-H(6)	119.2
C(7)-C(6)-H(6)	119.2
C(8)-C(7)-C(6)	121.4(3)
C(8)-C(7)-H(7)	119.3
C(6)-C(7)-H(7)	119.3
C(7)-C(8)-C(3)	117.5(3)
C(7)-C(8)-H(8)	121.3
C(3)-C(8)-H(8)	121.3
N(2)-C(9)-N(3)	122.1(3)
N(2)-C(9)-C(10)	131.6(3)
N(3)-C(9)-C(10)	105.4(2)
C(13)-C(10)-C(11)	121.3(3)
C(13)-C(10)-C(9)	131.6(3)
C(11)-C(10)-C(9)	107.1(2)
C(16)-C(11)-C(10)	120.4(3)
C(16)-C(11)-C(12)	132.1(3)
C(10)-C(11)-C(12)	107.4(2)
N(4)-C(12)-N(3)	122.1(3)
N(4)-C(12)-C(11)	132.3(3)
N(3)-C(12)-C(11)	104.8(2)
C(14)-C(13)-C(10)	117.3(3)
C(14)-C(13)-H(13)	121.3
C(10)-C(13)-H(13)	121.3

C(13)-C(14)-C(15)	121.5(3)
C(13)-C(14)-H(14)	119.3
C(15)-C(14)-H(14)	119.3
C(16)-C(15)-C(14)	121.8(3)
C(16)-C(15)-H(15)	119.1
C(14)-C(15)-H(15)	119.1
C(15)-C(16)-C(11)	117.5(3)
C(15)-C(16)-H(16)	121.2
C(11)-C(16)-H(16)	121.2
N(4)-C(17)-N(5)	122.6(3)
N(4)-C(17)-C(18)	131.2(3)
N(5)-C(17)-C(18)	105.2(2)
C(21)-C(18)-C(19)	120.5(3)
C(21)-C(18)-C(17)	131.9(3)
C(19)-C(18)-C(17)	107.5(2)
C(24)-C(19)-C(18)	120.6(3)
C(24)-C(19)-C(20)	132.7(3)
C(18)-C(19)-C(20)	106.6(2)
N(6)-C(20)-N(5)	122.0(2)
N(6)-C(20)-C(19)	130.7(3)
N(5)-C(20)-C(19)	105.6(2)
C(22)-C(21)-C(18)	118.0(3)
C(22)-C(21)-H(21)	121.0
C(18)-C(21)-H(21)	121.0
C(21)-C(22)-C(23)	121.5(3)
C(21)-C(22)-H(22)	119.3
C(23)-C(22)-H(22)	119.3
C(24)-C(23)-C(22)	121.4(3)
C(24)-C(23)-H(23)	119.3
C(22)-C(23)-H(23)	119.3
C(23)-C(24)-C(19)	117.9(3)
C(23)-C(24)-H(24)	121.0
C(19)-C(24)-H(24)	121.0
O(1)-C(25)-C(26)	109.2(2)
O(1)-C(25)-H(25A)	109.8
C(26)-C(25)-H(25A)	109.8
O(1)-C(25)-H(25B)	109.8
C(26)-C(25)-H(25B)	109.8
H(25A)-C(25)-H(25B)	108.3
C(27)-C(26)-C(30)	107.9(3)
C(27)-C(26)-C(25)	126.5(3)
C(30)-C(26)-C(25)	125.6(3)
C(27)-C(26)-Fe(1)	69.24(16)
C(30)-C(26)-Fe(1)	70.41(16)
C(25)-C(26)-Fe(1)	126.0(2)
C(26)-C(27)-C(28)	107.7(3)

C(26)-C(27)-Fe(1)	69.85(16)
C(28)-C(27)-Fe(1)	69.73(17)
C(26)-C(27)-H(27)	126.2
C(28)-C(27)-H(27)	126.2
Fe(1)-C(27)-H(27)	125.8
C(29)-C(28)-C(27)	108.3(3)
C(29)-C(28)-Fe(1)	70.76(18)
C(27)-C(28)-Fe(1)	69.25(17)
C(29)-C(28)-H(28)	125.8
C(27)-C(28)-H(28)	125.8
Fe(1)-C(28)-H(28)	125.7
C(28)-C(29)-C(30)	108.0(3)
C(28)-C(29)-Fe(1)	68.87(18)
C(30)-C(29)-Fe(1)	69.69(17)
C(28)-C(29)-H(29)	126.0
C(30)-C(29)-H(29)	126.0
Fe(1)-C(29)-H(29)	127.0
C(29)-C(30)-C(26)	108.1(3)
C(29)-C(30)-Fe(1)	69.98(17)
C(26)-C(30)-Fe(1)	68.96(16)
C(29)-C(30)-H(30)	125.9
C(26)-C(30)-H(30)	125.9
Fe(1)-C(30)-H(30)	126.7
C(35)-C(31)-C(32)	107.8(3)
C(35)-C(31)-Fe(1)	70.46(17)
C(32)-C(31)-Fe(1)	69.61(18)
C(35)-C(31)-H(31)	126.1
C(32)-C(31)-H(31)	126.1
Fe(1)-C(31)-H(31)	125.4
C(33)-C(32)-C(31)	107.5(3)
C(33)-C(32)-Fe(1)	70.87(17)
C(31)-C(32)-Fe(1)	69.40(17)
C(33)-C(32)-H(32)	126.2
C(31)-C(32)-H(32)	126.2
Fe(1)-C(32)-H(32)	125.1
C(34)-C(33)-C(32)	108.4(3)
C(34)-C(33)-Fe(1)	69.70(17)
C(32)-C(33)-Fe(1)	68.51(17)
C(34)-C(33)-H(33)	125.8
C(32)-C(33)-H(33)	125.8
Fe(1)-C(33)-H(33)	127.6
C(33)-C(34)-C(35)	108.1(3)
C(33)-C(34)-Fe(1)	70.43(17)
C(35)-C(34)-Fe(1)	69.65(17)
C(33)-C(34)-H(34)	126.0
C(35)-C(34)-H(34)	126.0

Fe(1)-C(34)-H(34)	125.5
C(31)-C(35)-C(34)	108.1(3)
C(31)-C(35)-Fe(1)	68.90(17)
C(34)-C(35)-Fe(1)	69.94(17)
C(31)-C(35)-H(35)	125.9
C(34)-C(35)-H(35)	125.9
Fe(1)-C(35)-H(35)	126.8
C(1)-N(1)-C(4)	113.0(2)
C(1)-N(1)-B(1)	122.5(2)
C(4)-N(1)-B(1)	122.8(2)
C(9)-N(2)-C(4)	116.5(2)
C(9)-N(3)-C(12)	113.9(2)
C(9)-N(3)-B(1)	123.4(2)
C(12)-N(3)-B(1)	122.6(2)
C(12)-N(4)-C(17)	116.7(2)
C(20)-N(5)-C(17)	113.5(2)
C(20)-N(5)-B(1)	123.1(2)
C(17)-N(5)-B(1)	122.6(2)
C(1)-N(6)-C(20)	117.3(2)
C(25)-O(1)-B(1)	117.0(2)
C(27)-Fe(1)-C(31)	112.67(13)
C(27)-Fe(1)-C(28)	41.02(12)
C(31)-Fe(1)-C(28)	146.19(14)
C(27)-Fe(1)-C(32)	145.23(12)
C(31)-Fe(1)-C(32)	40.99(13)
C(28)-Fe(1)-C(32)	172.52(13)
C(27)-Fe(1)-C(26)	40.91(11)
C(31)-Fe(1)-C(26)	105.79(12)
C(28)-Fe(1)-C(26)	68.68(11)
C(32)-Fe(1)-C(26)	113.84(12)
C(27)-Fe(1)-C(35)	107.14(13)
C(31)-Fe(1)-C(35)	40.65(12)
C(28)-Fe(1)-C(35)	115.99(13)
C(32)-Fe(1)-C(35)	68.38(13)
C(26)-Fe(1)-C(35)	129.39(12)
C(27)-Fe(1)-C(30)	68.46(12)
C(31)-Fe(1)-C(30)	130.21(12)
C(28)-Fe(1)-C(30)	68.09(13)
C(32)-Fe(1)-C(30)	108.86(13)
C(26)-Fe(1)-C(30)	40.63(11)
C(35)-Fe(1)-C(30)	168.68(12)
C(27)-Fe(1)-C(34)	131.61(13)
C(31)-Fe(1)-C(34)	68.38(12)
C(28)-Fe(1)-C(34)	110.69(12)
C(32)-Fe(1)-C(34)	68.26(12)
C(26)-Fe(1)-C(34)	169.17(13)

C(35)-Fe(1)-C(34)	40.41(12)
C(30)-Fe(1)-C(34)	149.97(13)
C(27)-Fe(1)-C(29)	68.45(13)
C(31)-Fe(1)-C(29)	170.17(13)
C(28)-Fe(1)-C(29)	40.38(13)
C(32)-Fe(1)-C(29)	133.02(13)
C(26)-Fe(1)-C(29)	68.29(12)
C(35)-Fe(1)-C(29)	149.14(13)
C(30)-Fe(1)-C(29)	40.32(12)
C(34)-Fe(1)-C(29)	118.74(12)
C(27)-Fe(1)-C(33)	171.21(12)
C(31)-Fe(1)-C(33)	68.17(13)
C(28)-Fe(1)-C(33)	133.99(12)
C(32)-Fe(1)-C(33)	40.62(12)
C(26)-Fe(1)-C(33)	147.87(12)
C(35)-Fe(1)-C(33)	67.44(13)
C(30)-Fe(1)-C(33)	118.18(13)
C(34)-Fe(1)-C(33)	39.87(12)
C(29)-Fe(1)-C(33)	112.33(13)
O(1)-B(1)-N(5)	111.1(2)
O(1)-B(1)-N(3)	116.0(2)
N(5)-B(1)-N(3)	103.1(2)
O(1)-B(1)-N(1)	118.1(2)
N(5)-B(1)-N(1)	104.3(2)
N(3)-B(1)-N(1)	102.7(2)

Symmetry transformations used to generate equivalent atoms:

Table 4. Anisotropic displacement parameters (A^2 x 10^3) for a0022.
The anisotropic displacement factor exponent takes the form:
-2 pi^2 [h^2 a*^2 U11 + ... + 2 h k a* b* U12]

	U11	U22	U33	U23	U13	U12
C(1)	20(1)	26(1)	17(1)	-1(1)	8(1)	1(1)
C(2)	20(1)	25(1)	18(1)	1(1)	7(1)	2(1)
C(3)	23(1)	24(1)	18(1)	1(1)	8(1)	2(1)
C(4)	21(1)	26(1)	19(1)	2(1)	8(1)	2(1)
C(5)	22(1)	30(1)	17(1)	-1(1)	5(1)	1(1)
C(6)	29(1)	36(2)	16(1)	-3(1)	7(1)	1(1)

C(7)	30(1)	35(2)	19(1)	4(1)	12(1)	2(1)
C(8)	25(1)	28(1)	21(1)	3(1)	9(1)	3(1)
C(9)	25(1)	24(1)	21(1)	-1(1)	12(1)	-0(1)
C(10)	24(1)	28(1)	22(1)	-5(1)	12(1)	-0(1)
C(11)	22(1)	30(1)	22(1)	-6(1)	12(1)	0(1)
C(12)	21(1)	30(1)	17(1)	-3(1)	9(1)	-0(1)
C(13)	29(1)	29(1)	29(1)	-4(1)	18(1)	-3(1)
C(14)	29(2)	32(2)	40(2)	-9(1)	21(1)	-6(1)
C(15)	21(1)	40(2)	33(2)	-12(1)	13(1)	-5(1)
C(16)	24(1)	37(2)	24(1)	-7(1)	12(1)	-0(1)
C(17)	22(1)	30(1)	15(1)	1(1)	8(1)	3(1)
C(18)	25(1)	27(1)	19(1)	1(1)	13(1)	2(1)
C(19)	25(1)	26(1)	20(1)	4(1)	13(1)	4(1)
C(20)	23(1)	25(1)	18(1)	-0(1)	12(1)	-1(1)
C(21)	27(1)	37(2)	19(1)	4(1)	10(1)	7(1)
C(22)	38(2)	34(2)	28(2)	11(1)	15(1)	17(1)
C(23)	41(2)	29(2)	30(2)	5(1)	19(1)	9(1)
C(24)	32(1)	26(1)	23(1)	1(1)	15(1)	2(1)
C(25)	29(1)	31(2)	20(1)	-1(1)	11(1)	2(1)
C(26)	23(1)	26(1)	18(1)	0(1)	7(1)	2(1)
C(27)	28(1)	27(1)	23(1)	1(1)	10(1)	5(1)
C(28)	34(2)	34(2)	22(1)	-1(1)	11(1)	9(1)
C(29)	24(1)	45(2)	20(1)	2(1)	10(1)	4(1)
C(30)	23(1)	34(2)	20(1)	-1(1)	6(1)	0(1)
C(31)	23(1)	41(2)	23(1)	-2(1)	7(1)	3(1)
C(32)	32(2)	25(1)	25(1)	-2(1)	8(1)	3(1)
C(33)	32(2)	29(2)	21(1)	5(1)	9(1)	4(1)
C(34)	28(1)	36(2)	19(1)	-4(1)	5(1)	1(1)
C(35)	26(1)	31(2)	28(2)	-2(1)	7(1)	-2(1)
N(1)	22(1)	22(1)	17(1)	1(1)	8(1)	0(1)
N(2)	27(1)	23(1)	20(1)	-1(1)	11(1)	0(1)
N(3)	22(1)	25(1)	16(1)	-0(1)	8(1)	1(1)
N(4)	23(1)	31(1)	16(1)	-1(1)	8(1)	1(1)
N(5)	23(1)	23(1)	15(1)	-1(1)	9(1)	-0(1)
N(6)	22(1)	23(1)	18(1)	0(1)	9(1)	-0(1)
O(1)	33(1)	26(1)	17(1)	-1(1)	12(1)	-6(1)
Fe(1)	24(1)	27(1)	17(1)	-0(1)	8(1)	1(1)
B(1)	22(1)	24(1)	16(1)	1(1)	9(1)	1(1)

Table 5. Hydrogen coordinates (x 10^4) and isotropic displacement parameters (A^2 x 10^3) for a0022.

	x	y	z	U(eq)
H(5)	5366	-804	2074	29
H(6)	5330	0	862	33
H(7)	5563	1970	788	33
H(8)	5888	3185	1946	30
H(13)	7215	5268	4492	32
H(14)	7973	5947	5554	37
H(15)	8352	4886	6759	37
H(16)	7998	3088	6951	33
H(21)	7441	-1393	7035	33
H(22)	7335	-3469	6932	39
H(23)	6669	-4339	5828	38
H(24)	6097	-3167	4764	31
H(25A)	5310	3267	4474	31
H(25B)	5868	3743	5079	31
H(27)	5519	5459	5790	32
H(28)	5089	5390	6765	36
H(29)	4800	3268	6813	36
H(30)	5059	2008	5882	32
H(31)	6654	3531	6692	36
H(32)	6323	1623	7076	34
H(33)	6030	2150	8180	34
H(34)	6136	4371	8427	35
H(35)	6548	5220	7543	36

Table 6. Torsion angles [deg] for a0022.

N(6)-C(1)-C(2)-C(5)	13.5(5)
N(1)-C(1)-C(2)-C(5)	178.7(3)
N(6)-C(1)-C(2)-C(3)	-159.4(3)
N(1)-C(1)-C(2)-C(3)	5.8(3)
C(5)-C(2)-C(3)-C(8)	0.5(4)
C(1)-C(2)-C(3)-C(8)	174.5(2)
C(5)-C(2)-C(3)-C(4)	-173.4(2)
C(1)-C(2)-C(3)-C(4)	0.6(3)
C(8)-C(3)-C(4)-N(2)	-15.3(5)
C(2)-C(3)-C(4)-N(2)	157.7(3)
C(8)-C(3)-C(4)-N(1)	-179.8(3)
C(2)-C(3)-C(4)-N(1)	-6.7(3)
C(3)-C(2)-C(5)-C(6)	-1.0(4)
C(1)-C(2)-C(5)-C(6)	-173.2(3)
C(2)-C(5)-C(6)-C(7)	-0.2(4)

C(5)-C(6)-C(7)-C(8)	1.8(5)
C(6)-C(7)-C(8)-C(3)	-2.2(4)
C(2)-C(3)-C(8)-C(7)	1.0(4)
C(4)-C(3)-C(8)-C(7)	173.2(3)
N(2)-C(9)-C(10)-C(13)	18.5(5)
N(3)-C(9)-C(10)-C(13)	-172.8(3)
N(2)-C(9)-C(10)-C(11)	-161.8(3)
N(3)-C(9)-C(10)-C(11)	6.9(3)
C(13)-C(10)-C(11)-C(16)	0.6(4)
C(9)-C(10)-C(11)-C(16)	-179.2(3)
C(13)-C(10)-C(11)-C(12)	179.9(3)
C(9)-C(10)-C(11)-C(12)	0.1(3)
C(16)-C(11)-C(12)-N(4)	-18.7(5)
C(10)-C(11)-C(12)-N(4)	162.1(3)
C(16)-C(11)-C(12)-N(3)	172.1(3)
C(10)-C(11)-C(12)-N(3)	-7.1(3)
C(11)-C(10)-C(13)-C(14)	-3.5(4)
C(9)-C(10)-C(13)-C(14)	176.2(3)
C(10)-C(13)-C(14)-C(15)	3.0(4)
C(13)-C(14)-C(15)-C(16)	0.5(5)
C(14)-C(15)-C(16)-C(11)	-3.4(4)
C(10)-C(11)-C(16)-C(15)	2.9(4)
C(12)-C(11)-C(16)-C(15)	-176.2(3)
N(4)-C(17)-C(18)-C(21)	15.3(5)
N(5)-C(17)-C(18)-C(21)	-176.5(3)
N(4)-C(17)-C(18)-C(19)	-161.7(3)
N(5)-C(17)-C(18)-C(19)	6.5(3)
C(21)-C(18)-C(19)-C(24)	1.0(4)
C(17)-C(18)-C(19)-C(24)	178.4(2)
C(21)-C(18)-C(19)-C(20)	-176.7(2)
C(17)-C(18)-C(19)-C(20)	0.7(3)
C(24)-C(19)-C(20)-N(6)	-19.5(5)
C(18)-C(19)-C(20)-N(6)	157.8(3)
C(24)-C(19)-C(20)-N(5)	175.0(3)
C(18)-C(19)-C(20)-N(5)	-7.7(3)
C(19)-C(18)-C(21)-C(22)	-3.0(4)
C(17)-C(18)-C(21)-C(22)	-179.6(3)
C(18)-C(21)-C(22)-C(23)	2.0(5)
C(21)-C(22)-C(23)-C(24)	1.1(5)
C(22)-C(23)-C(24)-C(19)	-3.0(4)
C(18)-C(19)-C(24)-C(23)	2.0(4)
C(20)-C(19)-C(24)-C(23)	179.0(3)
O(1)-C(25)-C(26)-C(27)	148.1(3)
O(1)-C(25)-C(26)-C(30)	-32.1(4)
O(1)-C(25)-C(26)-Fe(1)	58.5(3)
C(30)-C(26)-C(27)-C(28)	0.3(3)

C(25)-C(26)-C(27)-C(28)	-179.8(3)
Fe(1)-C(26)-C(27)-C(28)	-59.7(2)
C(30)-C(26)-C(27)-Fe(1)	60.0(2)
C(25)-C(26)-C(27)-Fe(1)	-120.1(3)
C(26)-C(27)-C(28)-C(29)	-0.4(3)
Fe(1)-C(27)-C(28)-C(29)	-60.2(2)
C(26)-C(27)-C(28)-Fe(1)	59.8(2)
C(27)-C(28)-C(29)-C(30)	0.4(3)
Fe(1)-C(28)-C(29)-C(30)	-58.9(2)
C(27)-C(28)-C(29)-Fe(1)	59.3(2)
C(28)-C(29)-C(30)-C(26)	-0.2(3)
Fe(1)-C(29)-C(30)-C(26)	-58.56(19)
C(28)-C(29)-C(30)-Fe(1)	58.4(2)
C(27)-C(26)-C(30)-C(29)	-0.1(3)
C(25)-C(26)-C(30)-C(29)	-180.0(3)
Fe(1)-C(26)-C(30)-C(29)	59.2(2)
C(27)-C(26)-C(30)-Fe(1)	-59.3(2)
C(25)-C(26)-C(30)-Fe(1)	120.8(3)
C(35)-C(31)-C(32)-C(33)	-0.5(3)
Fe(1)-C(31)-C(32)-C(33)	-60.9(2)
C(35)-C(31)-C(32)-Fe(1)	60.4(2)
C(31)-C(32)-C(33)-C(34)	1.6(3)
Fe(1)-C(32)-C(33)-C(34)	-58.4(2)
C(31)-C(32)-C(33)-Fe(1)	60.0(2)
C(32)-C(33)-C(34)-C(35)	-2.1(3)
Fe(1)-C(33)-C(34)-C(35)	-59.7(2)
C(32)-C(33)-C(34)-Fe(1)	57.6(2)
C(32)-C(31)-C(35)-C(34)	-0.7(3)
Fe(1)-C(31)-C(35)-C(34)	59.1(2)
C(32)-C(31)-C(35)-Fe(1)	-59.9(2)
C(33)-C(34)-C(35)-C(31)	1.7(3)
Fe(1)-C(34)-C(35)-C(31)	-58.5(2)
C(33)-C(34)-C(35)-Fe(1)	60.2(2)
N(6)-C(1)-N(1)-C(4)	155.8(3)
C(2)-C(1)-N(1)-C(4)	-10.7(3)
N(6)-C(1)-N(1)-B(1)	-9.7(4)
C(2)-C(1)-N(1)-B(1)	-176.2(2)
N(2)-C(4)-N(1)-C(1)	-154.6(3)
C(3)-C(4)-N(1)-C(1)	11.1(3)
N(2)-C(4)-N(1)-B(1)	10.9(4)
C(3)-C(4)-N(1)-B(1)	176.5(2)
N(3)-C(9)-N(2)-C(4)	-6.6(4)
C(10)-C(9)-N(2)-C(4)	160.5(3)
N(1)-C(4)-N(2)-C(9)	10.1(4)
C(3)-C(4)-N(2)-C(9)	-152.0(3)
N(2)-C(9)-N(3)-C(12)	157.7(3)

C(10)-C(9)-N(3)-C(12)	-12.3(3)
N(2)-C(9)-N(3)-B(1)	-18.2(4)
C(10)-C(9)-N(3)-B(1)	171.7(2)
N(4)-C(12)-N(3)-C(9)	-158.3(3)
C(11)-C(12)-N(3)-C(9)	12.3(3)
N(4)-C(12)-N(3)-B(1)	17.7(4)
C(11)-C(12)-N(3)-B(1)	-171.7(2)
N(3)-C(12)-N(4)-C(17)	7.4(4)
C(11)-C(12)-N(4)-C(17)	-160.2(3)
N(5)-C(17)-N(4)-C(12)	-9.8(4)
C(18)-C(17)-N(4)-C(12)	156.7(3)
N(6)-C(20)-N(5)-C(17)	-154.4(2)
C(19)-C(20)-N(5)-C(17)	12.7(3)
N(6)-C(20)-N(5)-B(1)	15.7(4)
C(19)-C(20)-N(5)-B(1)	-177.2(2)
N(4)-C(17)-N(5)-C(20)	157.2(2)
C(18)-C(17)-N(5)-C(20)	-12.3(3)
N(4)-C(17)-N(5)-B(1)	-12.9(4)
C(18)-C(17)-N(5)-B(1)	177.6(2)
N(1)-C(1)-N(6)-C(20)	-10.2(4)
C(2)-C(1)-N(6)-C(20)	152.8(3)
N(5)-C(20)-N(6)-C(1)	7.4(4)
C(19)-C(20)-N(6)-C(1)	-156.1(3)
C(26)-C(25)-O(1)-B(1)	-160.9(2)
C(26)-C(27)-Fe(1)-C(31)	88.18(19)
C(28)-C(27)-Fe(1)-C(31)	-153.10(19)
C(26)-C(27)-Fe(1)-C(28)	-118.7(3)
C(26)-C(27)-Fe(1)-C(32)	54.6(3)
C(28)-C(27)-Fe(1)-C(32)	173.3(2)
C(28)-C(27)-Fe(1)-C(26)	118.7(3)
C(26)-C(27)-Fe(1)-C(35)	131.16(18)
C(28)-C(27)-Fe(1)-C(35)	-110.1(2)
C(26)-C(27)-Fe(1)-C(30)	-37.78(17)
C(28)-C(27)-Fe(1)-C(30)	80.9(2)
C(26)-C(27)-Fe(1)-C(34)	168.80(18)
C(28)-C(27)-Fe(1)-C(34)	-72.5(2)
C(26)-C(27)-Fe(1)-C(29)	-81.28(19)
C(28)-C(27)-Fe(1)-C(29)	37.44(19)
C(26)-C(27)-Fe(1)-C(33)	-178(22)
C(28)-C(27)-Fe(1)-C(33)	-59.4(9)
C(35)-C(31)-Fe(1)-C(27)	90.2(2)
C(32)-C(31)-Fe(1)-C(27)	-151.23(17)
C(35)-C(31)-Fe(1)-C(28)	58.0(3)
C(32)-C(31)-Fe(1)-C(28)	176.5(2)
C(35)-C(31)-Fe(1)-C(32)	-118.6(3)
C(35)-C(31)-Fe(1)-C(26)	133.08(19)

C(32)-C(31)-Fe(1)-C(26)	-108.36(18)
C(32)-C(31)-Fe(1)-C(35)	118.6(3)
C(35)-C(31)-Fe(1)-C(30)	170.55(18)
C(32)-C(31)-Fe(1)-C(30)	-70.9(2)
C(35)-C(31)-Fe(1)-C(34)	-37.27(19)
C(32)-C(31)-Fe(1)-C(34)	81.29(19)
C(35)-C(31)-Fe(1)-C(29)	-175.2(7)
C(32)-C(31)-Fe(1)-C(29)	-56.7(8)
C(35)-C(31)-Fe(1)-C(33)	-80.3(2)
C(32)-C(31)-Fe(1)-C(33)	38.23(17)
C(29)-C(28)-Fe(1)-C(27)	119.2(3)
C(29)-C(28)-Fe(1)-C(31)	167.8(2)
C(27)-C(28)-Fe(1)-C(31)	48.6(3)
C(29)-C(28)-Fe(1)-C(32)	-30.0(10)
C(27)-C(28)-Fe(1)-C(32)	-149.2(9)
C(29)-C(28)-Fe(1)-C(26)	81.14(18)
C(27)-C(28)-Fe(1)-C(26)	-38.07(18)
C(29)-C(28)-Fe(1)-C(35)	-154.28(17)
C(27)-C(28)-Fe(1)-C(35)	86.5(2)
C(29)-C(28)-Fe(1)-C(30)	37.29(17)
C(27)-C(28)-Fe(1)-C(30)	-81.92(19)
C(29)-C(28)-Fe(1)-C(34)	-110.44(19)
C(27)-C(28)-Fe(1)-C(34)	130.35(19)
C(27)-C(28)-Fe(1)-C(29)	-119.2(3)
C(29)-C(28)-Fe(1)-C(33)	-71.3(2)
C(27)-C(28)-Fe(1)-C(33)	169.47(18)
C(33)-C(32)-Fe(1)-C(27)	169.2(2)
C(31)-C(32)-Fe(1)-C(27)	51.2(3)
C(33)-C(32)-Fe(1)-C(31)	118.1(3)
C(33)-C(32)-Fe(1)-C(28)	-46.9(10)
C(31)-C(32)-Fe(1)-C(28)	-165.0(9)
C(33)-C(32)-Fe(1)-C(26)	-155.07(18)
C(31)-C(32)-Fe(1)-C(26)	86.85(19)
C(33)-C(32)-Fe(1)-C(35)	80.1(2)
C(31)-C(32)-Fe(1)-C(35)	-37.98(18)
C(33)-C(32)-Fe(1)-C(30)	-111.60(19)
C(31)-C(32)-Fe(1)-C(30)	130.31(18)
C(33)-C(32)-Fe(1)-C(34)	36.47(18)
C(31)-C(32)-Fe(1)-C(34)	-81.62(19)
C(33)-C(32)-Fe(1)-C(29)	-73.2(2)
C(31)-C(32)-Fe(1)-C(29)	168.75(17)
C(31)-C(32)-Fe(1)-C(33)	-118.1(3)
C(30)-C(26)-Fe(1)-C(27)	-118.9(2)
C(25)-C(26)-Fe(1)-C(27)	120.7(3)
C(27)-C(26)-Fe(1)-C(31)	-106.58(19)
C(30)-C(26)-Fe(1)-C(31)	134.48(18)

C(25)-C(26)-Fe(1)-C(31)	14.1(3)
C(27)-C(26)-Fe(1)-C(28)	38.16(18)
C(30)-C(26)-Fe(1)-C(28)	-80.78(19)
C(25)-C(26)-Fe(1)-C(28)	158.9(3)
C(27)-C(26)-Fe(1)-C(32)	-149.47(18)
C(30)-C(26)-Fe(1)-C(32)	91.6(2)
C(25)-C(26)-Fe(1)-C(32)	-28.8(3)
C(27)-C(26)-Fe(1)-C(35)	-68.6(2)
C(30)-C(26)-Fe(1)-C(35)	172.47(18)
C(25)-C(26)-Fe(1)-C(35)	52.1(3)
C(27)-C(26)-Fe(1)-C(30)	118.9(2)
C(25)-C(26)-Fe(1)-C(30)	-120.3(3)
C(27)-C(26)-Fe(1)-C(34)	-50.6(7)
C(30)-C(26)-Fe(1)-C(34)	-169.5(6)
C(25)-C(26)-Fe(1)-C(34)	70.1(7)
C(27)-C(26)-Fe(1)-C(29)	81.71(19)
C(30)-C(26)-Fe(1)-C(29)	-37.23(18)
C(25)-C(26)-Fe(1)-C(29)	-157.6(3)
C(27)-C(26)-Fe(1)-C(33)	179.5(2)
C(30)-C(26)-Fe(1)-C(33)	60.5(3)
C(25)-C(26)-Fe(1)-C(33)	-59.8(4)
C(31)-C(35)-Fe(1)-C(27)	-105.1(2)
C(34)-C(35)-Fe(1)-C(27)	135.21(19)
C(34)-C(35)-Fe(1)-C(31)	-119.7(3)
C(31)-C(35)-Fe(1)-C(28)	-148.35(19)
C(34)-C(35)-Fe(1)-C(28)	91.9(2)
C(31)-C(35)-Fe(1)-C(32)	38.30(19)
C(34)-C(35)-Fe(1)-C(32)	-81.4(2)
C(31)-C(35)-Fe(1)-C(26)	-65.4(2)
C(34)-C(35)-Fe(1)-C(26)	174.86(18)
C(31)-C(35)-Fe(1)-C(30)	-39.7(7)
C(34)-C(35)-Fe(1)-C(30)	-159.4(6)
C(31)-C(35)-Fe(1)-C(34)	119.7(3)
C(31)-C(35)-Fe(1)-C(29)	178.4(2)
C(34)-C(35)-Fe(1)-C(29)	58.7(3)
C(31)-C(35)-Fe(1)-C(33)	82.3(2)
C(34)-C(35)-Fe(1)-C(33)	-37.43(18)
C(29)-C(30)-Fe(1)-C(27)	-81.7(2)
C(26)-C(30)-Fe(1)-C(27)	38.03(17)
C(29)-C(30)-Fe(1)-C(31)	176.29(19)
C(26)-C(30)-Fe(1)-C(31)	-64.0(2)
C(29)-C(30)-Fe(1)-C(28)	-37.34(19)
C(26)-C(30)-Fe(1)-C(28)	82.35(19)
C(29)-C(30)-Fe(1)-C(32)	135.37(19)
C(26)-C(30)-Fe(1)-C(32)	-104.94(18)
C(29)-C(30)-Fe(1)-C(26)	-119.7(3)

C(29)-C(30)-Fe(1)-C(35)	-150.7(6)
C(26)-C(30)-Fe(1)-C(35)	-31.0(7)
C(29)-C(30)-Fe(1)-C(34)	56.4(3)
C(26)-C(30)-Fe(1)-C(34)	176.1(2)
C(26)-C(30)-Fe(1)-C(29)	119.7(3)
C(29)-C(30)-Fe(1)-C(33)	92.0(2)
C(26)-C(30)-Fe(1)-C(33)	-148.31(17)
C(33)-C(34)-Fe(1)-C(27)	176.91(18)
C(35)-C(34)-Fe(1)-C(27)	-64.2(2)
C(33)-C(34)-Fe(1)-C(31)	-81.4(2)
C(35)-C(34)-Fe(1)-C(31)	37.48(19)
C(33)-C(34)-Fe(1)-C(28)	134.92(19)
C(35)-C(34)-Fe(1)-C(28)	-106.2(2)
C(33)-C(34)-Fe(1)-C(32)	-37.13(19)
C(35)-C(34)-Fe(1)-C(32)	81.7(2)
C(33)-C(34)-Fe(1)-C(26)	-140.5(6)
C(35)-C(34)-Fe(1)-C(26)	-21.6(7)
C(33)-C(34)-Fe(1)-C(35)	-118.9(3)
C(33)-C(34)-Fe(1)-C(30)	53.2(3)
C(35)-C(34)-Fe(1)-C(30)	172.1(2)
C(33)-C(34)-Fe(1)-C(29)	91.1(2)
C(35)-C(34)-Fe(1)-C(29)	-150.01(19)
C(35)-C(34)-Fe(1)-C(33)	118.9(3)
C(28)-C(29)-Fe(1)-C(27)	-38.02(17)
C(30)-C(29)-Fe(1)-C(27)	81.68(19)
C(28)-C(29)-Fe(1)-C(31)	-136.5(7)
C(30)-C(29)-Fe(1)-C(31)	-16.8(8)
C(30)-C(29)-Fe(1)-C(28)	119.7(3)
C(28)-C(29)-Fe(1)-C(32)	174.90(18)
C(30)-C(29)-Fe(1)-C(32)	-65.4(2)
C(28)-C(29)-Fe(1)-C(26)	-82.19(18)
C(30)-C(29)-Fe(1)-C(26)	37.51(18)
C(28)-C(29)-Fe(1)-C(35)	49.5(3)
C(30)-C(29)-Fe(1)-C(35)	169.2(2)
C(28)-C(29)-Fe(1)-C(30)	-119.7(3)
C(28)-C(29)-Fe(1)-C(34)	88.7(2)
C(30)-C(29)-Fe(1)-C(34)	-151.61(18)
C(28)-C(29)-Fe(1)-C(33)	132.54(18)
C(30)-C(29)-Fe(1)-C(33)	-107.76(19)
C(34)-C(33)-Fe(1)-C(27)	-15.3(9)
C(32)-C(33)-Fe(1)-C(27)	-135.8(8)
C(34)-C(33)-Fe(1)-C(31)	82.0(2)
C(32)-C(33)-Fe(1)-C(31)	-38.56(18)
C(34)-C(33)-Fe(1)-C(28)	-67.0(3)
C(32)-C(33)-Fe(1)-C(28)	172.41(19)
C(34)-C(33)-Fe(1)-C(32)	120.5(3)

C(34)-C(33)-Fe(1)-C(26)	167.0(2)
C(32)-C(33)-Fe(1)-C(26)	46.5(3)
C(34)-C(33)-Fe(1)-C(35)	37.93(19)
C(32)-C(33)-Fe(1)-C(35)	-82.6(2)
C(34)-C(33)-Fe(1)-C(30)	-152.97(18)
C(32)-C(33)-Fe(1)-C(30)	86.5(2)
C(32)-C(33)-Fe(1)-C(34)	-120.5(3)
C(34)-C(33)-Fe(1)-C(29)	-108.6(2)
C(32)-C(33)-Fe(1)-C(29)	130.84(19)
C(25)-O(1)-B(1)-N(5)	173.0(2)
C(25)-O(1)-B(1)-N(3)	55.8(3)
C(25)-O(1)-B(1)-N(1)	-66.7(3)
C(20)-N(5)-B(1)-O(1)	97.7(3)
C(17)-N(5)-B(1)-O(1)	-93.1(3)
C(20)-N(5)-B(1)-N(3)	-137.4(2)
C(17)-N(5)-B(1)-N(3)	31.8(3)
C(20)-N(5)-B(1)-N(1)	-30.5(3)
C(17)-N(5)-B(1)-N(1)	138.7(2)
C(9)-N(3)-B(1)-O(1)	-97.1(3)
C(12)-N(3)-B(1)-O(1)	87.3(3)
C(9)-N(3)-B(1)-N(5)	141.4(2)
C(12)-N(3)-B(1)-N(5)	-34.3(3)
C(9)-N(3)-B(1)-N(1)	33.2(3)
C(12)-N(3)-B(1)-N(1)	-142.4(2)
C(1)-N(1)-B(1)-O(1)	-96.3(3)
C(4)-N(1)-B(1)-O(1)	99.6(3)
C(1)-N(1)-B(1)-N(5)	27.4(3)
C(4)-N(1)-B(1)-N(5)	-136.7(2)
C(1)-N(1)-B(1)-N(3)	134.7(2)
C(4)-N(1)-B(1)-N(3)	-29.4(3)

Symmetry transformations used to generate equivalent atoms:

Table 7. Hydrogen bonds for a0022 [A and deg.].

D-H...A	d(D-H)	d(H...A)	d(D...A)	<(DHA)

CIF Information for Compound 3

Table 1. Crystal data and structure refinement for a0005.

Identification code	a0005
Empirical formula	C35 H21 B Fe N6 O2
Formula weight	624.24
Temperature	123(2) K
Wavelength	1.54187 A
Crystal system, space group	Monoclinic, P21/c
Unit cell dimensions	a = 17.2645(8) A alpha = 90 deg. b = 7.7863(2) A beta = 95.019(7) deg. c = 20.6276(14) A gamma = 90 deg.
Volume	2762.3(2) A^3
Z, Calculated density	4, 1.501 Mg/m^3
Absorption coefficient	4.757 mm^-1
F(000)	1280
Crystal size	0.22 x 0.20 x 0.18 mm
Theta range for data collection	6.53 to 68.41 deg.
Limiting indices	-20<=h<=20, -9<=k<=9, -17<=l<=24
Reflections collected / unique	29594 / 5040 [R(int) = 0.0647]
Completeness to theta = 68.41	99.1 %
Absorption correction	Semi-empirical from equivalents
Max. and min. transmission	0.4814 and 0.4209
Refinement method	Full-matrix least-squares on F^2
Data / restraints / parameters	5040 / 0 / 406

Goodness-of-fit on F^2 1.092

Final R indices [I>2sigma(I)] R1 = 0.0657, wR2 = 0.1817

R indices (all data) R1 = 0.0815, wR2 = 0.2060

Largest diff. peak and hole 0.618 and -0.971 e.A^-3

Table 2. Atomic coordinates (x 10^4) and equivalent isotropic displacement parameters (A^2 x 10^3) for a0005.
U(eq) is defined as one third of the trace of the orthogonalized Uij tensor.

	x	y	z	U(eq)
Fe(1)	5097(1)	1443(1)	1278(1)	46(1)
O(1)	6890(1)	506(3)	444(1)	43(1)
O(2)	7240(2)	1668(3)	1422(1)	50(1)
N(1)	8302(2)	601(4)	258(2)	40(1)
N(2)	8977(2)	367(4)	1309(2)	43(1)
N(3)	7905(2)	-1471(3)	1001(2)	38(1)
N(4)	7408(2)	-4139(4)	580(2)	43(1)
N(5)	7510(2)	-1733(4)	-114(2)	39(1)
N(6)	8152(2)	-66(4)	-873(2)	42(1)
C(1)	8484(2)	840(5)	-364(2)	42(1)
C(2)	9203(2)	1829(5)	-318(2)	43(1)
C(3)	9464(2)	1934(5)	351(2)	43(1)
C(4)	8900(2)	1048(4)	709(2)	41(1)
C(5)	9654(2)	2483(5)	-788(2)	48(1)
C(6)	10351(2)	3277(5)	-572(2)	52(1)
C(7)	10606(2)	3354(5)	82(2)	50(1)
C(8)	10180(2)	2680(5)	551(2)	49(1)
C(9)	8512(2)	-945(5)	1430(2)	41(1)
C(10)	8650(2)	-2333(5)	1899(2)	42(1)
C(11)	8160(2)	-3711(5)	1675(2)	43(1)
C(12)	7731(2)	-3174(5)	1071(2)	44(1)
C(13)	9207(2)	-2558(5)	2416(2)	45(1)
C(14)	9251(2)	-4128(5)	2730(2)	54(1)
C(15)	8757(2)	-5467(5)	2518(2)	56(1)
C(16)	8211(2)	-5298(5)	1993(2)	53(1)
C(17)	7342(2)	-3426(4)	-12(2)	40(1)
C(18)	7288(2)	-4219(5)	-653(2)	43(1)
C(19)	7515(2)	-2967(5)	-1103(2)	42(1)

C(20)	7709(2)	-1406(4)	-726(2)	40(1)
C(21)	7128(2)	-5897(5)	-860(2)	47(1)
C(22)	7182(2)	-6288(5)	-1505(2)	49(1)
C(23)	7398(2)	-5055(5)	-1955(2)	50(1)
C(24)	7570(2)	-3379(5)	-1749(2)	46(1)
C(25)	6774(2)	1527(4)	946(2)	42(1)
C(26)	6017(2)	2406(4)	862(2)	41(1)
C(27)	5409(2)	2021(5)	371(2)	45(1)
C(28)	4753(2)	3041(5)	502(2)	52(1)
C(29)	4951(3)	3994(6)	1068(2)	57(1)
C(30)	5739(2)	3635(4)	1301(2)	48(1)
C(31)	4985(3)	-1155(5)	1362(2)	59(1)
C(32)	4254(3)	-338(6)	1383(3)	65(1)
C(33)	4316(3)	781(7)	1923(3)	70(1)
C(34)	5080(3)	696(6)	2225(2)	67(1)
C(35)	5485(3)	-504(5)	1873(2)	57(1)
B(1)	7618(2)	-453(5)	417(2)	42(1)

Table 3. Bond lengths [A] and angles [deg] for a0005.

Fe(1)-C(26)	2.016(4)
Fe(1)-C(35)	2.028(4)
Fe(1)-C(30)	2.034(4)
Fe(1)-C(32)	2.035(4)
Fe(1)-C(27)	2.040(4)
Fe(1)-C(31)	2.040(4)
Fe(1)-C(33)	2.041(5)
Fe(1)-C(34)	2.042(5)
Fe(1)-C(29)	2.043(4)
Fe(1)-C(28)	2.071(4)
O(1)-C(25)	1.334(4)
O(1)-B(1)	1.467(4)
O(2)-C(25)	1.218(4)
N(1)-C(1)	1.359(5)
N(1)-C(4)	1.374(4)
N(1)-B(1)	1.498(5)
N(2)-C(9)	1.336(5)
N(2)-C(4)	1.342(5)
N(3)-C(12)	1.370(4)
N(3)-C(9)	1.373(4)
N(3)-B(1)	1.490(5)
N(4)-C(17)	1.337(5)
N(4)-C(12)	1.343(5)
N(5)-C(20)	1.362(5)

N(5)-C(17)	1.369(4)
N(5)-B(1)	1.480(5)
N(6)-C(20)	1.343(4)
N(6)-C(1)	1.350(5)
C(1)-C(2)	1.457(5)
C(2)-C(5)	1.392(5)
C(2)-C(3)	1.416(5)
C(3)-C(8)	1.396(5)
C(3)-C(4)	1.446(5)
C(5)-C(6)	1.391(5)
C(5)-H(5)	0.9500
C(6)-C(7)	1.384(6)
C(6)-H(6)	0.9500
C(7)-C(8)	1.370(5)
C(7)-H(7)	0.9500
C(8)-H(8)	0.9500
C(9)-C(10)	1.456(5)
C(10)-C(13)	1.385(5)
C(10)-C(11)	1.418(5)
C(11)-C(16)	1.398(5)
C(11)-C(12)	1.454(5)
C(13)-C(14)	1.382(6)
C(13)-H(13)	0.9500
C(14)-C(15)	1.393(6)
C(14)-H(14)	0.9500
C(15)-C(16)	1.380(5)
C(15)-H(15)	0.9500
C(16)-H(16)	0.9500
C(17)-C(18)	1.454(5)
C(18)-C(21)	1.394(5)
C(18)-C(19)	1.425(5)
C(19)-C(24)	1.382(5)
C(19)-C(20)	1.465(5)
C(21)-C(22)	1.377(5)
C(21)-H(21)	0.9500
C(22)-C(23)	1.408(6)
C(22)-H(22)	0.9500
C(23)-C(24)	1.397(5)
C(23)-H(23)	0.9500
C(24)-H(24)	0.9500
C(25)-C(26)	1.472(5)
C(26)-C(27)	1.425(5)
C(26)-C(30)	1.430(5)
C(27)-C(28)	1.428(5)
C(27)-H(27)	0.9500
C(28)-C(29)	1.399(6)

C(28)-H(28)	0.9500
C(29)-C(30)	1.430(6)
C(29)-H(29)	0.9500
C(30)-H(30)	0.9500
C(31)-C(35)	1.398(6)
C(31)-C(32)	1.418(6)
C(31)-H(31)	0.9500
C(32)-C(33)	1.410(7)
C(32)-H(32)	0.9500
C(33)-C(34)	1.410(6)
C(33)-H(33)	0.9500
C(34)-C(35)	1.407(6)
C(34)-H(34)	0.9500
C(35)-H(35)	0.9500

C(26)-Fe(1)-C(35)	107.71(16)
C(26)-Fe(1)-C(30)	41.36(15)
C(35)-Fe(1)-C(30)	117.52(17)
C(26)-Fe(1)-C(32)	153.73(19)
C(35)-Fe(1)-C(32)	68.14(18)
C(30)-Fe(1)-C(32)	164.27(19)
C(26)-Fe(1)-C(27)	41.14(14)
C(35)-Fe(1)-C(27)	128.29(17)
C(30)-Fe(1)-C(27)	69.50(17)
C(32)-Fe(1)-C(27)	119.80(19)
C(26)-Fe(1)-C(31)	119.25(18)
C(35)-Fe(1)-C(31)	40.18(16)
C(30)-Fe(1)-C(31)	152.27(18)
C(32)-Fe(1)-C(31)	40.71(18)
C(27)-Fe(1)-C(31)	109.34(18)
C(26)-Fe(1)-C(33)	164.04(19)
C(35)-Fe(1)-C(33)	67.60(19)
C(30)-Fe(1)-C(33)	125.9(2)
C(32)-Fe(1)-C(33)	40.48(19)
C(27)-Fe(1)-C(33)	153.56(19)
C(31)-Fe(1)-C(33)	67.8(2)
C(26)-Fe(1)-C(34)	126.23(18)
C(35)-Fe(1)-C(34)	40.45(17)
C(30)-Fe(1)-C(34)	105.63(19)
C(32)-Fe(1)-C(34)	68.5(2)
C(27)-Fe(1)-C(34)	165.18(18)
C(31)-Fe(1)-C(34)	68.07(19)
C(33)-Fe(1)-C(34)	40.40(18)
C(26)-Fe(1)-C(29)	68.61(16)
C(35)-Fe(1)-C(29)	151.97(19)
C(30)-Fe(1)-C(29)	41.05(16)

C(32)-Fe(1)-C(29)	127.52(18)
C(27)-Fe(1)-C(29)	68.25(18)
C(31)-Fe(1)-C(29)	166.10(18)
C(33)-Fe(1)-C(29)	107.9(2)
C(34)-Fe(1)-C(29)	117.9(2)
C(26)-Fe(1)-C(28)	68.35(15)
C(35)-Fe(1)-C(28)	166.84(18)
C(30)-Fe(1)-C(28)	68.46(17)
C(32)-Fe(1)-C(28)	109.46(18)
C(27)-Fe(1)-C(28)	40.63(14)
C(31)-Fe(1)-C(28)	129.70(17)
C(33)-Fe(1)-C(28)	119.62(18)
C(34)-Fe(1)-C(28)	152.00(18)
C(29)-Fe(1)-C(28)	39.75(17)
C(25)-O(1)-B(1)	121.3(3)
C(1)-N(1)-C(4)	112.4(3)
C(1)-N(1)-B(1)	122.3(3)
C(4)-N(1)-B(1)	123.5(3)
C(9)-N(2)-C(4)	117.6(3)
C(12)-N(3)-C(9)	112.5(3)
C(12)-N(3)-B(1)	122.7(3)
C(9)-N(3)-B(1)	122.9(3)
C(17)-N(4)-C(12)	116.9(3)
C(20)-N(5)-C(17)	113.3(3)
C(20)-N(5)-B(1)	122.3(3)
C(17)-N(5)-B(1)	123.3(3)
C(20)-N(6)-C(1)	116.3(3)
N(6)-C(1)-N(1)	122.9(3)
N(6)-C(1)-C(2)	128.9(4)
N(1)-C(1)-C(2)	106.1(3)
C(5)-C(2)-C(3)	120.6(4)
C(5)-C(2)-C(1)	132.3(4)
C(3)-C(2)-C(1)	106.8(4)
C(8)-C(3)-C(2)	120.6(4)
C(8)-C(3)-C(4)	131.8(4)
C(2)-C(3)-C(4)	107.4(3)
N(2)-C(4)-N(1)	122.1(3)
N(2)-C(4)-C(3)	130.0(3)
N(1)-C(4)-C(3)	106.0(3)
C(6)-C(5)-C(2)	117.3(4)
C(6)-C(5)-H(5)	121.3
C(2)-C(5)-H(5)	121.3
C(7)-C(6)-C(5)	121.7(4)
C(7)-C(6)-H(6)	119.2
C(5)-C(6)-H(6)	119.2
C(8)-C(7)-C(6)	121.8(4)

C(8)-C(7)-H(7)	119.1
C(6)-C(7)-H(7)	119.1
C(7)-C(8)-C(3)	117.9(4)
C(7)-C(8)-H(8)	121.1
C(3)-C(8)-H(8)	121.1
N(2)-C(9)-N(3)	123.0(3)
N(2)-C(9)-C(10)	128.8(3)
N(3)-C(9)-C(10)	106.1(3)
C(13)-C(10)-C(11)	120.6(3)
C(13)-C(10)-C(9)	131.9(3)
C(11)-C(10)-C(9)	106.7(3)
C(16)-C(11)-C(10)	120.3(4)
C(16)-C(11)-C(12)	131.5(4)
C(10)-C(11)-C(12)	107.8(3)
N(4)-C(12)-N(3)	122.8(3)
N(4)-C(12)-C(11)	129.2(3)
N(3)-C(12)-C(11)	105.6(3)
C(14)-C(13)-C(10)	118.6(4)
C(14)-C(13)-H(13)	120.7
C(10)-C(13)-H(13)	120.7
C(13)-C(14)-C(15)	120.6(4)
C(13)-C(14)-H(14)	119.7
C(15)-C(14)-H(14)	119.7
C(16)-C(15)-C(14)	122.1(4)
C(16)-C(15)-H(15)	118.9
C(14)-C(15)-H(15)	118.9
C(15)-C(16)-C(11)	117.6(4)
C(15)-C(16)-H(16)	121.2
C(11)-C(16)-H(16)	121.2
N(4)-C(17)-N(5)	122.5(3)
N(4)-C(17)-C(18)	130.3(3)
N(5)-C(17)-C(18)	105.5(3)
C(21)-C(18)-C(19)	120.0(4)
C(21)-C(18)-C(17)	132.2(4)
C(19)-C(18)-C(17)	107.6(3)
C(24)-C(19)-C(18)	121.0(4)
C(24)-C(19)-C(20)	132.2(4)
C(18)-C(19)-C(20)	106.5(3)
N(6)-C(20)-N(5)	123.3(3)
N(6)-C(20)-C(19)	129.3(4)
N(5)-C(20)-C(19)	105.8(3)
C(22)-C(21)-C(18)	118.4(4)
C(22)-C(21)-H(21)	120.8
C(18)-C(21)-H(21)	120.8
C(21)-C(22)-C(23)	122.1(4)
C(21)-C(22)-H(22)	119.0

C(23)-C(22)-H(22)	119.0
C(24)-C(23)-C(22)	119.9(4)
C(24)-C(23)-H(23)	120.1
C(22)-C(23)-H(23)	120.1
C(19)-C(24)-C(23)	118.7(4)
C(19)-C(24)-H(24)	120.7
C(23)-C(24)-H(24)	120.7
O(2)-C(25)-O(1)	123.1(3)
O(2)-C(25)-C(26)	124.8(4)
O(1)-C(25)-C(26)	112.1(3)
C(27)-C(26)-C(30)	108.8(3)
C(27)-C(26)-C(25)	125.3(3)
C(30)-C(26)-C(25)	125.5(3)
C(27)-C(26)-Fe(1)	70.4(2)
C(30)-C(26)-Fe(1)	70.0(2)
C(25)-C(26)-Fe(1)	120.1(2)
C(26)-C(27)-C(28)	107.2(4)
C(26)-C(27)-Fe(1)	68.5(2)
C(28)-C(27)-Fe(1)	70.8(2)
C(26)-C(27)-H(27)	126.4
C(28)-C(27)-H(27)	126.4
Fe(1)-C(27)-H(27)	125.8
C(29)-C(28)-C(27)	108.3(4)
C(29)-C(28)-Fe(1)	69.0(2)
C(27)-C(28)-Fe(1)	68.5(2)
C(29)-C(28)-H(28)	125.9
C(27)-C(28)-H(28)	125.9
Fe(1)-C(28)-H(28)	128.1
C(28)-C(29)-C(30)	109.4(4)
C(28)-C(29)-Fe(1)	71.2(2)
C(30)-C(29)-Fe(1)	69.1(2)
C(28)-C(29)-H(29)	125.3
C(30)-C(29)-H(29)	125.3
Fe(1)-C(29)-H(29)	126.0
C(29)-C(30)-C(26)	106.3(4)
C(29)-C(30)-Fe(1)	69.8(2)
C(26)-C(30)-Fe(1)	68.6(2)
C(29)-C(30)-H(30)	126.9
C(26)-C(30)-H(30)	126.9
Fe(1)-C(30)-H(30)	126.2
C(35)-C(31)-C(32)	107.9(4)
C(35)-C(31)-Fe(1)	69.4(2)
C(32)-C(31)-Fe(1)	69.5(3)
C(35)-C(31)-H(31)	126.1
C(32)-C(31)-H(31)	126.1
Fe(1)-C(31)-H(31)	126.6

C(33)-C(32)-C(31)	107.2(4)
C(33)-C(32)-Fe(1)	70.0(3)
C(31)-C(32)-Fe(1)	69.8(2)
C(33)-C(32)-H(32)	126.4
C(31)-C(32)-H(32)	126.4
Fe(1)-C(32)-H(32)	125.4
C(34)-C(33)-C(32)	108.9(4)
C(34)-C(33)-Fe(1)	69.8(3)
C(32)-C(33)-Fe(1)	69.6(3)
C(34)-C(33)-H(33)	125.6
C(32)-C(33)-H(33)	125.6
Fe(1)-C(33)-H(33)	126.6
C(35)-C(34)-C(33)	107.0(4)
C(35)-C(34)-Fe(1)	69.3(3)
C(33)-C(34)-Fe(1)	69.8(3)
C(35)-C(34)-H(34)	126.5
C(33)-C(34)-H(34)	126.5
Fe(1)-C(34)-H(34)	126.0
C(31)-C(35)-C(34)	109.1(4)
C(31)-C(35)-Fe(1)	70.4(2)
C(34)-C(35)-Fe(1)	70.3(3)
C(31)-C(35)-H(35)	125.5
C(34)-C(35)-H(35)	125.5
Fe(1)-C(35)-H(35)	125.5
O(1)-B(1)-N(5)	108.6(3)
O(1)-B(1)-N(3)	117.7(3)
N(5)-B(1)-N(3)	104.5(3)
O(1)-B(1)-N(1)	115.1(3)
N(5)-B(1)-N(1)	104.9(3)
N(3)-B(1)-N(1)	104.8(3)

Symmetry transformations used to generate equivalent atoms:

Table 4. Anisotropic displacement parameters (A^2 x 10^3) for a0005.
The anisotropic displacement factor exponent takes the form:
-2 pi^2 [h^2 a*^2 U11 + ... + 2 h k a* b* U12]

	U11	U22	U33	U23	U13	U12
Fe(1)	42(1)	44(1)	52(1)	-1(1)	3(1)	0(1)

O(1)	38(1)	48(2)	43(2)	-5(1)	-0(1)	5(1)
O(2)	47(2)	50(2)	51(2)	-6(1)	-6(1)	1(1)
N(1)	36(2)	38(2)	43(2)	-1(1)	-0(1)	1(1)
N(2)	41(2)	39(2)	49(2)	-2(2)	1(1)	-0(1)
N(3)	35(2)	40(2)	38(2)	-2(1)	-3(1)	2(1)
N(4)	41(2)	47(2)	40(2)	-4(2)	1(1)	-6(1)
N(5)	36(2)	44(2)	36(2)	-1(1)	-0(1)	1(1)
N(6)	45(2)	36(2)	46(2)	-1(1)	-1(1)	1(1)
C(1)	43(2)	40(2)	45(2)	1(2)	3(2)	7(2)
C(2)	40(2)	34(2)	55(3)	-3(2)	5(2)	2(2)
C(3)	43(2)	35(2)	51(3)	-0(2)	-1(2)	2(2)
C(4)	44(2)	35(2)	43(2)	-2(2)	-1(2)	1(2)
C(5)	52(2)	36(2)	57(3)	-4(2)	5(2)	6(2)
C(6)	43(2)	42(2)	70(3)	-5(2)	11(2)	2(2)
C(7)	39(2)	38(2)	72(3)	1(2)	3(2)	2(2)
C(8)	43(2)	35(2)	66(3)	-0(2)	-3(2)	2(2)
C(9)	40(2)	44(2)	39(2)	-2(2)	-1(2)	2(2)
C(10)	41(2)	41(2)	42(2)	-0(2)	-1(2)	1(2)
C(11)	44(2)	46(2)	38(2)	-1(2)	0(2)	-1(2)
C(12)	39(2)	45(2)	48(2)	2(2)	-0(2)	-0(2)
C(13)	42(2)	51(2)	41(2)	-3(2)	-0(2)	1(2)
C(14)	60(3)	50(2)	50(3)	3(2)	-8(2)	3(2)
C(15)	62(3)	50(2)	54(3)	9(2)	-8(2)	-4(2)
C(16)	58(2)	48(2)	51(3)	4(2)	-1(2)	-10(2)
C(17)	37(2)	43(2)	38(2)	-0(2)	-2(2)	-2(2)
C(18)	39(2)	42(2)	48(2)	0(2)	3(2)	3(2)
C(19)	34(2)	45(2)	45(2)	-6(2)	2(2)	6(2)
C(20)	39(2)	41(2)	41(2)	-2(2)	-1(2)	5(2)
C(21)	47(2)	41(2)	54(3)	1(2)	1(2)	-2(2)
C(22)	55(2)	47(2)	45(3)	-9(2)	-1(2)	-2(2)
C(23)	51(2)	56(2)	41(2)	-7(2)	3(2)	1(2)
C(24)	43(2)	45(2)	51(3)	-5(2)	0(2)	3(2)
C(25)	41(2)	42(2)	42(2)	1(2)	3(2)	-5(2)
C(26)	40(2)	40(2)	43(2)	-1(2)	6(2)	-1(2)
C(27)	41(2)	44(2)	51(3)	3(2)	2(2)	3(2)
C(28)	42(2)	55(2)	60(3)	7(2)	8(2)	10(2)
C(29)	58(3)	45(2)	68(3)	0(2)	5(2)	13(2)
C(30)	52(2)	40(2)	53(3)	-10(2)	9(2)	-1(2)
C(31)	77(3)	40(2)	58(3)	6(2)	2(2)	-11(2)
C(32)	50(2)	71(3)	75(4)	8(3)	1(2)	-13(2)
C(33)	62(3)	78(3)	72(4)	13(3)	22(3)	6(3)
C(34)	88(4)	64(3)	50(3)	-3(2)	14(3)	-9(3)
C(35)	59(3)	53(2)	58(3)	9(2)	3(2)	-2(2)
B(1)	38(2)	42(2)	45(3)	-3(2)	0(2)	1(2)

Table 5. Hydrogen coordinates (x 10^4) and isotropic displacement parameters (A^2 x 10^3) for a0005.

	x	y	z	U(eq)
H(5)	9492	2390	-1239	58
H(6)	10659	3779	-882	62
H(7)	11090	3889	209	60
H(8)	10367	2719	998	58
H(13)	9552	-1652	2553	54
H(14)	9621	-4294	3093	65
H(15)	8798	-6533	2743	68
H(16)	7881	-6226	1852	63
H(21)	6985	-6748	-563	57
H(22)	7070	-7425	-1651	59
H(23)	7426	-5363	-2398	59
H(24)	7721	-2538	-2047	56
H(27)	5434	1232	22	55
H(28)	4266	3069	249	62
H(29)	4614	4759	1266	69
H(30)	6020	4117	1674	58
H(31)	5113	-1995	1055	70
H(32)	3806	-513	1089	79
H(33)	3910	1479	2060	83
H(34)	5282	1328	2596	80
H(35)	6015	-822	1967	68

Table 6. Torsion angles [deg] for a0005.

C(20)-N(6)-C(1)-N(1)	-9.5(5)
C(20)-N(6)-C(1)-C(2)	152.1(4)
C(4)-N(1)-C(1)-N(6)	153.7(3)
B(1)-N(1)-C(1)-N(6)	-11.3(5)
C(4)-N(1)-C(1)-C(2)	-11.6(4)
B(1)-N(1)-C(1)-C(2)	-176.5(3)
N(6)-C(1)-C(2)-C(5)	17.6(7)
N(1)-C(1)-C(2)-C(5)	-178.4(4)
N(6)-C(1)-C(2)-C(3)	-156.5(4)
N(1)-C(1)-C(2)-C(3)	7.5(4)
C(5)-C(2)-C(3)-C(8)	-0.6(5)

C(1)-C(2)-C(3)-C(8)	174.4(3)
C(5)-C(2)-C(3)-C(4)	-176.1(3)
C(1)-C(2)-C(3)-C(4)	-1.2(4)
C(9)-N(2)-C(4)-N(1)	9.0(5)
C(9)-N(2)-C(4)-C(3)	-152.8(4)
C(1)-N(1)-C(4)-N(2)	-154.8(3)
B(1)-N(1)-C(4)-N(2)	9.9(5)
C(1)-N(1)-C(4)-C(3)	10.8(4)
B(1)-N(1)-C(4)-C(3)	175.6(3)
C(8)-C(3)-C(4)-N(2)	-16.2(7)
C(2)-C(3)-C(4)-N(2)	158.6(4)
C(8)-C(3)-C(4)-N(1)	179.7(4)
C(2)-C(3)-C(4)-N(1)	-5.5(4)
C(3)-C(2)-C(5)-C(6)	-1.9(5)
C(1)-C(2)-C(5)-C(6)	-175.3(4)
C(2)-C(5)-C(6)-C(7)	2.7(5)
C(5)-C(6)-C(7)-C(8)	-1.2(6)
C(6)-C(7)-C(8)-C(3)	-1.3(5)
C(2)-C(3)-C(8)-C(7)	2.2(5)
C(4)-C(3)-C(8)-C(7)	176.5(4)
C(4)-N(2)-C(9)-N(3)	-8.5(5)
C(4)-N(2)-C(9)-C(10)	152.6(4)
C(12)-N(3)-C(9)-N(2)	153.4(4)
B(1)-N(3)-C(9)-N(2)	-11.2(5)
C(12)-N(3)-C(9)-C(10)	-11.4(4)
B(1)-N(3)-C(9)-C(10)	-175.9(3)
N(2)-C(9)-C(10)-C(13)	12.8(7)
N(3)-C(9)-C(10)-C(13)	176.3(4)
N(2)-C(9)-C(10)-C(11)	-157.2(4)
N(3)-C(9)-C(10)-C(11)	6.3(4)
C(13)-C(10)-C(11)-C(16)	2.8(6)
C(9)-C(10)-C(11)-C(16)	174.2(4)
C(13)-C(10)-C(11)-C(12)	-171.0(4)
C(9)-C(10)-C(11)-C(12)	0.4(4)
C(17)-N(4)-C(12)-N(3)	7.7(5)
C(17)-N(4)-C(12)-C(11)	-152.2(4)
C(9)-N(3)-C(12)-N(4)	-152.5(4)
B(1)-N(3)-C(12)-N(4)	12.1(6)
C(9)-N(3)-C(12)-C(11)	11.5(4)
B(1)-N(3)-C(12)-C(11)	176.1(3)
C(16)-C(11)-C(12)-N(4)	-17.2(8)
C(10)-C(11)-C(12)-N(4)	155.7(4)
C(16)-C(11)-C(12)-N(3)	-179.8(4)
C(10)-C(11)-C(12)-N(3)	-6.9(4)
C(11)-C(10)-C(13)-C(14)	-3.1(6)
C(9)-C(10)-C(13)-C(14)	-171.9(4)

C(10)-C(13)-C(14)-C(15)	1.6(6)
C(13)-C(14)-C(15)-C(16)	0.2(7)
C(14)-C(15)-C(16)-C(11)	-0.5(7)
C(10)-C(11)-C(16)-C(15)	-1.0(6)
C(12)-C(11)-C(16)-C(15)	171.1(4)
C(12)-N(4)-C(17)-N(5)	-7.3(5)
C(12)-N(4)-C(17)-C(18)	155.7(4)
C(20)-N(5)-C(17)-N(4)	155.4(3)
B(1)-N(5)-C(17)-N(4)	-13.2(5)
C(20)-N(5)-C(17)-C(18)	-11.3(4)
B(1)-N(5)-C(17)-C(18)	-179.8(3)
N(4)-C(17)-C(18)-C(21)	15.3(7)
N(5)-C(17)-C(18)-C(21)	-179.6(4)
N(4)-C(17)-C(18)-C(19)	-158.8(4)
N(5)-C(17)-C(18)-C(19)	6.4(4)
C(21)-C(18)-C(19)-C(24)	1.0(5)
C(17)-C(18)-C(19)-C(24)	175.9(3)
C(21)-C(18)-C(19)-C(20)	-174.8(3)
C(17)-C(18)-C(19)-C(20)	0.1(4)
C(1)-N(6)-C(20)-N(5)	8.6(5)
C(1)-N(6)-C(20)-C(19)	-154.6(4)
C(17)-N(5)-C(20)-N(6)	-155.2(3)
B(1)-N(5)-C(20)-N(6)	13.5(5)
C(17)-N(5)-C(20)-C(19)	11.3(4)
B(1)-N(5)-C(20)-C(19)	-180.0(3)
C(24)-C(19)-C(20)-N(6)	-16.3(6)
C(18)-C(19)-C(20)-N(6)	158.9(4)
C(24)-C(19)-C(20)-N(5)	178.3(4)
C(18)-C(19)-C(20)-N(5)	-6.5(4)
C(19)-C(18)-C(21)-C(22)	-1.2(5)
C(17)-C(18)-C(21)-C(22)	-174.6(4)
C(18)-C(21)-C(22)-C(23)	0.5(6)
C(21)-C(22)-C(23)-C(24)	0.4(6)
C(18)-C(19)-C(24)-C(23)	-0.1(5)
C(20)-C(19)-C(24)-C(23)	174.5(4)
C(22)-C(23)-C(24)-C(19)	-0.6(6)
B(1)-O(1)-C(25)-O(2)	-3.5(5)
B(1)-O(1)-C(25)-C(26)	178.0(3)
O(2)-C(25)-C(26)-C(27)	-167.7(4)
O(1)-C(25)-C(26)-C(27)	10.7(5)
O(2)-C(25)-C(26)-C(30)	4.3(6)
O(1)-C(25)-C(26)-C(30)	-177.2(3)
O(2)-C(25)-C(26)-Fe(1)	-81.5(4)
O(1)-C(25)-C(26)-Fe(1)	97.0(3)
C(35)-Fe(1)-C(26)-C(27)	128.5(2)
C(30)-Fe(1)-C(26)-C(27)	-119.7(3)

C(32)-Fe(1)-C(26)-C(27)	52.2(5)
C(31)-Fe(1)-C(26)-C(27)	86.3(2)
C(33)-Fe(1)-C(26)-C(27)	-161.2(6)
C(34)-Fe(1)-C(26)-C(27)	169.4(2)
C(29)-Fe(1)-C(26)-C(27)	-81.0(2)
C(28)-Fe(1)-C(26)-C(27)	-38.1(2)
C(35)-Fe(1)-C(26)-C(30)	-111.8(3)
C(32)-Fe(1)-C(26)-C(30)	171.9(4)
C(27)-Fe(1)-C(26)-C(30)	119.7(3)
C(31)-Fe(1)-C(26)-C(30)	-154.0(2)
C(33)-Fe(1)-C(26)-C(30)	-41.6(7)
C(34)-Fe(1)-C(26)-C(30)	-70.9(3)
C(29)-Fe(1)-C(26)-C(30)	38.7(3)
C(28)-Fe(1)-C(26)-C(30)	81.5(3)
C(35)-Fe(1)-C(26)-C(25)	8.4(3)
C(30)-Fe(1)-C(26)-C(25)	120.2(4)
C(32)-Fe(1)-C(26)-C(25)	-67.9(5)
C(27)-Fe(1)-C(26)-C(25)	-120.1(4)
C(31)-Fe(1)-C(26)-C(25)	-33.8(4)
C(33)-Fe(1)-C(26)-C(25)	78.6(7)
C(34)-Fe(1)-C(26)-C(25)	49.3(4)
C(29)-Fe(1)-C(26)-C(25)	158.9(3)
C(28)-Fe(1)-C(26)-C(25)	-158.2(3)
C(30)-C(26)-C(27)-C(28)	1.0(4)
C(25)-C(26)-C(27)-C(28)	174.2(4)
Fe(1)-C(26)-C(27)-C(28)	60.6(3)
C(30)-C(26)-C(27)-Fe(1)	-59.6(3)
C(25)-C(26)-C(27)-Fe(1)	113.6(4)
C(35)-Fe(1)-C(27)-C(26)	-71.7(3)
C(30)-Fe(1)-C(27)-C(26)	37.8(2)
C(32)-Fe(1)-C(27)-C(26)	-156.2(2)
C(31)-Fe(1)-C(27)-C(26)	-112.7(2)
C(33)-Fe(1)-C(27)-C(26)	168.5(4)
C(34)-Fe(1)-C(27)-C(26)	-35.4(8)
C(29)-Fe(1)-C(27)-C(26)	82.0(2)
C(28)-Fe(1)-C(27)-C(26)	118.2(3)
C(26)-Fe(1)-C(27)-C(28)	-118.2(3)
C(35)-Fe(1)-C(27)-C(28)	170.1(2)
C(30)-Fe(1)-C(27)-C(28)	-80.4(3)
C(32)-Fe(1)-C(27)-C(28)	85.5(3)
C(31)-Fe(1)-C(27)-C(28)	129.1(3)
C(33)-Fe(1)-C(27)-C(28)	50.3(5)
C(34)-Fe(1)-C(27)-C(28)	-153.7(6)
C(29)-Fe(1)-C(27)-C(28)	-36.3(2)
C(26)-C(27)-C(28)-C(29)	-1.4(5)
Fe(1)-C(27)-C(28)-C(29)	57.7(3)

C(26)-C(27)-C(28)-Fe(1)	-59.1(3)
C(26)-Fe(1)-C(28)-C(29)	-82.2(3)
C(35)-Fe(1)-C(28)-C(29)	-157.1(7)
C(30)-Fe(1)-C(28)-C(29)	-37.5(2)
C(32)-Fe(1)-C(28)-C(29)	125.8(3)
C(27)-Fe(1)-C(28)-C(29)	-120.7(4)
C(31)-Fe(1)-C(28)-C(29)	167.1(3)
C(33)-Fe(1)-C(28)-C(29)	82.5(3)
C(34)-Fe(1)-C(28)-C(29)	45.3(5)
C(26)-Fe(1)-C(28)-C(27)	38.6(2)
C(35)-Fe(1)-C(28)-C(27)	-36.3(8)
C(30)-Fe(1)-C(28)-C(27)	83.2(3)
C(32)-Fe(1)-C(28)-C(27)	-113.4(3)
C(31)-Fe(1)-C(28)-C(27)	-72.1(3)
C(33)-Fe(1)-C(28)-C(27)	-156.8(3)
C(34)-Fe(1)-C(28)-C(27)	166.0(4)
C(29)-Fe(1)-C(28)-C(27)	120.7(4)
C(27)-C(28)-C(29)-C(30)	1.3(5)
Fe(1)-C(28)-C(29)-C(30)	58.7(3)
C(27)-C(28)-C(29)-Fe(1)	-57.4(3)
C(26)-Fe(1)-C(29)-C(28)	81.4(3)
C(35)-Fe(1)-C(29)-C(28)	169.1(3)
C(30)-Fe(1)-C(29)-C(28)	120.4(4)
C(32)-Fe(1)-C(29)-C(28)	-74.6(3)
C(27)-Fe(1)-C(29)-C(28)	37.1(2)
C(31)-Fe(1)-C(29)-C(28)	-45.6(9)
C(33)-Fe(1)-C(29)-C(28)	-115.1(3)
C(34)-Fe(1)-C(29)-C(28)	-157.8(2)
C(26)-Fe(1)-C(29)-C(30)	-39.0(3)
C(35)-Fe(1)-C(29)-C(30)	48.7(5)
C(32)-Fe(1)-C(29)-C(30)	165.0(3)
C(27)-Fe(1)-C(29)-C(30)	-83.3(3)
C(31)-Fe(1)-C(29)-C(30)	-166.0(7)
C(33)-Fe(1)-C(29)-C(30)	124.5(3)
C(34)-Fe(1)-C(29)-C(30)	81.8(3)
C(28)-Fe(1)-C(29)-C(30)	-120.4(4)
C(28)-C(29)-C(30)-C(26)	-0.7(5)
Fe(1)-C(29)-C(30)-C(26)	59.3(3)
C(28)-C(29)-C(30)-Fe(1)	-60.0(3)
C(27)-C(26)-C(30)-C(29)	-0.2(4)
C(25)-C(26)-C(30)-C(29)	-173.3(4)
Fe(1)-C(26)-C(30)-C(29)	-60.0(3)
C(27)-C(26)-C(30)-Fe(1)	59.9(3)
C(25)-C(26)-C(30)-Fe(1)	-113.3(4)
C(26)-Fe(1)-C(30)-C(29)	117.6(4)
C(35)-Fe(1)-C(30)-C(29)	-156.5(3)

C(32)-Fe(1)-C(30)-C(29)	-49.0(8)
C(27)-Fe(1)-C(30)-C(29)	80.0(3)
C(31)-Fe(1)-C(30)-C(29)	172.8(4)
C(33)-Fe(1)-C(30)-C(29)	-75.4(3)
C(34)-Fe(1)-C(30)-C(29)	-114.7(3)
C(28)-Fe(1)-C(30)-C(29)	36.4(3)
C(35)-Fe(1)-C(30)-C(26)	85.8(3)
C(32)-Fe(1)-C(30)-C(26)	-166.7(6)
C(27)-Fe(1)-C(30)-C(26)	-37.6(2)
C(31)-Fe(1)-C(30)-C(26)	55.2(5)
C(33)-Fe(1)-C(30)-C(26)	167.0(2)
C(34)-Fe(1)-C(30)-C(26)	127.7(3)
C(29)-Fe(1)-C(30)-C(26)	-117.6(4)
C(28)-Fe(1)-C(30)-C(26)	-81.3(2)
C(26)-Fe(1)-C(31)-C(35)	82.9(3)
C(30)-Fe(1)-C(31)-C(35)	44.5(5)
C(32)-Fe(1)-C(31)-C(35)	-119.4(4)
C(27)-Fe(1)-C(31)-C(35)	127.0(3)
C(33)-Fe(1)-C(31)-C(35)	-81.1(3)
C(34)-Fe(1)-C(31)-C(35)	-37.4(3)
C(29)-Fe(1)-C(31)-C(35)	-155.5(7)
C(28)-Fe(1)-C(31)-C(35)	168.1(3)
C(26)-Fe(1)-C(31)-C(32)	-157.6(3)
C(35)-Fe(1)-C(31)-C(32)	119.4(4)
C(30)-Fe(1)-C(31)-C(32)	163.9(4)
C(27)-Fe(1)-C(31)-C(32)	-113.6(3)
C(33)-Fe(1)-C(31)-C(32)	38.3(3)
C(34)-Fe(1)-C(31)-C(32)	82.0(3)
C(29)-Fe(1)-C(31)-C(32)	-36.1(9)
C(28)-Fe(1)-C(31)-C(32)	-72.5(4)
C(35)-C(31)-C(32)-C(33)	-1.3(5)
Fe(1)-C(31)-C(32)-C(33)	-60.3(3)
C(35)-C(31)-C(32)-Fe(1)	59.0(3)
C(26)-Fe(1)-C(32)-C(33)	166.5(3)
C(35)-Fe(1)-C(32)-C(33)	80.7(3)
C(30)-Fe(1)-C(32)-C(33)	-33.7(8)
C(27)-Fe(1)-C(32)-C(33)	-156.7(3)
C(31)-Fe(1)-C(32)-C(33)	117.9(4)
C(34)-Fe(1)-C(32)-C(33)	37.0(3)
C(29)-Fe(1)-C(32)-C(33)	-72.4(4)
C(28)-Fe(1)-C(32)-C(33)	-113.2(3)
C(26)-Fe(1)-C(32)-C(31)	48.6(5)
C(35)-Fe(1)-C(32)-C(31)	-37.3(3)
C(30)-Fe(1)-C(32)-C(31)	-151.6(6)
C(27)-Fe(1)-C(32)-C(31)	85.4(3)
C(33)-Fe(1)-C(32)-C(31)	-117.9(4)

C(34)-Fe(1)-C(32)-C(31)	-81.0(3)
C(29)-Fe(1)-C(32)-C(31)	169.7(3)
C(28)-Fe(1)-C(32)-C(31)	128.9(3)
C(31)-C(32)-C(33)-C(34)	1.3(5)
Fe(1)-C(32)-C(33)-C(34)	-58.9(3)
C(31)-C(32)-C(33)-Fe(1)	60.2(3)
C(26)-Fe(1)-C(33)-C(34)	-37.6(8)
C(35)-Fe(1)-C(33)-C(34)	38.2(3)
C(30)-Fe(1)-C(33)-C(34)	-70.4(4)
C(32)-Fe(1)-C(33)-C(34)	120.3(4)
C(27)-Fe(1)-C(33)-C(34)	170.8(3)
C(31)-Fe(1)-C(33)-C(34)	81.8(3)
C(29)-Fe(1)-C(33)-C(34)	-112.3(3)
C(28)-Fe(1)-C(33)-C(34)	-154.0(3)
C(26)-Fe(1)-C(33)-C(32)	-157.9(6)
C(35)-Fe(1)-C(33)-C(32)	-82.1(3)
C(30)-Fe(1)-C(33)-C(32)	169.3(3)
C(27)-Fe(1)-C(33)-C(32)	50.4(5)
C(31)-Fe(1)-C(33)-C(32)	-38.5(3)
C(34)-Fe(1)-C(33)-C(32)	-120.3(4)
C(29)-Fe(1)-C(33)-C(32)	127.4(3)
C(28)-Fe(1)-C(33)-C(32)	85.6(3)
C(32)-C(33)-C(34)-C(35)	-0.8(5)
Fe(1)-C(33)-C(34)-C(35)	-59.5(3)
C(32)-C(33)-C(34)-Fe(1)	58.7(3)
C(26)-Fe(1)-C(34)-C(35)	-73.9(3)
C(30)-Fe(1)-C(34)-C(35)	-114.3(3)
C(32)-Fe(1)-C(34)-C(35)	81.1(3)
C(27)-Fe(1)-C(34)-C(35)	-45.6(8)
C(31)-Fe(1)-C(34)-C(35)	37.1(3)
C(33)-Fe(1)-C(34)-C(35)	118.2(4)
C(29)-Fe(1)-C(34)-C(35)	-156.7(3)
C(28)-Fe(1)-C(34)-C(35)	172.3(3)
C(26)-Fe(1)-C(34)-C(33)	168.0(3)
C(35)-Fe(1)-C(34)-C(33)	-118.2(4)
C(30)-Fe(1)-C(34)-C(33)	127.6(3)
C(32)-Fe(1)-C(34)-C(33)	-37.0(3)
C(27)-Fe(1)-C(34)-C(33)	-163.8(6)
C(31)-Fe(1)-C(34)-C(33)	-81.0(3)
C(29)-Fe(1)-C(34)-C(33)	85.1(3)
C(28)-Fe(1)-C(34)-C(33)	54.2(5)
C(32)-C(31)-C(35)-C(34)	0.8(5)
Fe(1)-C(31)-C(35)-C(34)	59.8(3)
C(32)-C(31)-C(35)-Fe(1)	-59.0(3)
C(33)-C(34)-C(35)-C(31)	0.0(5)
Fe(1)-C(34)-C(35)-C(31)	-59.9(3)

C(33)-C(34)-C(35)-Fe(1)	59.9(3)
C(26)-Fe(1)-C(35)-C(31)	-114.6(3)
C(30)-Fe(1)-C(35)-C(31)	-158.4(3)
C(32)-Fe(1)-C(35)-C(31)	37.7(3)
C(27)-Fe(1)-C(35)-C(31)	-73.7(3)
C(33)-Fe(1)-C(35)-C(31)	81.6(3)
C(34)-Fe(1)-C(35)-C(31)	119.8(4)
C(29)-Fe(1)-C(35)-C(31)	167.8(4)
C(28)-Fe(1)-C(35)-C(31)	-44.2(8)
C(26)-Fe(1)-C(35)-C(34)	125.6(3)
C(30)-Fe(1)-C(35)-C(34)	81.8(3)
C(32)-Fe(1)-C(35)-C(34)	-82.0(3)
C(27)-Fe(1)-C(35)-C(34)	166.5(3)
C(31)-Fe(1)-C(35)-C(34)	-119.8(4)
C(33)-Fe(1)-C(35)-C(34)	-38.2(3)
C(29)-Fe(1)-C(35)-C(34)	48.0(5)
C(28)-Fe(1)-C(35)-C(34)	-164.0(7)
C(25)-O(1)-B(1)-N(5)	167.9(3)
C(25)-O(1)-B(1)-N(3)	49.5(4)
C(25)-O(1)-B(1)-N(1)	-74.9(4)
C(20)-N(5)-B(1)-O(1)	94.0(4)
C(17)-N(5)-B(1)-O(1)	-98.4(4)
C(20)-N(5)-B(1)-N(3)	-139.5(3)
C(17)-N(5)-B(1)-N(3)	28.1(4)
C(20)-N(5)-B(1)-N(1)	-29.5(4)
C(17)-N(5)-B(1)-N(1)	138.1(3)
C(12)-N(3)-B(1)-O(1)	93.2(4)
C(9)-N(3)-B(1)-O(1)	-103.9(4)
C(12)-N(3)-B(1)-N(5)	-27.4(5)
C(9)-N(3)-B(1)-N(5)	135.5(3)
C(12)-N(3)-B(1)-N(1)	-137.5(3)
C(9)-N(3)-B(1)-N(1)	25.5(5)
C(1)-N(1)-B(1)-O(1)	-90.8(4)
C(4)-N(1)-B(1)-O(1)	105.9(4)
C(1)-N(1)-B(1)-N(5)	28.5(4)
C(4)-N(1)-B(1)-N(5)	-134.8(3)
C(1)-N(1)-B(1)-N(3)	138.3(3)
C(4)-N(1)-B(1)-N(3)	-25.0(5)

Symmetry transformations used to generate equivalent atoms:

Table 7. Hydrogen bonds for a0005 [A and deg.].

D-H...A	d(D-H)	d(H...A)	d(D...A)	<(DHA)